A HIGHLY LINEAR AND EFFICIENT OUT-PHASING TRANSMITTER FOR MULTI-BAND, MULTI-MODE APPLICATIONS

A Dissertation
Presented to
The Academic Faculty

by

Joonhoi Hur

In Partial Fulfillment
Of the Requirements for the Degree
Doctor of Philosophy in the
School of Electrical and Computer Engineering

Georgia Institute of Technology
December 2010

A HIGHLY LINEAR AND EFFICIENT OUT-PHASING TRANSMITTER FOR MULTI-BAND, MULTI-MODE APPLICATIONS

Approved by:

Dr. James Stevenson Kenney, Advisor
School of Electrical and Computer Engineering
Georgia Institute of Technology

Dr. Emmanouil M. Tentzeris
School of Electrical and Computer Engineering
Georgia Institute of Technology

Dr. Shyh-Chiang Shen
School of Electrical and Computer Engineering
Georgia Institute of Technology

Dr. Jongman Kim
School of Electrical and Computer Engineering
Georgia Institute of Technology

Dr. Sung Ha Kang
School of Mathematics
Georgia Institute of Technology

Date Approved: Oct. 20, 2010

ACKNOWLEDGEMENTS

First of all, I would like to acknowledge monumental support and enthusiastic supervision of my research advisor, Professor James Stevenson Kenney. Without his guidance and inspiration, I would not have achieved this research goal.

I am also grateful to all the committee members, Professor, Emmanouil M. Tentzeris, Professor Shyh-Chiang Shen, Professor Jongman Kim, and Professor Sung Ha Kang for their time and effort in reviewing my dissertation and serving as my defense committee members.

I would like to specially express my gratitude to Dr. Joy Laskar, Dr. Kyutae Lim, and Dr. Chang-Ho Lee for their great support and guidance throughout this research.

I am greatly indebted my colleague members in Microwave Application Group (MAG) for making good environment as a team supporting each other. I owe special thanks to the cognitive radio (CR) team and the Samsung Design Center (SDC) members for their numerous technical discussions in circuit and system design.

And most of all, I am especially grateful to my parents, Hun-Koo Hur and Kyung-Sook Kong, and my parents-in-law, Jin-Tae Kim and He-Sook Kwon, for their unconditional love. I can't express my love and gratitude enough to my wife, Sei-Eun Kim, for her endless support throughout my life. Without their encouragement and support, I would not be able to complete this work.

TABLE OF CONTENTS

LIST OF TABLES

LIST OF FIGURES

SUMMARY

There have been many efforts to improve efficiency of transmitter while meeting stringent linearity requirement of modern communication system. Among the technology to enhance efficiency of linear transmitter, the out-phasing technologies, also called the linear amplification with nonlinear components (LINC), is considered as a promising technology. LINC has been studied long times, since it provides excellent linearity with high efficiency by allowing adopt high efficient switch-mode power amplifiers. However, The LINC transmitter has some technical challenges: linearity degradation due to amplitude and phase mismatches, efficiency degradation due to poor combining efficiency, and narrow frequency bandwidth due to output matching network of switching power amplifier.

In this thesis, some state-of-the-art techniques for solving the problems of LINC transmitters are presented. An unbalanced phase calibration technique compensates amplitude/phase mismatches between two parallel paths in the LINC system, and multi-level LINC (MLINC) and an uneven multi-level LINC (UMLINC) structure improve the overall power efficiency. And the reconfigurable Class-D switching PA enables multi-band operation with high efficiency and good linearity. With these techniques, the new multi-band out-phasing transmitter improves the efficiency without sacrificing the linearity performance.

CHAPTER 1

INTRODUCTION

1.1. MOTIVATION

The higher data rate in wireless communications is one of most important factors in modern wireless communication [1]. Figure 1 shows the evolution of wireless communication trends. As shown in the figure, new emerging wireless standard requires higher data rate.

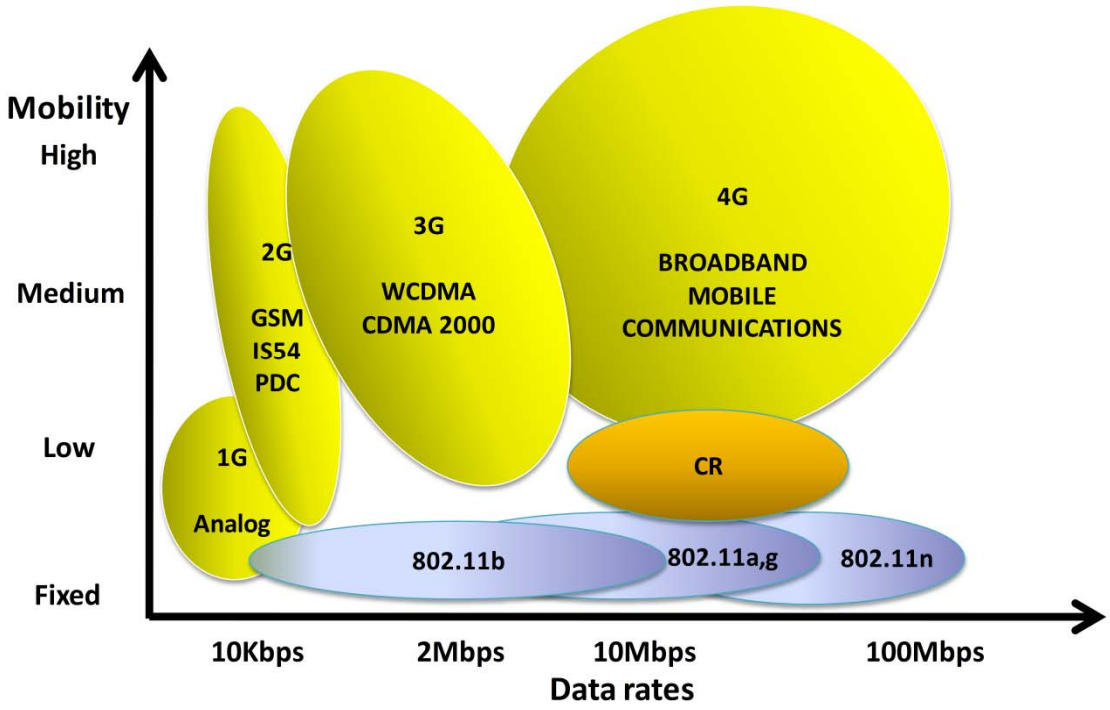

Figure 1. Trend of wireless communication standards.

To deal with the high data rate, one of the solutions can be increasing the speed of symbol rate. However, increasing symbol ratio requires broad bandwidth and limits the number of users in a given bandwidth.

Another choice for higher date rate is increasing spectral efficiency. To increase the spectral efficiency, baseband signals should have complex I/Q symbols, which require both amplitude and phase modulation. For example, the 64QAM signal which is shown in Figure 2(b) can transfer 16 times of date of QPSK signal which is shown in Figure 2(a) at the same spectrum bandwidth. However, to transfer more information, amplitude modulated signals have high peak-to-average power ratio (PAPR), a substantial back-off in its power amplifier (PA) is generally needed to ensure adequate transmitter linearity; thus the average power efficiency is significantly degraded [2].

In an effort to increase the efficiency of a PA, Out-phasing power amplification, also called linear amplification using nonlinear components (LINC), was proposed as one solution that may offer high efficiency with good linearity [3]. LINC eliminates the high linearity demands on a single PA by summing the outputs of two nonlinear PAs via a power combiner to amplify non-constant envelope signals. This technique produces an amplifier with the linearity of a moderate back-off linear PA at an efficiency approaching that of a switching amplifier. However, despite the efficiency improvement, the out-phasing topology has not been widely used in commercial amplifiers due to its strict branch matching requirements for both phase and amplitude [4], [5] and signal distortion and efficiency degradation caused by the RF power combiner [6], . In addition, narrow bandwidth of the switching PA limits the operational frequency bandwidth of LINC system.

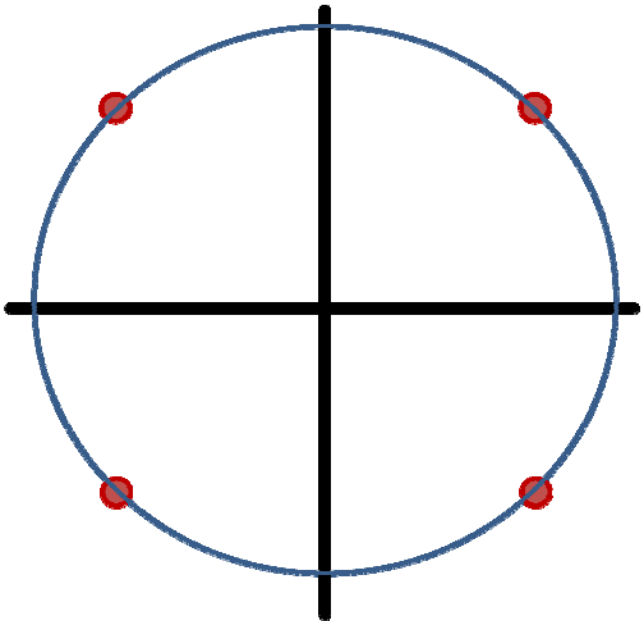

(a)

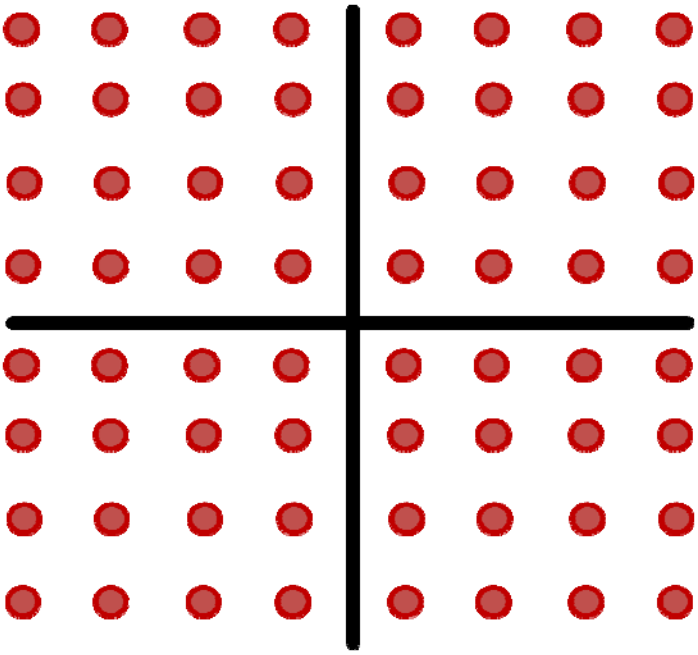

(b)

Figure 2. Different signal source for the wireless communications: (a) QPSK, (b) 64QAM

1.2. ORGANIZATION

The dissertation is organized as follows:

Chapter 1 is an introduction of this dissertation and demonstrates the necessity of highly efficient and linear RF transmitter in emerging wireless communications and the origin of the problems of out-phasing RF transmitter is introduced. Following that, the organization of the dissertation is described.

In Chapter 2, efficiencies of various RF transmitters are presented as a background. The basic concepts of highly efficient transmitters such as polar transmitter and LINC transmitter are presented as a background.

In Chapter 3 deals with a mismatch calibration technique for the LINC system that calibrates both phase and amplitude mismatches with only phase control. The technique detects mismatches between two paths without any iteration using pre-defined five test vector signals. After all, the linearity is significantly improved with the technique.

Chapter 4 focused on efficiency improvement techniques for LINC transmitter. The multi-level LINC improve the efficiency performance, the uneven-multi LINC (UMLINC) architecture that further increases system efficiency without increasing complexity with a given number of power supplies.

Chapter 5 describes a multi-band multi-mode LINC technique which employs tunable series resonators in the Class D power amplifier which have good efficiency for both high power and low power mode. The 3dB bandwidth of the LINC system was from 450 MHz to 730 MHz, which covers the cognitive radio white spectrum standard.

Finally, chapter 6 summarizes the dissertation and provides guidance towards future research possibilities.

CHAPTER 2
BACKGROUND

2.1. EFFICIENCY OF POWER AMPLIFIERS

To deals with modern communications which have high peak to average power ratio, highly linear transmitter is required. Some linear amplifier topologies can meet the linearity requirement of modern communication specification; however, they usually yield poor efficiency.

2.1.1. Linear Power Amplifiers

The linear power amplifier usually has good linearity with a cost of efficiency. Brief explanation and basic functionality of each PA topology is presented [7] [8].

2.1.1-(a) Class A PA

Figure 3 shows the basic structure of Class A PA which is working linearly for the all input range. For the Class A operation, the gate bias is set for the quiescent current to be large enough that the transistor remains at all times in the active region. So that, ideally, Class A PA works as a current source. Consequently, in fixed load, the output current and voltage waveforms are linear with the input voltage [9]. However, because it consumes power even if there is no output RF-signals, the efficiency of Class A power amplifier is low.

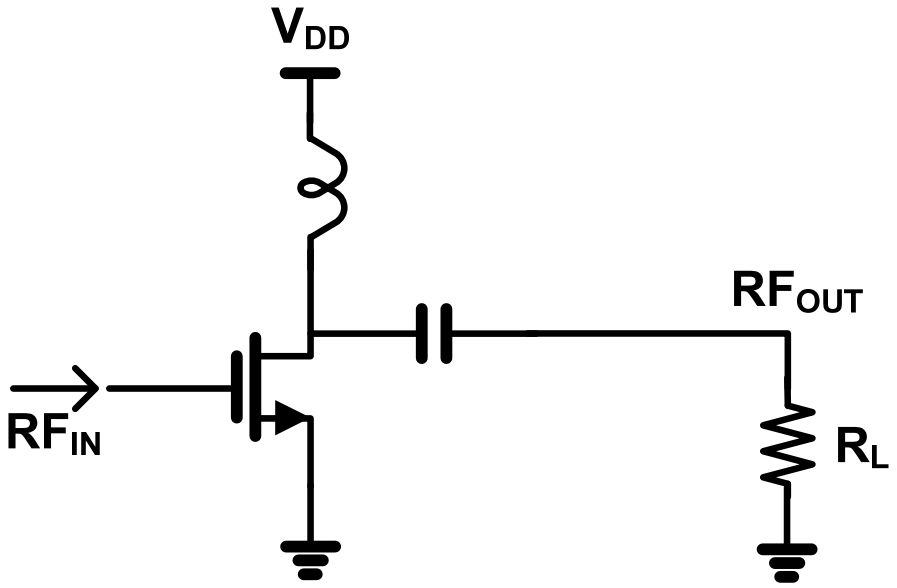

Figure 3. Overall structure of Class A power amplifier

The efficiency of the Class A power amplifier is following.

$$\eta_{PA}(ClassA) = 0.5 \times \frac{P_{OUT}}{(P_{OUT})_{MAX}} \tag{2.1}$$

where,

P_{OUT} = output power of the PA,

$(P_{OUT})_{MAX}$ = peak output power of the PA

η_{PA} = Instance Efficiency of the PA

According to (2.1), the maximum efficiency of the Class A power amplifier is 50% when the PA is saturated. Furthermore, the efficiency is even worse when the output power of the PA is less than maximum output power.

2.1.1-B Class B PA

The efficiency of Class B power amplifier is higher than that of Class A power amplifier [10]. The gate bias in a class-B PA is set at the threshold of conduction so that the quiescent drain current is zero. As a result, the transistor is active half of the time and the drain current is a half sinusoid. Figure 4-(a) shows a Class B PA using transformer. The two transistors are working as complementary with the two differential RF input signals. The Class B PA can be implemented without transformer. Figure 4-(b) shows a Class B PA using RLC tank shunts harmonics to ground. The efficiency of Class B PA is as following.

$$\eta_{PA}(ClassB) = \frac{\pi}{4} \times \left(\frac{P_{OUT}}{(P_{OUT})_{MAX}} \right)^{0.5} \qquad (2.2)$$

According to the equation (2.2), the maximum efficiency is 78.5% when the PA is saturated. And for the lower output power, the power efficiency is less than the maximum efficiency.

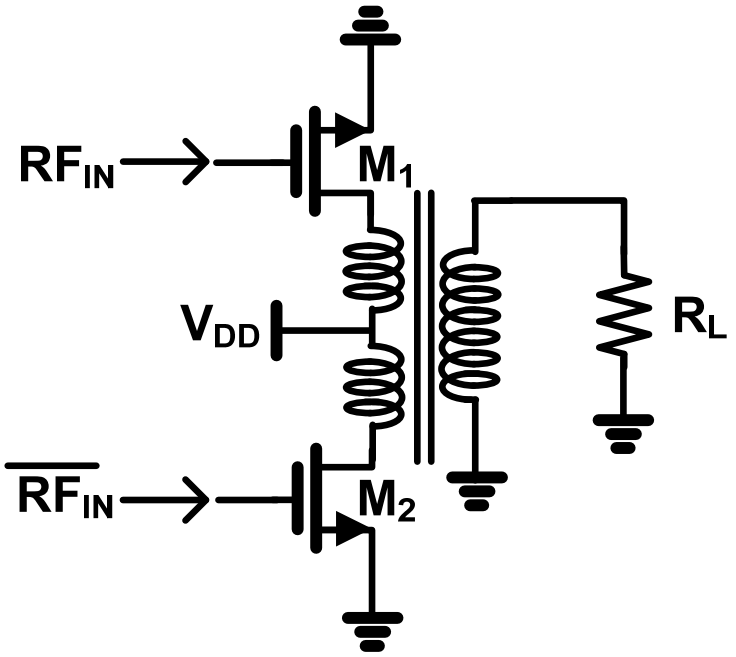

(a)

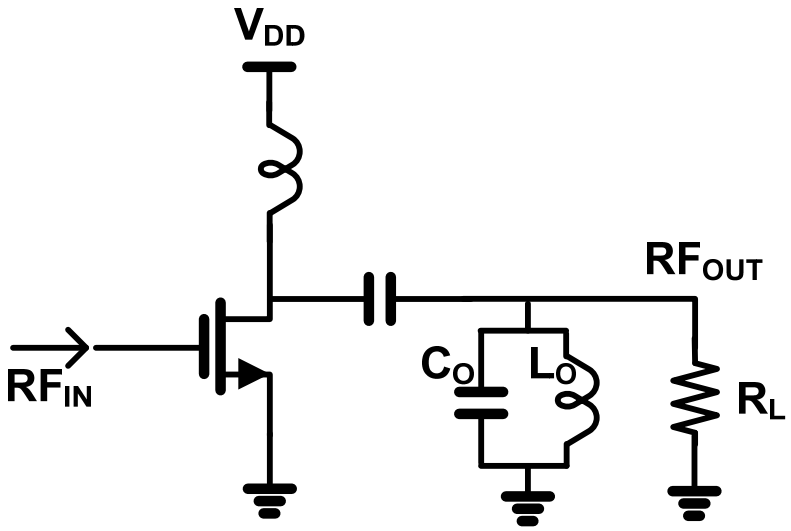

(b)

Figure 4. Class B PA: (a) with a transformer, (b) with a parallel resonator.

2.1.2 Switching Power Amplifiers

If give up linearity, then some intrinsically efficient amplifiers can be created using switches. An ideal switch does not dissipate any power since either the voltage or current is zero. So that the Switching power amplifiers have very good efficiency compared with linear power amplifier.

2.1.2-(a) Class D Power Amplifier

Class-D PAs usually use two transistors as inverting switches to generate a square voltage waveform in a drain [11]. A series LC output filter only allows the fundamental-frequency component into the load as shown in Figure 5. Since current is drawn only through the transistor that is on, Class-D Pas have ideally 100-percent efficiency.

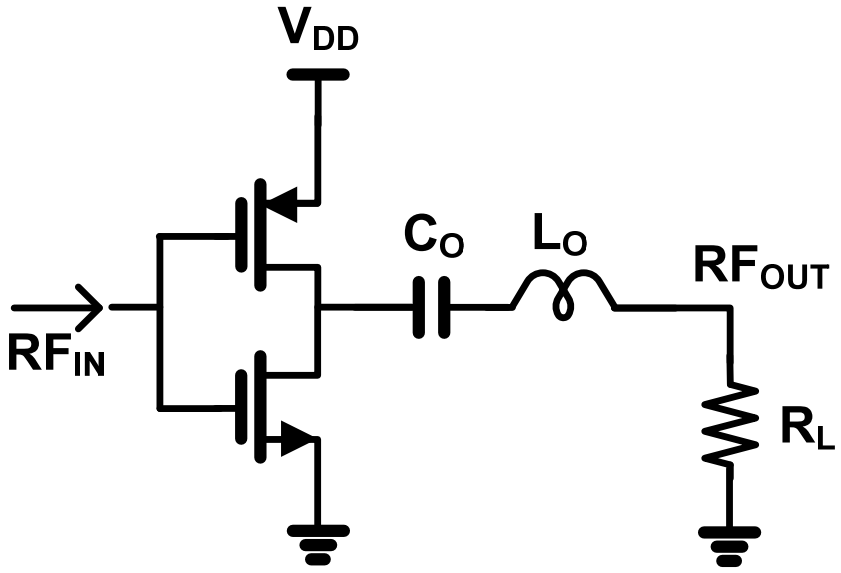

Figure 5. Class D Power amplifier

2.1.2-B Class E Power Amplifier

The overall structure of Class E power amplifier is shown in Figure 6. The Class E power amplifier employs a single transistor operated as a switch. The drain voltage waveform is the result of the sum of the DC and RF currents charging the drain-shunt capacitance [12]. In optimum class E, the drain voltage drops to zero and has a zero slope just as the transistor turns on. The result is an ideal efficiency of 100 percent.

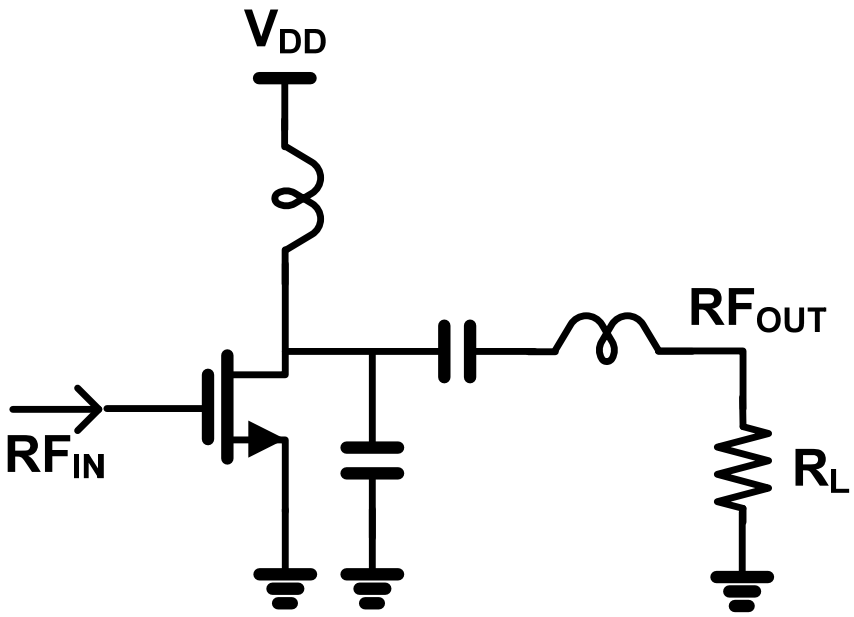

Figure 6. Class E Power amplifier

2.1.2-(c) Class F Power Amplifier

The Class F PA boosts both efficiency and output by using harmonic resonators in the output network to shape the drain waveforms [13]. The voltage waveform includes one or more odd harmonics and approximates a square wave, while the current includes even harmonics and approximates a half sine wave. Figure 7 shows a Class F PA using a quarter wave transformer converter. A quarter-waver transformer converts the low impedance at the load at harmonics of the fundamental to high impedance for all odd harmonics. In theory, a perfect square wave at the drain of the transistor can be created and thus achieve 100% efficiency.

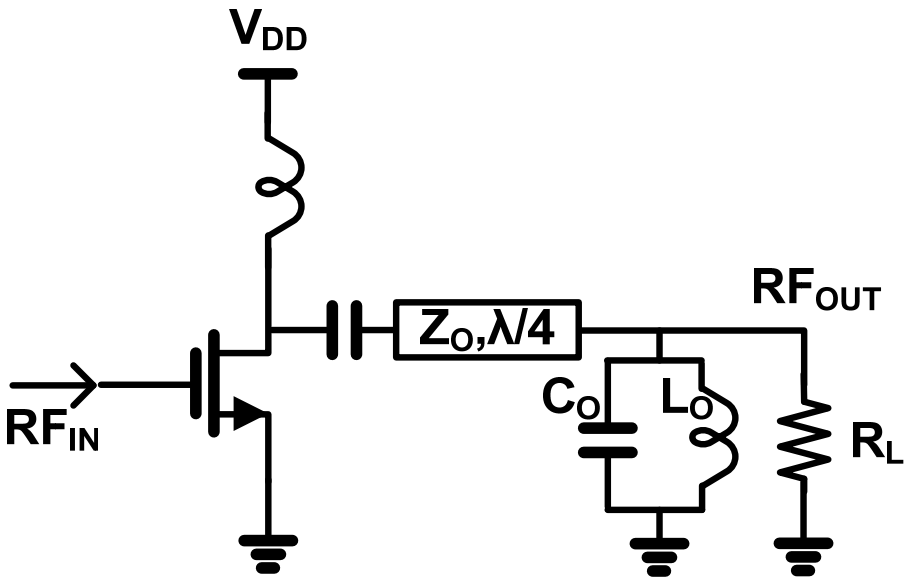

Figure 7. Overall Structure of Class F PA

2.2 HIGHLY EFFICIENT LINEAR TRANSMITTER USING SWITCHING PA

2.2.1 Polar Transmitter

The overall structure of Envelope Elimination and Restoration (EER) technique is shown in Figure 8. EER transmitter combines a highly efficient but nonlinear RF power amplifier (PA) with a highly efficient envelope amplifier to implement a high efficiency linear RF power amplifier [14].

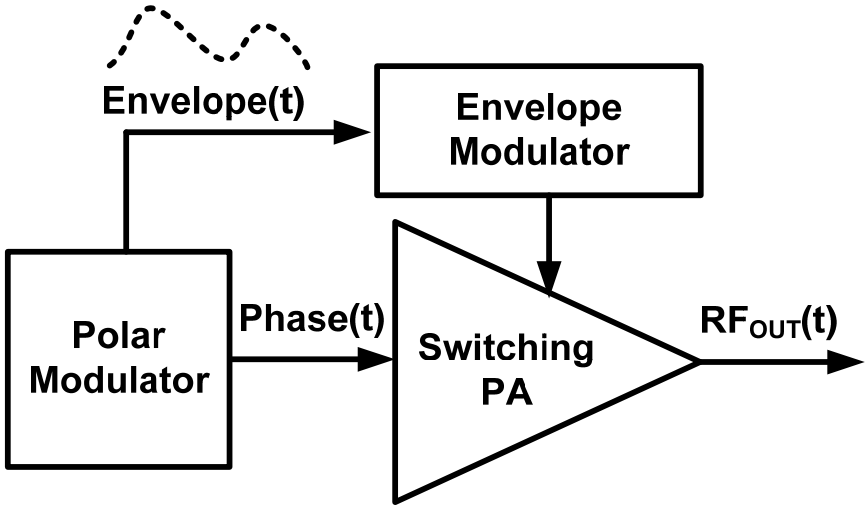

Figure 8. Envelope Elimination and Restoration Transmitter

In its classic form, a limiter eliminates the envelope, allowing the constant-amplitude phase modulated carrier to be amplified efficiently by Switching PAs [13].

Amplitude modulation of the final RF PA restores the envelope to the phase modulated carrier creating an amplified replica of the input signal.

EER is based upon the equivalence of any narrowband signal to simultaneous amplitude (envelope) and phase modulations. The polar transmitter basically operates by converting complex I/Q symbols into envelope and constant envelope phase signals. The

constant envelope signal is amplified through a highly efficient nonlinear PA with a separate envelope control path.

In a modern implementation, both the envelope and the phase-modulated carrier are generated by a DSP. In contrast to linear amplifiers, a Kahn-technique transmitter operates with high efficiency over a wide dynamic range and therefore produces a high average efficiency for a wide range of signals and power (back-off) levels.

However, despite the efficiency improvement, the separate amplitude modulation through a low dropout (LDO) regulator, DC/DC converter, ΣΔ modulator, or PWM has a significant bandwidth limitation and efficiency degradation problems in commercial wideband systems. Transmitters based upon the Kahn technique generally have excellent linearity because linearity depends upon the modulator rather than RF power transistors. The two most important factors affecting the linearity are the envelope bandwidth and alignment of the envelope and phase modulations. As a rule of thumb, the envelope bandwidth must be at least twice the RF bandwidth and the misalignment must not exceed one tenth of the inverse of the RF bandwidth [15].

2.2.2 Out-phasing Transmitter

The purpose of the LINC system is to increase the efficiency of a PA. If the linear signal is decomposed into two constant envelope signals, the LINC system is able to employ high-efficiency, nonlinear PAs instead of a low-efficiency, linear PA. Figure 9 shows the decomposing principle of the LINC system. The non-constant envelope signal such as OFDM can be represented in a polar notation as

$$S_I(t) = |S_I(t)| \angle \phi(t). \tag{2.3}$$

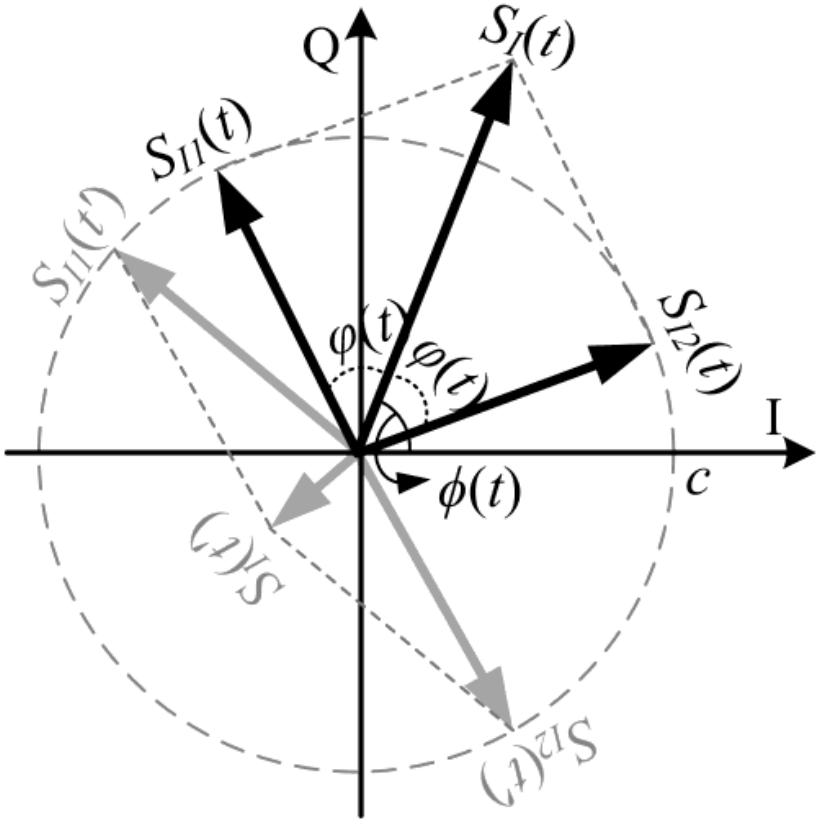

Figure 9. The out-phasing vector decomposition diagram.

As shown in Figure 9, the original input signal can also be expressed by a sum of two phase-modulated signals:

$$S_{I1}(t) = c\angle\theta_1(t) = c\angle(\phi(t) + \varphi(t)), \tag{2.4}$$

$$S_{I2}(t)) = c\angle\theta_2(t) = c\angle(\phi(t) - \varphi(t)), \tag{2.5}$$

where $c=0.5\cdot|S_I|_{MAX}$ and $|S_I|_{MAX}$ is the maximum envelope of the input signal.

These two phase-modulated constant-envelope signals are amplified individually by high efficiency nonlinear PAs as shown in Figure 10. When the output magnitudes of the PAs are α, the outputs of the nonlinear PAs are expressed as

$$S_{O1}(t) = \alpha\angle(\theta_1(t)), \tag{2.6}$$

$$S_{O2}(t) = \alpha\angle(\theta_2(t)). \tag{2.7}$$

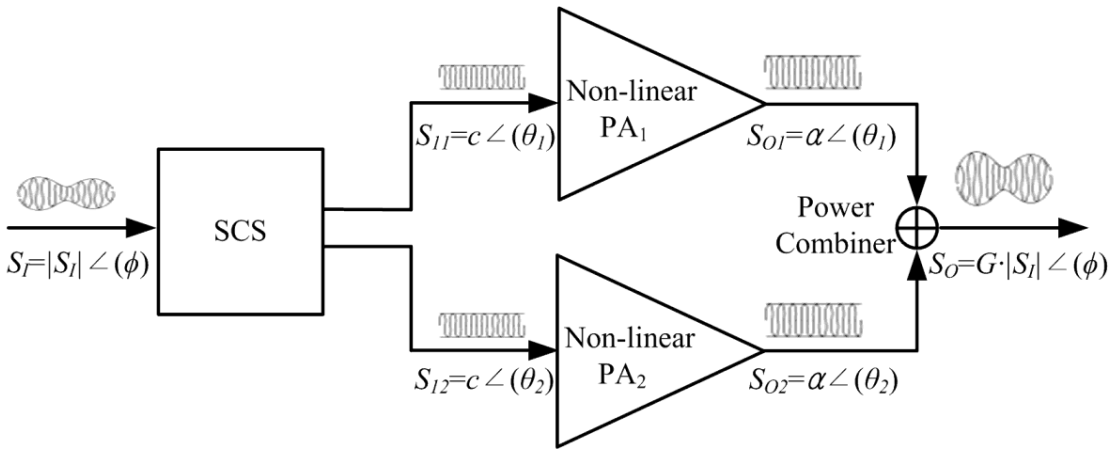

Figure 10. Block diagram of the LINC system.

The outputs of the PAs are summed in a power combiner, and the output of the power combiner can be expressed as follows:

$$S_O(t) = S_{O1}(t) + S_{O2}(t) = \alpha\angle(\theta_1(t)) + \alpha\angle(\theta_2(t)) = \frac{\alpha}{c} \cdot S_I(t) = G \cdot S_I(t), \qquad (2.8)$$

where G is the voltage gain of the PA.

In (2.8), it can be understood that the output signal is proportional to the input signal. In this way, the LINC system can maintain linearity while using high efficiency, nonlinear PAs.

CHAPTER 3
HIGHLY LINEAR UNBALANCED LINC ARCHITECTURE

3.1 INTRODUCTION

In an effort to increase the efficiency of a PA, the linear amplifier with nonlinear components (LINC) architecture has been proposed. Although the LINC architecture, which separates a non-constant envelope input signal into two constant envelope signals, is highly efficient, by using two highly efficient nonlinear PAs, it has poor linearity if path mismatches such as amplitude and phase mismatches occur between the two signal paths.

In order to improve the linearity performance, many researchers have tried to calibrate path mismatches: A phase calibration method based on a multiplier was proposed in [16], however, the amplitude mismatches still degraded amplifier linearity. To adjust both amplitude and phase mismatches, [17] and [18] used a direct searching scheme and [19] used a baseband pre-preconditioning and DC adjustment methods. In addition, Zhang et al. in [20], [21], [22] proposed a digital pre-distortion approach that controls a baseband DSP and a down-conversion loop.

Although these techniques have good calibration performance, most of them need time- and power-consuming iterations to detect mismatches. In addition, in order to correct an amplitude mismatch of a nonlinear PA, they require additional blocks such as fine resolution DC/DC converters or low drop output regulators (LDO) [23]. To reduce

the iterations, [24] proposed a calibration method using pre-defined test vector signal, but it still needs some iterations due to AM/PM and AM/AM distortions of the PAs and also requires additional amplitude control blocks to control the output power of the PAs.

In order to calibrate the both amplitude and phase mismatches without additional amplitude mismatch correction blocks or iterations, this chapter proposed the concept of the new unbalanced phase-only calibration in [25]. In order to verify the system feasibility and to evaluate the enhanced linearity performance of the proposed system, the LINC system is implemented with an automatic calibration algorithm using the proposed calibration technique.

3.2 MISMATCH EFFECTS OF THE LINC SYSTEM

In the LINC architecture, an amplitude mismatch (Δα) and a phase mismatch (Δθ) between the two signal paths produce poor linearity, as shown in Figure 11. With these mismatches, the outputs of the PAs can be expressed as

$$S_{O1}(t) = \alpha \angle(\theta_1(t)), \tag{3.1}$$

$$S_{O2}(t) = (\alpha + \Delta\alpha)\angle(\theta_2(t) + \Delta\theta). \tag{3.2}$$

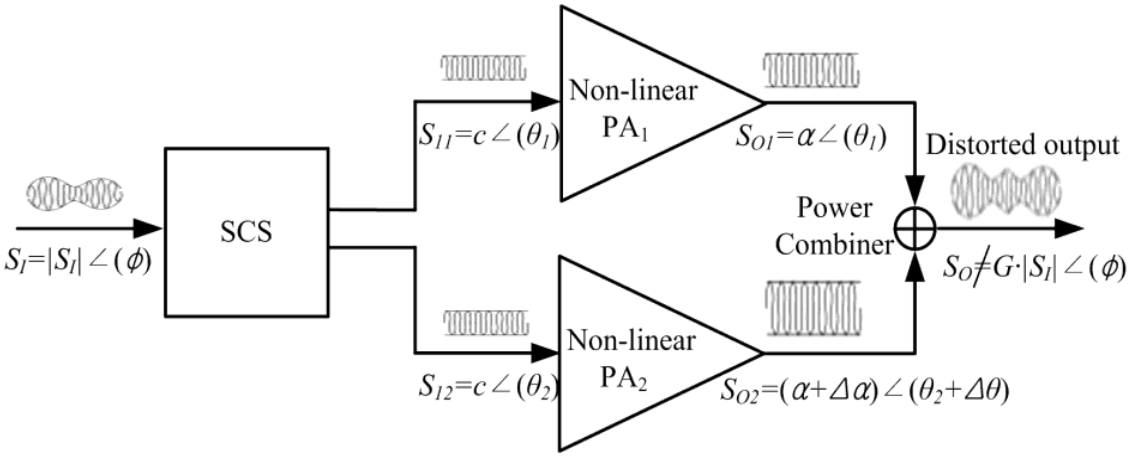

Figure 11. Path mismatches in the LINC system.

In this case, the output signal of the LINC system is not proportional to the input signal. This nonlinear error degrades system linearity. For example, when error vector magnitude (EVM) values are measured with a 7 MHz bandwidth 64QAM WiMAX signal using a two-port RF vector signal generator (SMU 200ATM), the path mismatches of the LINC system degrade the EVM values, as shown in Figure 12.

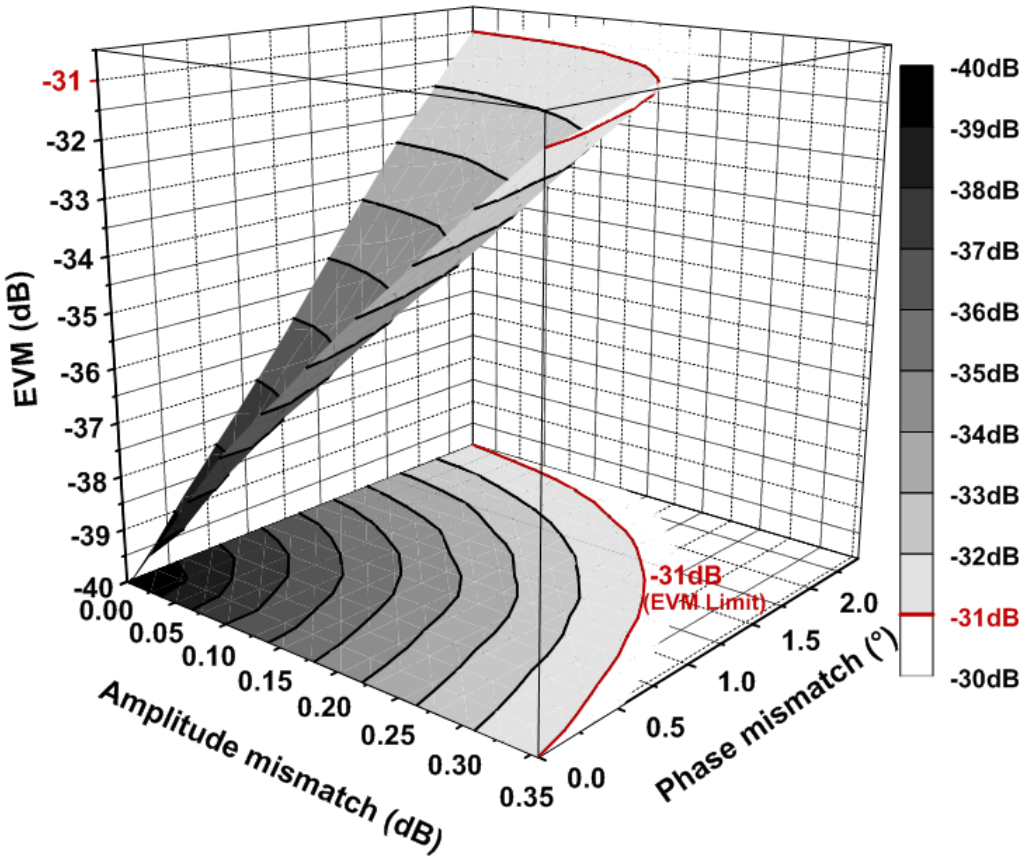

Figure 12. EVM with path mismatches in the LINC system with a 7MHz 64QAM WiMAX signal.

To satisfy the EVM requirement of the 64-QAM WiMAX system, the amplitude and phase mismatches should be less than a 0.37 dB and a 2.45°, respectively, when only one type of mismatch exists. In reality, both types of mismatches coexist, further restricting the mismatch requirement. Overcoming the linearity degradation due to path mismatch effects, mismatch detection, and mismatch compensation methods are required.

3.3 CONVENTIONAL MISMATCH CANCELLATION TECHNIQUES

To compensate the linearity degradation due to the amplitude mismatched of LINC transmitter, conventional mismatch calibration algorithms use additional bias control block as shown in Figure 13. Because the output power of the PA is proportional to its drain bias, by decreasing the drain DC bias of the PA which has higher output power between the two PAs in LINC system, the two outputs of the PAs can have the same value. However, this method requires additional bias-control blocks such as DC-DC converter of low drop output regulator.

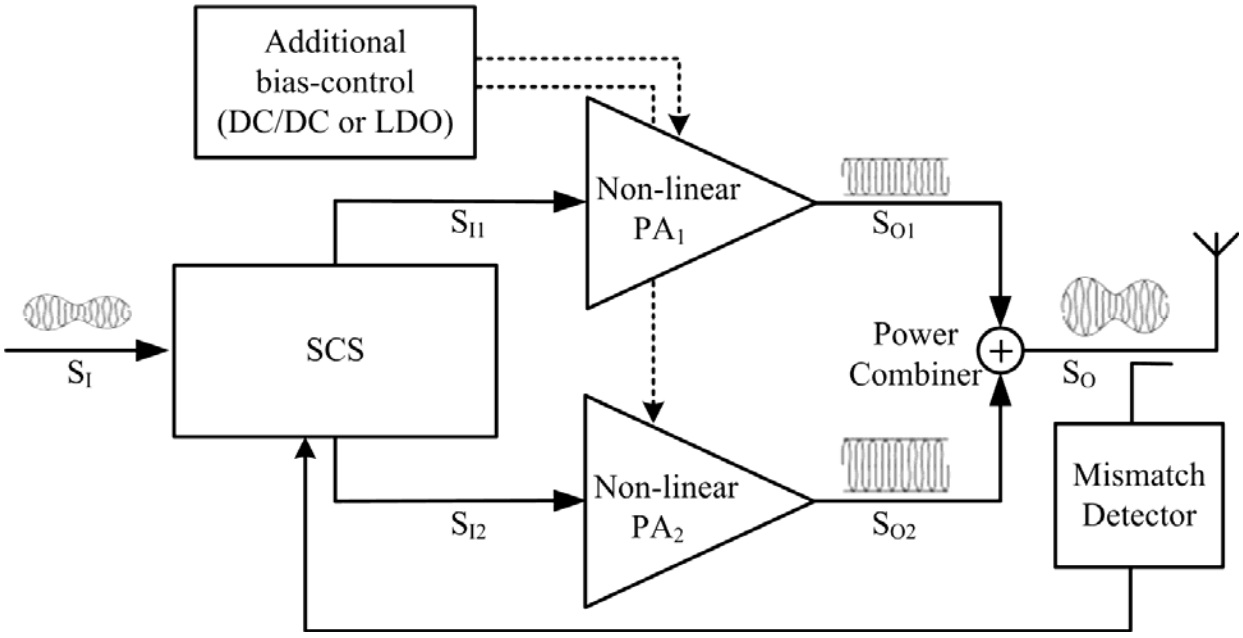

Figure 13. Conventional Mismatch Calibration Structure.

3.4 UNBALANCED MISMATCH CALIBRATION ALGORITHMS

3.4.1 Overal Structure

The linearity of the LINC system can be improved by calibrating the mismatches in the two RF paths (S1 and S2). In a conventional calibration technique, the amplitude mismatches can be calibrated using additional power supply blocks for amplitude control such as DC/DC converters or LDOs. However, these additional blocks consume additional power and increase system costs [26], [27]. In addition, when the bias is controlled to control the output power of nonlinear PAs, the mismatch parameters could be unintentionally changed because of the AM/AM and AM/PM characteristics of the PA [28]. Therefore, iterations are required to measure and correct the varying mismatches due to changing bias.

Figure 14 illustrates the overall structure of the proposed LINC system using the proposed calibration technique.

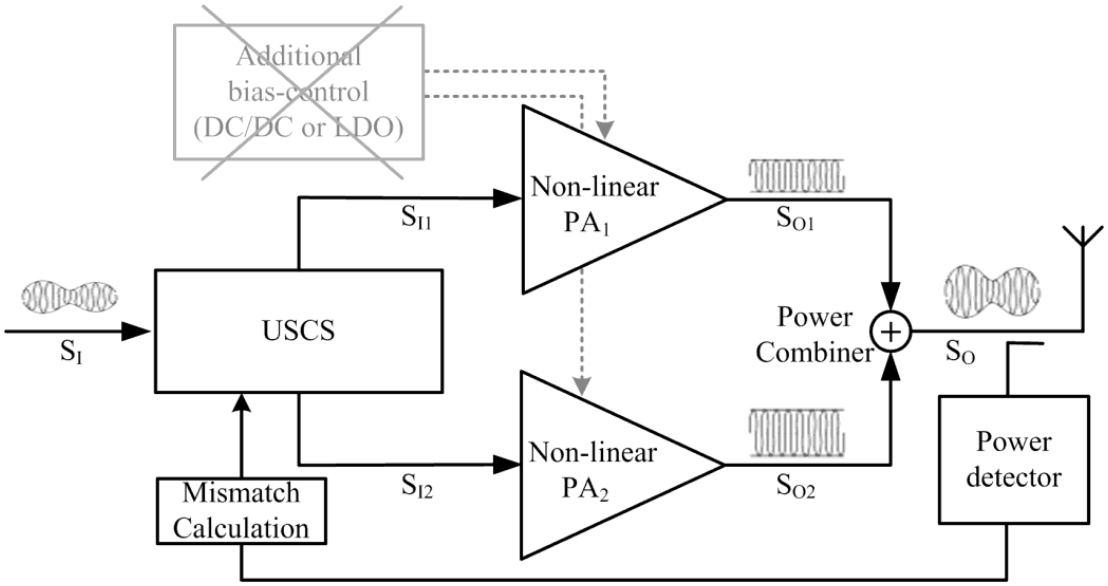

Figure 14. The overall structure of the proposed LINC system.

Without additional amplitude control blocks, the proposed LINC system compensates for both phase and amplitude mismatches using the unbalanced signal component separator (USCS), which generates unbalanced phase signals. Only an additional power detector is used for the mismatch detection. Figure 15 depicts the overall flowchart of the proposed calibration technique, which is composed of the proposed mismatch detection and the proposed mismatch correction.

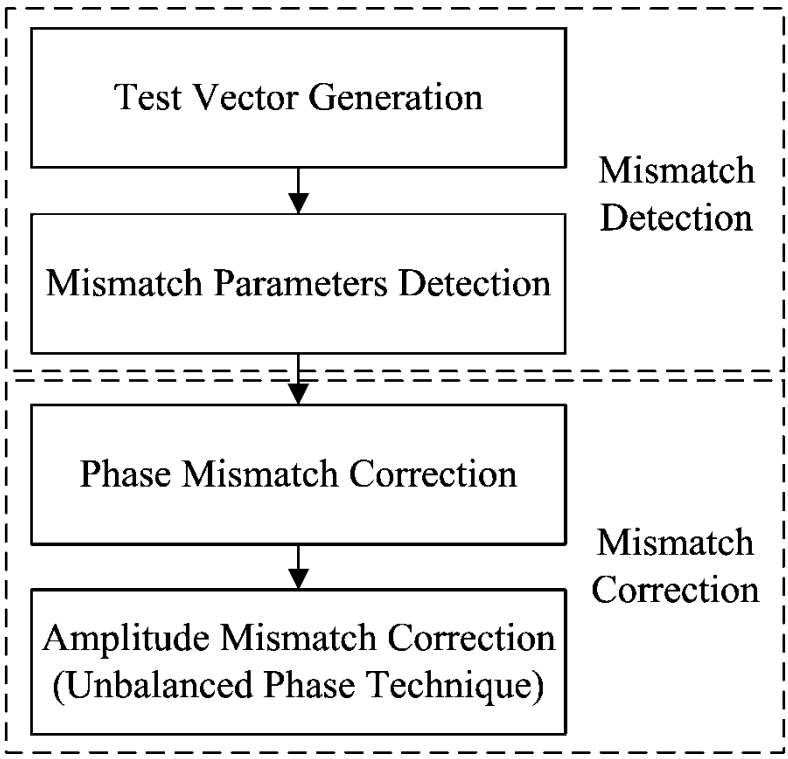

Figure 15. The overall flowchart of proposed calibration system.

To detect the mismatches, the proposed calibration technique uses phase-only test vector signals. Using a closed-form equation with the test vector signals, the mismatch detection algorithm can detect mismatch parameters that are used in the proposed mismatch correction. With the mismatch parameters, the proposed mismatch correction algorithm calibrates both phase and amplitude mismatches with phase-only controls. The detailed operation of the proposed mismatch detection and mismatch correction techniques are explained in the following sections.

3.4.2 Proposed Mismatch Detection Technique

Compared to several other mismatch detection techniques, the mismatch detection algorithm using test vector signals can reduce detection time by decreasing the number of iterations. Even though the test vector methods decrease the number of iterations, if the system requires the output power change of the PAs, it still requires time- and power-consuming iterative steps that result from the AM/AM and AM/PM distortions of the PA. To avoid the AM/AM and AM/PM distortions of the PAs, the proposed calibration does not change the output power of the PAs in either the mismatch detection or the mismatch correction procedures. In the proposed mismatch detection, mismatch parameters that will be used in the mismatch correction are detected using the five test vector signals. To detect the magnitude of the amplitude mismatch and the phase mismatch, the output powers of a power combiner are measured for the three test vector signals that are shown in Figure 16(a)-(c).

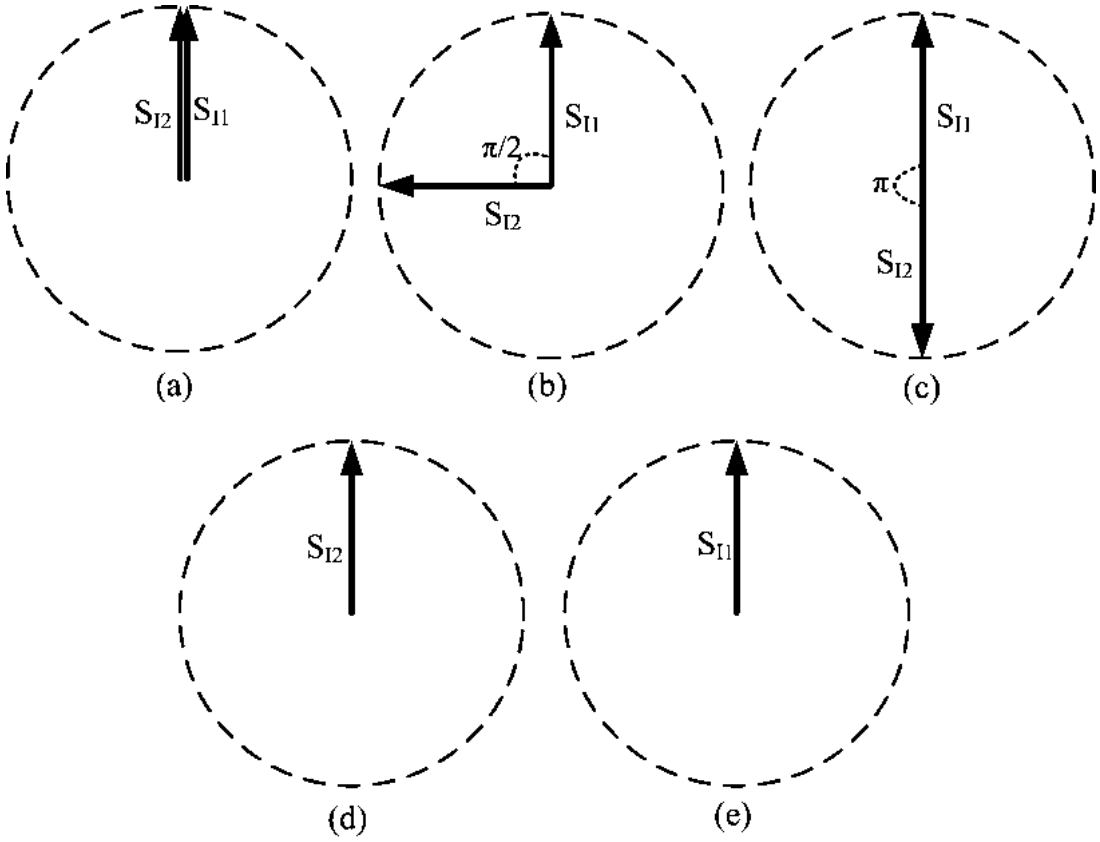

Figure 16. Test vector signals for mismatch detection.

When a phase mismatch of Δθ and an amplitude mismatch of Δα occur, the output of the LINC system can be expressed as the sum of (7) and (8) as

$$S_O(\theta_1,\theta_2) = \alpha\angle(\theta_1) + (\alpha+\Delta\alpha)\angle(\theta_2+\Delta\theta). \tag{3.3}$$

From (33), the LINC system outputs for the first three input test vector signals can be expressed as follows:

$$S_O(0,0) = \alpha\angle(0) + (\alpha+\Delta\alpha)\angle(0+\Delta\theta), \tag{3.4}$$

$$S_O(0,\frac{\pi}{2}) = \alpha\angle(0) + (\alpha+\Delta\alpha)\angle(\frac{\pi}{2}+\Delta\theta), \tag{3.5}$$

$$S_O(0,\pi) = \alpha\angle(0) + (\alpha+\Delta\alpha)\angle(\pi+\Delta\theta). \tag{3.6}$$

From the cosine law, the output powers of the test vectors can be expressed as

$$\begin{aligned} \left|S_O(0,0)\right|^2 &= \alpha^2 + (\alpha+\Delta\alpha)^2 - 2\cdot\alpha\cdot(\alpha+\Delta\alpha)\cdot\cos(\pi-\Delta\theta) \\ &= \alpha^2 + (\alpha+\Delta\alpha)^2 + 2\cdot\alpha\cdot(\alpha+\Delta\alpha)\cdot\cos(\Delta\theta) = A, \end{aligned} \tag{3.7}$$

$$\begin{aligned} \left|S_O(0,\pi/2)\right|^2 &= \alpha^2 + (\alpha+\Delta\alpha)^2 - 2\cdot\alpha\cdot(\alpha+\Delta\alpha)\cdot\cos(\pi-\frac{\pi}{2}-\Delta\theta) \\ &= \alpha^2 + (\alpha+\Delta\alpha)^2 + 2\cdot\alpha\cdot(\alpha+\Delta\alpha)\cdot\sin(\Delta\theta) = B, \end{aligned} \tag{3.8}$$

$$\begin{aligned} \left|S_O(0,\pi)\right|^2 &= \alpha^2 + (\alpha+\Delta\alpha)^2 - 2\cdot\alpha\cdot(\alpha+\Delta\alpha)\cdot\cos(\pi-\pi-\Delta\theta) \\ &= \alpha^2 + (\alpha+\Delta\alpha)^2 - 2\cdot\alpha\cdot(\alpha+\Delta\alpha)\cdot\cos(\Delta\theta) = C \end{aligned}. \tag{3.9}$$

From the measured output powers of the test vector signals in a power detector, a parameter D can be derived as follows:

$$A + C = 2\cdot(\alpha^2 + (\alpha+\Delta\alpha)^2) = D. \tag{3.10}$$

From (3.8) and (3.10), we can derive,

$$\sin(\Delta\theta) = \frac{2 \cdot B - D}{4 \cdot \alpha \cdot (\alpha + \Delta\alpha)}, \tag{3.11}$$

and from (3.7) and (3.9), we can derive

$$\cos(\Delta\theta) = \frac{A - C}{4 \cdot \alpha \cdot (\alpha + \Delta\alpha)}. \tag{3.12}$$

The tangent of the phase mismatch can be determined from (3.11) and (3.12) as follows

$$\tan(\Delta\theta) = \frac{\sin(\Delta\theta)}{\cos(\Delta\theta)} = \frac{2 \cdot B - D}{A - C}. \tag{3.13}$$

Finally, the phase mismatch can be determined from (3.13) as follows:

$$\Delta\theta = \tan^{-1}\left(\frac{2 \cdot B - D}{A - C}\right). \tag{3.14}$$

Likewise, from (3.7), (3.9), (3.10), and (3.14), the absolute values of the amplitude mismatch, |Δα|, and the maximum output signal amplitude, |SO|MAX, can be calculated as

$$\left|\Delta\alpha\right| = \sqrt{\{(\alpha + \Delta\alpha) - \Delta\alpha\}^2} = \sqrt{\frac{D}{2} - \frac{A - C}{2 \cdot \cos(\Delta\theta)}}, \tag{3.15}$$

$$|S_O|_{MAX} = 2\alpha + \Delta\alpha = \sqrt{\frac{D}{2} + \frac{A - C}{2 \cdot \cos(\Delta\theta)}}. \tag{3.16}$$

By comparing the measured output power of each PA without supplying an RF input for the other PA, the sign of the amplitude mismatch can be determined, which can be measured using the two test vectors in Figure 9(d)-(e). When the output power using the fourth test vector is greater than that using the fifth test vector, the amplitude mismatch has a negative value. Otherwise, the amplitude mismatch has a positive value.

3.4.3 Proposed Mismatch Correction Technique

After detecting amplitude and phase mismatches with the proposed mismatch detection technique, the proposed mismatch correction technique calibrates both amplitude and phase mismatches without the amplitude controls of the PAs. Figure 17 illustrates the flowchart of the proposed unbalanced phase calibration.

The first step of mismatch correction is phase mismatch calibration. Because the nonlinear PA has a linear phase characteristic, the phase mismatch can be compensated by phase mismatch cancellation by deducting the phase mismatch within the proposed USCS block [29].

When the original two phase outputs of USCS are θ1, θ2, the two outputs of USCS can be expressed as follows:

$$S_{I1} = c\angle\theta_1 = c\angle(\phi - \varphi_1), \tag{3.17}$$

$$S_{I2} = c\angle(\theta_2 - \Delta\theta) = c\angle(\phi - \varphi_2 - \Delta\theta). \tag{3.18}$$

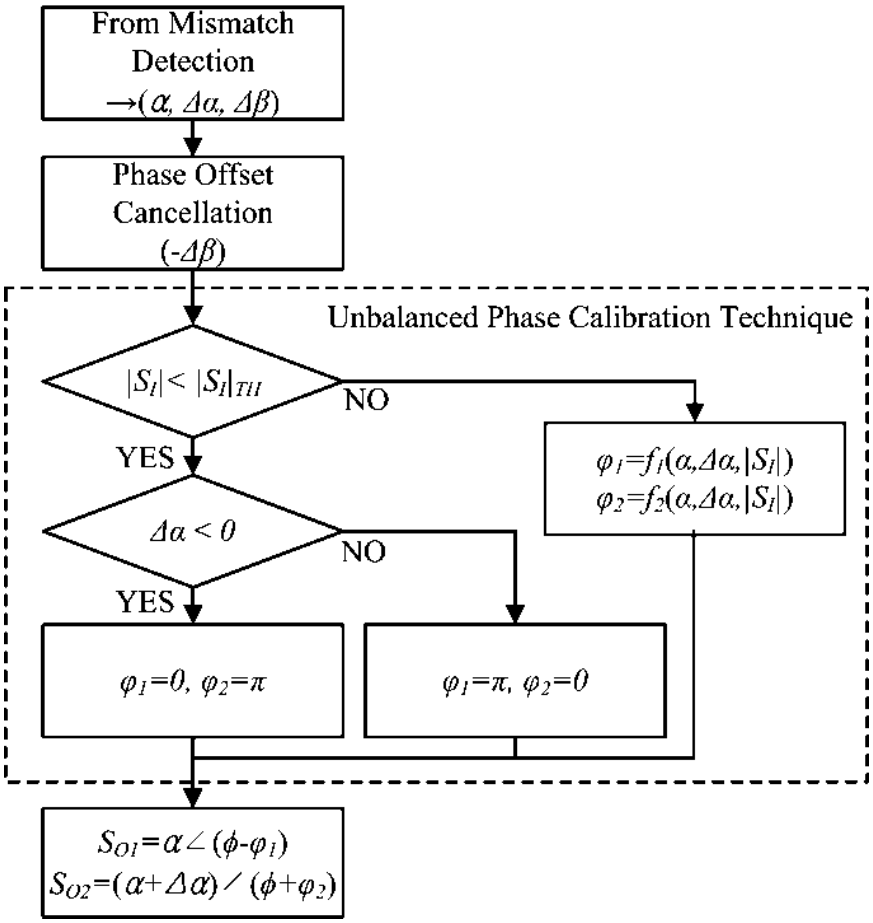

Figure 17. Flowchart of the proposed mismatch correction technique.

These two phase modulated outputs of USCS are connected to the switching PAs and the outputs of the PAs can be expressed as follows.

$$S_{O1} = \alpha\angle(\phi - \varphi_1), \tag{3.19}$$

$$S_{O2} = (\alpha + \Delta\alpha)\angle(\phi + \varphi_2). \tag{3.20}$$

After the phase mismatch cancellation, the next step is amplitude mismatch cancellation using the unbalanced phase calibration technique. The basic concept of the

unbalanced calibration system is to use unbalanced φ1 and φ2 to compensate for an amplitude mismatch; however, the conventional LINC system defines φ1 and φ2 as the same values.

Because the two vector signals have an amplitude difference of $|\Delta\alpha|$, the proposed system, however, cannot generate output powers that are less than $|\Delta\alpha|$. To minimize the linearity degradation from this limitation, the proposed unbalanced calibration system has two different operational modes: the unbalanced mode and the minimum output mode, as shown in Figure 18. Figure 18(a) shows the first mode operation of the proposed system when the output signal amplitude, $|S_O|$, exceeds the amplitude mismatch, $|\Delta\alpha|$. This condition also indicates that the input signal amplitude, $|S_I|$, is larger than the threshold level, $|S_I|_{TH}=|S_I|_{MAX} \cdot|\Delta\alpha|/(2\alpha+\Delta\alpha)$, which was calculated in the previous mismatch detection step. In this case, the proposed USCS generates two phase signals, φ_1 and φ_2, determined via the cosine law as follows.

$$\varphi_1 = \cos^{-1}\left(\frac{(2\alpha+\Delta\alpha)^2|S_I|^2 + 4c^2\left\{(\alpha+\Delta\alpha)^2-\alpha^2\right\}}{8c^2\cdot(2\alpha+\Delta\alpha)^2|S_I|\cdot(\alpha+\Delta\alpha)}\right), \tag{3.21}$$

$$\varphi_2 = \cos^{-1}\left(\frac{(2\alpha+\Delta\alpha)^2|S_I|^2 + 4c^2\left\{\alpha^2-(\alpha+\Delta\alpha)^2\right\}}{8c^2\cdot(2\alpha+\Delta\alpha)^2|S_I|\cdot\alpha}\right). \tag{3.22}$$

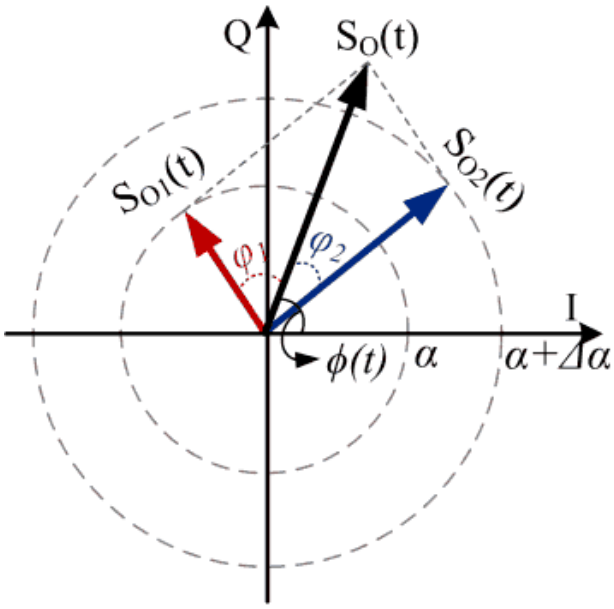

(a)

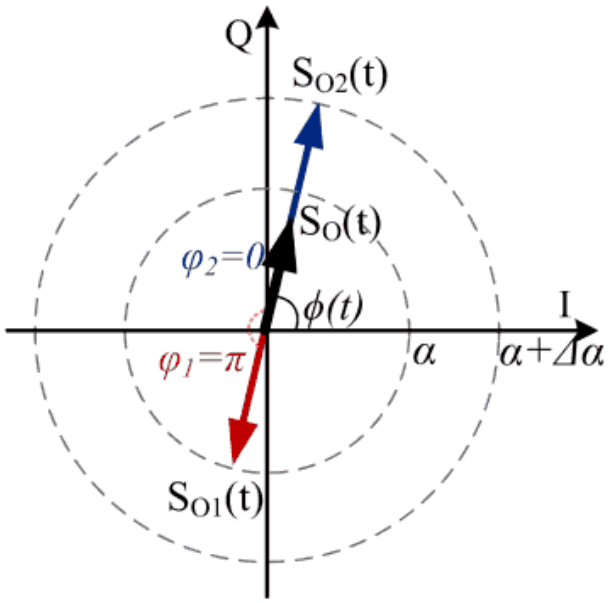

(b)

Figure 18. Two modes of the proposed unbalanced phase calibration: (a) when the signal output (S_O) is bigger than an amplitude mismatch ($\Delta\alpha$); (b) when the signal output (S_O) is smaller than an amplitude mismatch ($\Delta\alpha$).

The operation of the proposed USCS in the second mode is shown in Figure 18(b). When the amplitude of an input signal is smaller than the threshold level, $|S_I|_{TH}$, the system output should be smaller than the amplitude mismatch, $|\Delta\alpha|$. To maximize the linearity performance of the proposed LINC system, amplitude and phase distortions have to be minimized [30]. In the second mode, an amplitude distortion is minimized, using USCS to generate φ_1 and φ_2 in opposite directions. Then, a phase distortion is eliminated by ensuring that the output phase of USCS follows the input phase, ϕ, by generating a phase output of ϕ to the one path of the LINC system that has larger amplitude and generating a phase output of $\phi+\pi$ to the other path. Therefore, when the amplitude mismatch, $\Delta\alpha$, has a negative value, USCS assigns φ_1 to 0, and φ_2 to π, and in the other case, when the amplitude mismatch, $\Delta\alpha$, has a positive value, the USCS assigns φ_1 to π, and φ_2 to 0.

3.5 IMPLEMENTATION OF THE PROPOSED LINC SYSTEM

To prove the effectiveness of the proposed mismatch calibration technique, a LINC system is built with the proposed mismatch detection and correction methods. Figure 19 illustrates a block diagram of the LINC system.

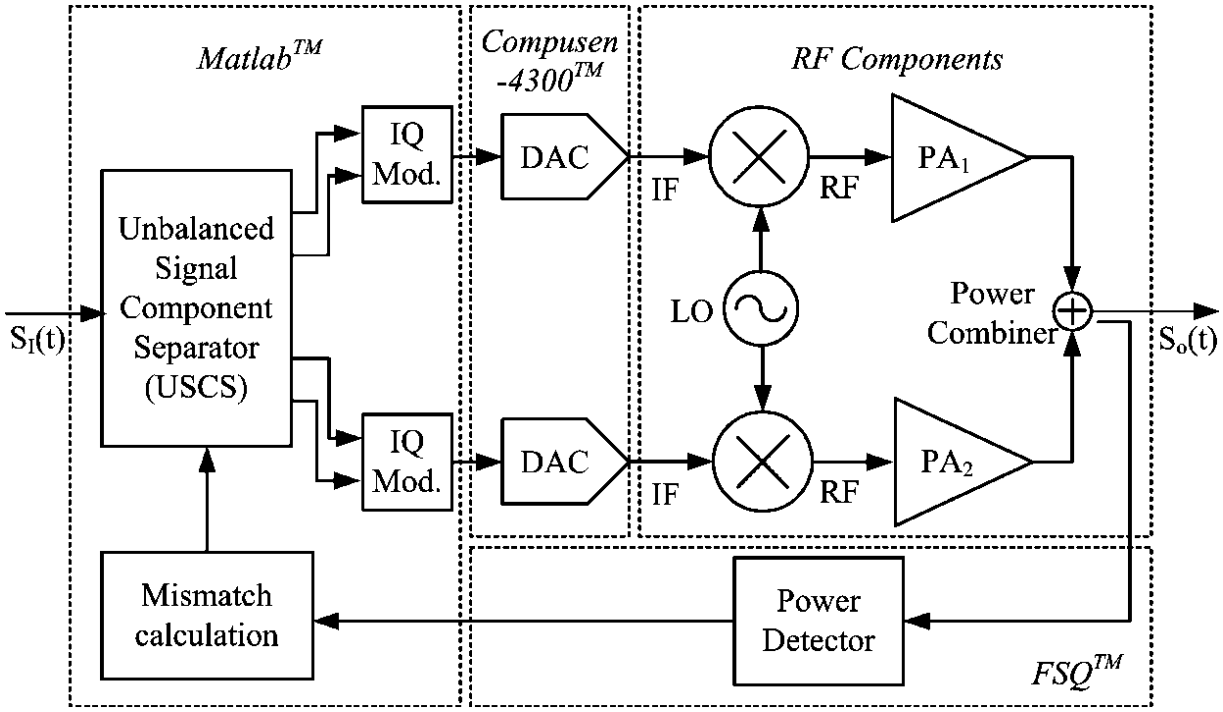

Figure 19. Experiment setup of proposed LINC system.

To minimize the effects of IQ mismatches, a digital intermediate frequency (IF) LINC modulator is employed [31]. The USCS block and IQ modulator blocks are implemented with Matlab™. The USCS generates two digital phase outputs, which are

digitally modulated to IF frequency IQ signals. The digital IF frequency signal is converted to a 30MHz IF frequency analog signal with 100MHz sampling in a DAC board (a Gage Compusen 4300) controlled by Matlab^{TM}.

The two outputs of the DAC board are up-converted to 670MHz RF signals using a 640MHz local oscillator (SMU 200ATM) and off-chip mixers (ZX05-42MH). The up-converted RF signals are sent to the two switching PAs as the two RF input signals of the LINC system.

To implement the high-efficiency, nonlinear PA class-E switching PAs are fabricated in a standard 0.18-μm CMOS process. The schematic diagram of the PA is shown in Figure 20.

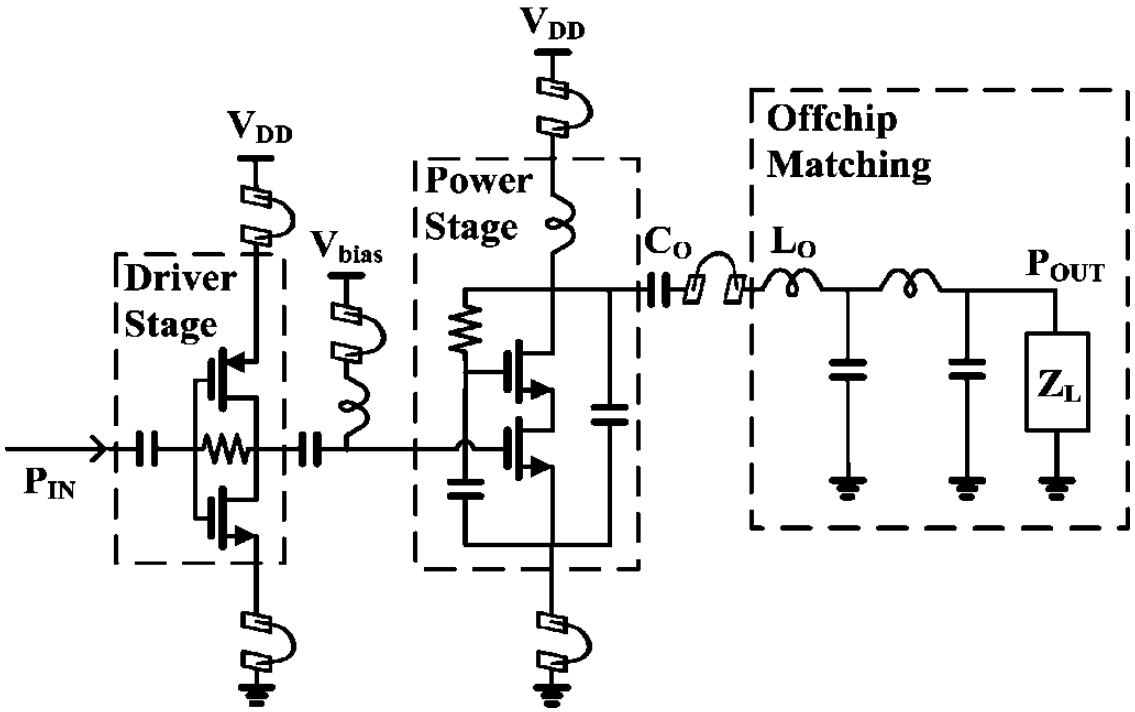

Figure 20. Schematic diagram of a fabricated Class-E CMOS power amplifier.

The PA consists of a driver stage and a power stage, and its external output matching circuits are designed to operate at 550~750 MHz. The power stage operates on a 3.3V supply, and the thick oxide cascode structure with a self-bias scheme is used to prevent a gate oxide breakdown in a high voltage operation. A chip die-photo is shown in Figure 21 and the die area is 1450 μm × 850 μm.

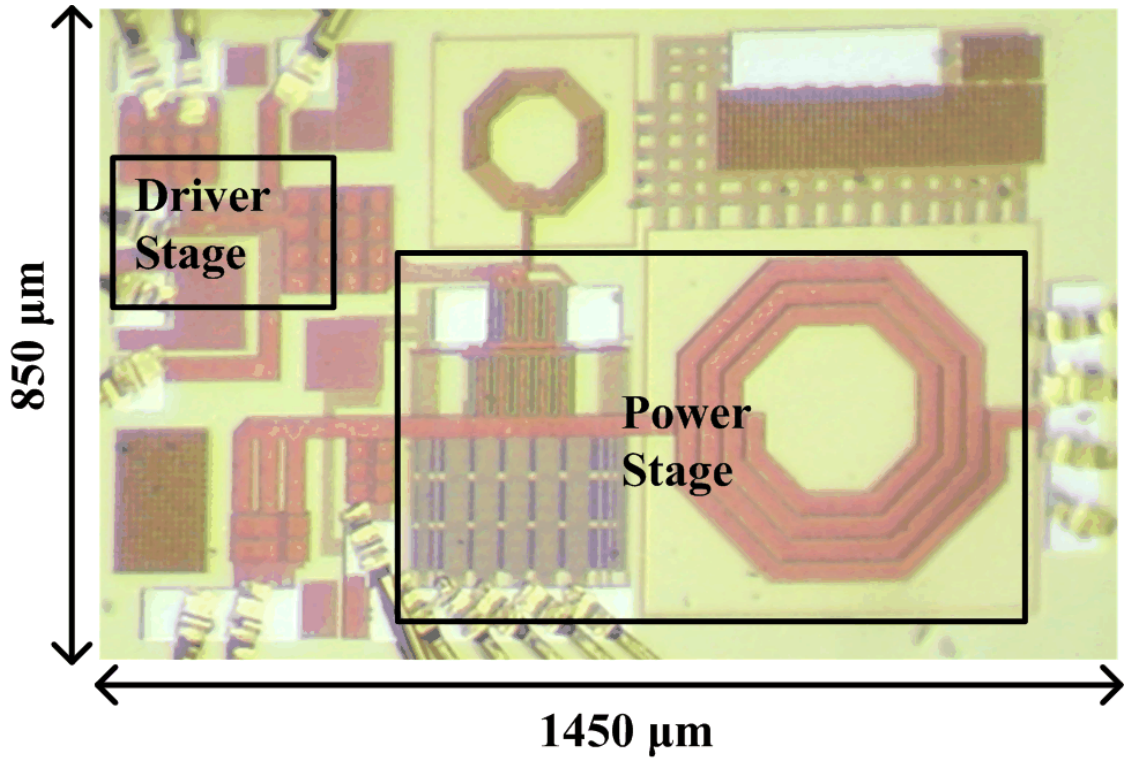

Figure 21. Die-photograph of fabricated Class-E CMOS power amplifier.

The measurement results of the PA are shown in Figure 22. The maximum output power of the PA at the input level of 0dBm is 21.15dBm with a power-added efficiency (PAE) of 45% at 670 MHz.

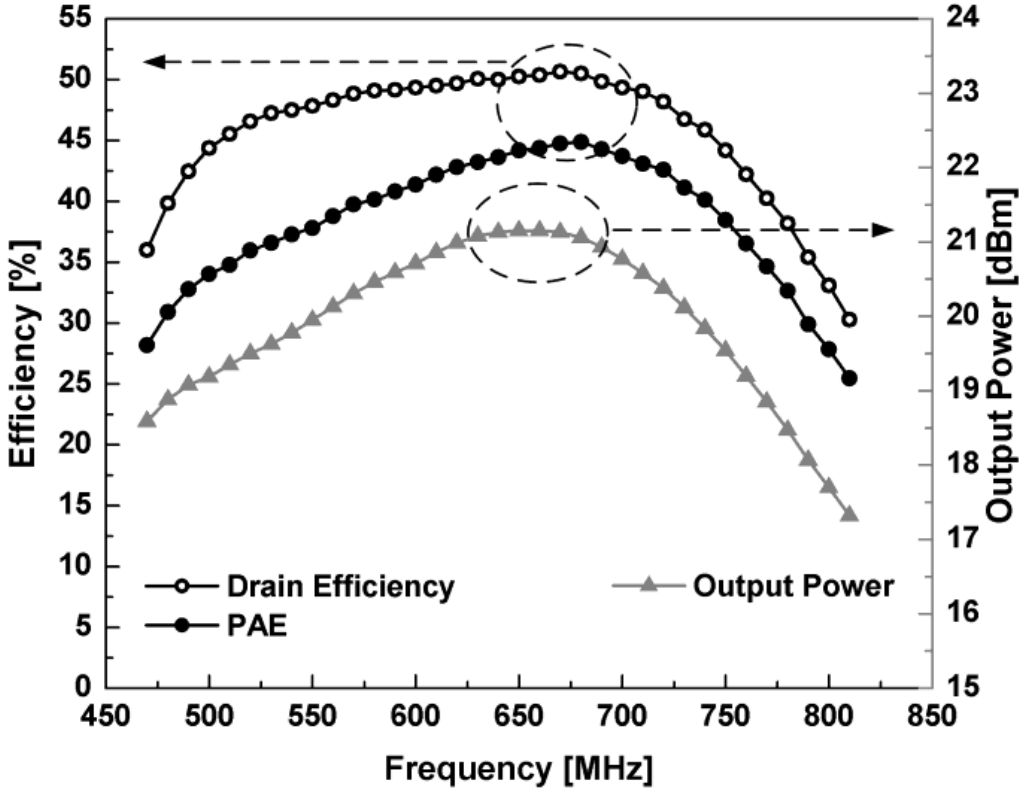

Figure 22. Measurement results of a Class-E CMOS power amplifier.

The outputs of the two PAs are combined with an isolated power combiner (a Walenton D6163-102™), and a spectrum analyzer (FSQ 26™) was used to detect the output power of the combiner. The proposed LINC system sends the output power values to Matlab™ directly via an Ethernet port to calculate the mismatch parameters, which are automatically adapted to the proposed mismatch calibration technique in Matlab™. To evaluate the linearity performance, the EVM and the spectrum mask are also measured by an FSQ 26™. All the sequences are automatically controlled by Matlab™ code. The photo diagram of the system configuration is shown in Figure 23.

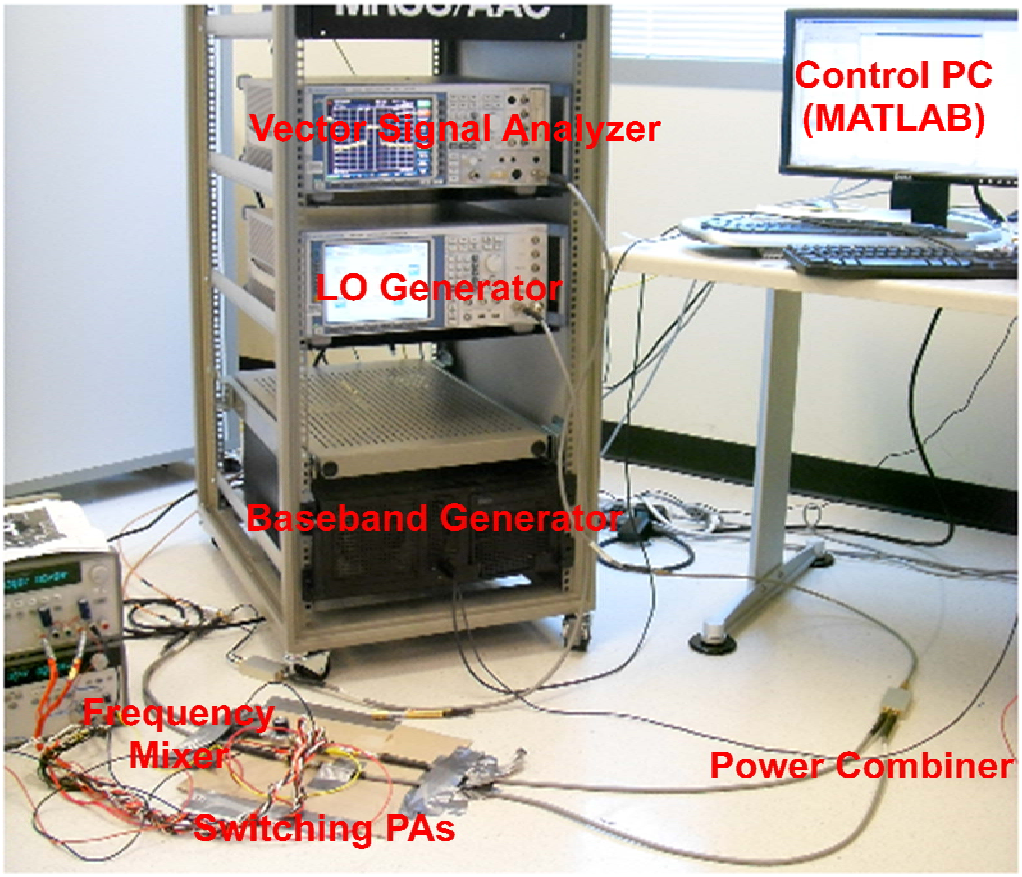

Figure 23. Photo of the System Configuration

3.6 EXPERIMENTAL RESULTS

3.6.1 The Spectrum Mask and the Constellation

The feasibility and performance of the proposed LINC system were determined using the 64-QAM OFDM signals with a channel bandwidth of 7 MHz in the UHF band. Using the proposed mismatch detection technique, a phase mismatch of 6.4° and an amplitude mismatch of 1.12 dB are detected. After the proposed mismatch detection technique, the proposed unbalanced mismatch correction technique was automatically applied. Figure 24 shows the constellation and spectrum masks before and after the proposed mismatch technique.

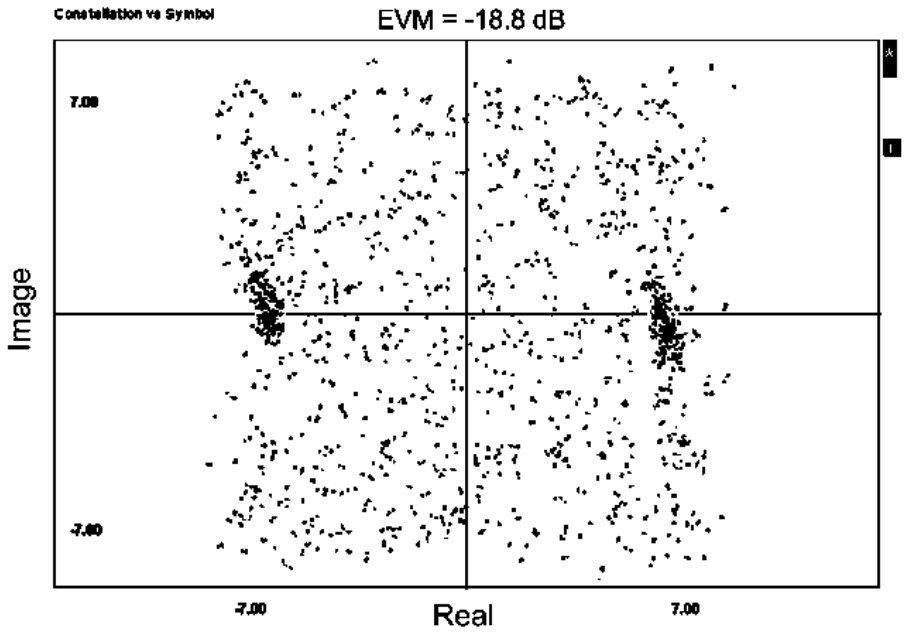

(a)

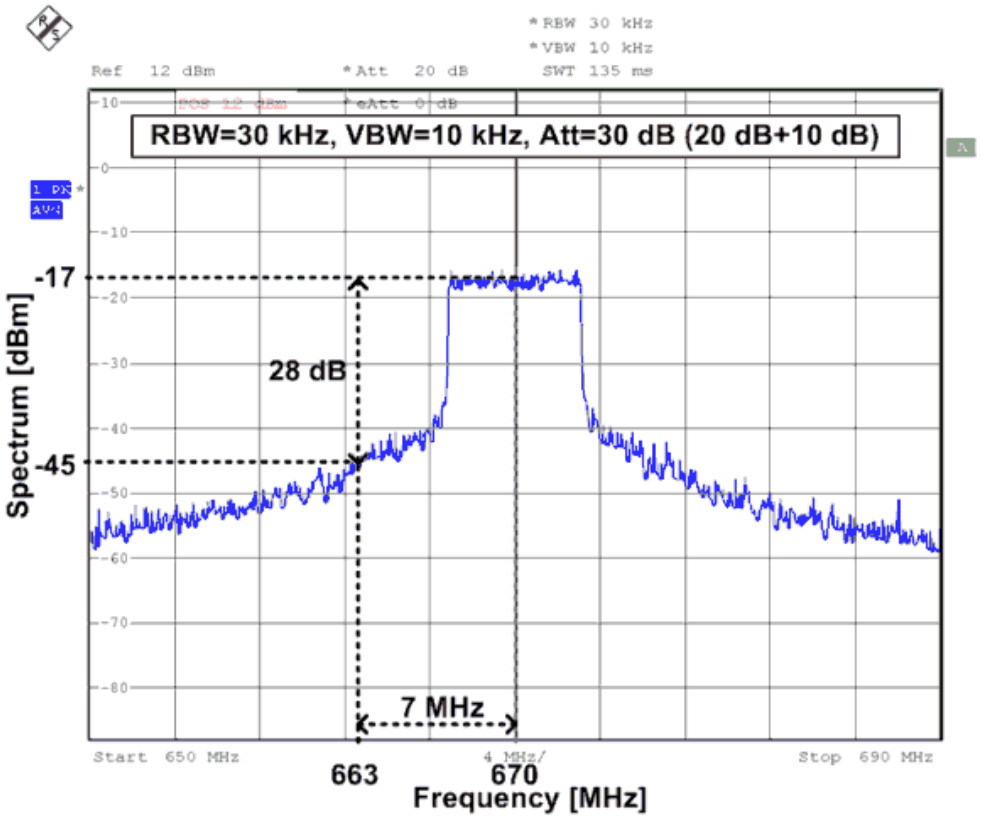
*RBW 30 kHz
*VBW 10 kHz
Ref 12 dBm
*Att 20 dB
SWT 135 ms
RBW=30 kHz, VBW=10 kHz, Att=30 dB (20 dB+10 dB)
-17
-45
28 dB
7 MHz
Spectrum [dBm]
Start 650 MHz
4 MHz/
Stop 690 MHz
663
670
Frequency [MHz]

(b)

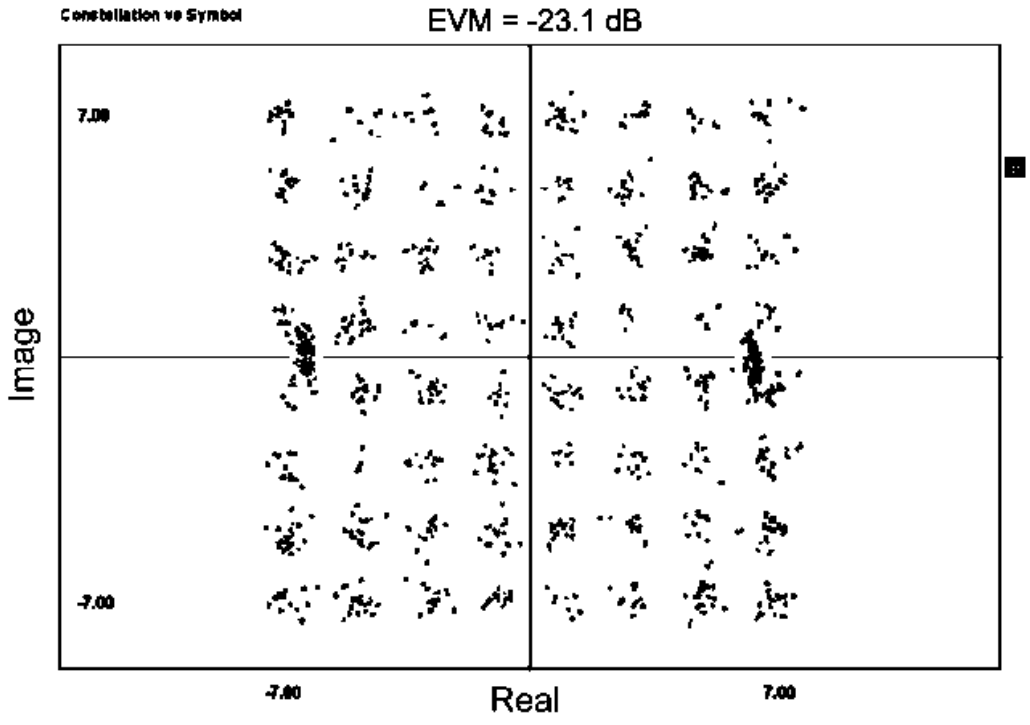
Constellation vs Symbol
EVM = -23.1 dB
7.00
-7.00
Image
-7.00
Real
7.00

(c)

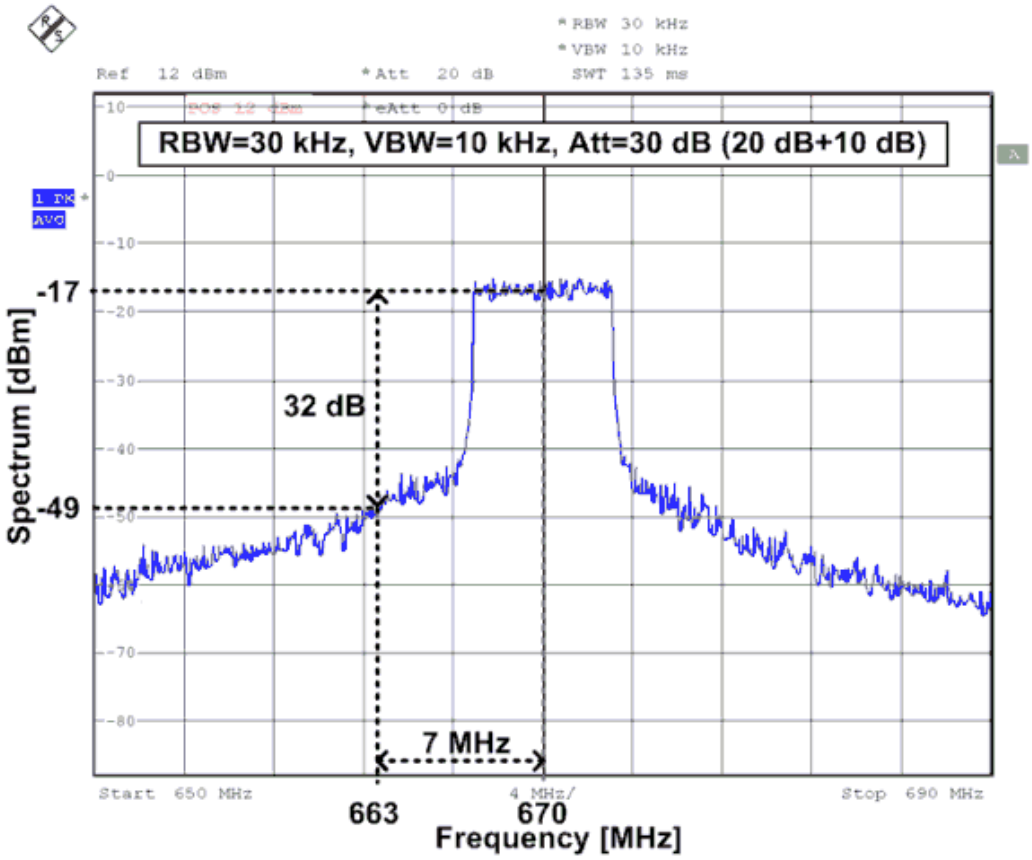
*RBW 30 kHz
*VBW 10 kHz
Ref 12 dBm
*Att 20 dB
SWT 135 ms
RBW=30 kHz, VBW=10 kHz, Att=30 dB (20 dB+10 dB)
1 PK
AVG
-17
-49
32 dB
7 MHz
Spectrum [dBm]
Start 650 MHz
4 MHz/
Stop 690 MHz
663
670
Frequency [MHz]

(d)

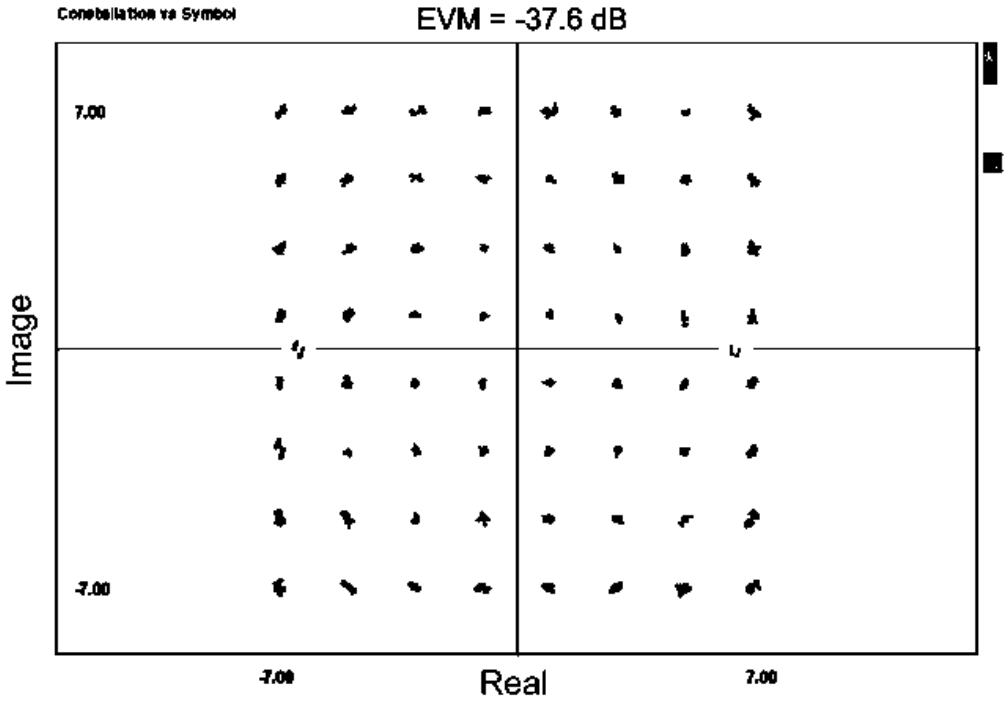
Constellation vs Symbol
EVM = -37.6 dB
7.00
-7.00
Image
-7.00
Real
7.00

(e)

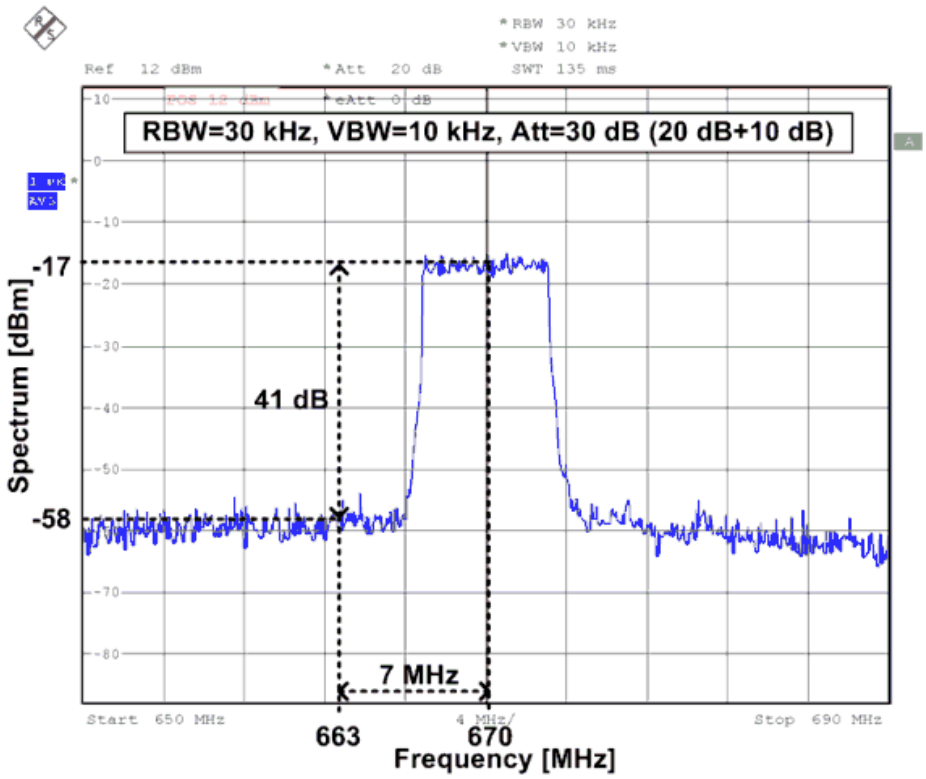

(f)

Figure 24. Measured 64-QAM constellations and spectrum mask: (a, b) before the calibration, (c, d) after the phase mismatch calibration, and (e, f) after the proposed unbalanced phase calibration.

Figure 24(a) shows the constellation before calibration, and Figure 24(c) shows the constellation after phase mismatch calibration. The error vector magnitude (EVM) values improved from -18.8 dB to -23.1 dB, but it was still far from complying with the WiMAX standard specification of -31 dB. However, after adapting the proposed unbalanced phase calibration, the EVM improved to -37.6dB, and the measured EVM values satisfied the WiMAX standard specification, shown in Figure 24(e). Figure 24 also illustrates the spectrum mask. With phase offset cancellation, the adjacent channel power ratio (ACPR) at 7 MHz improved from -28 dBc to -32 dBc, as shown in Figure

24(b) and Figure 24(d). After the proposed unbalanced phase calibration technique, the ACPR finally improved to -41dBc, as shown in Figure 24(f).

3.6.2 The Maximum Tolerance of the Amplitude Mismatch

The EVM values are related to both the amplitude and phase distortions. Although the proposed calibration technique reduces the amplitude distortion in the case of $|S_O|<|\Delta\alpha|$ by assigning opposite phases in the USCS, some amplitude distortions were still observed. As the amplitude mismatch increases, the EVM degrades further. The sensitivity of the proposed calibration regarding the amplitude mismatch was measured using the EVM for 7 MHz WiMAX OFDM signals. To vary the degree of amplitude mismatches, an external adjustable attenuator is used in one of the two paths of the LINC system. The measured results are shown in Figure 25 and Figure 26.

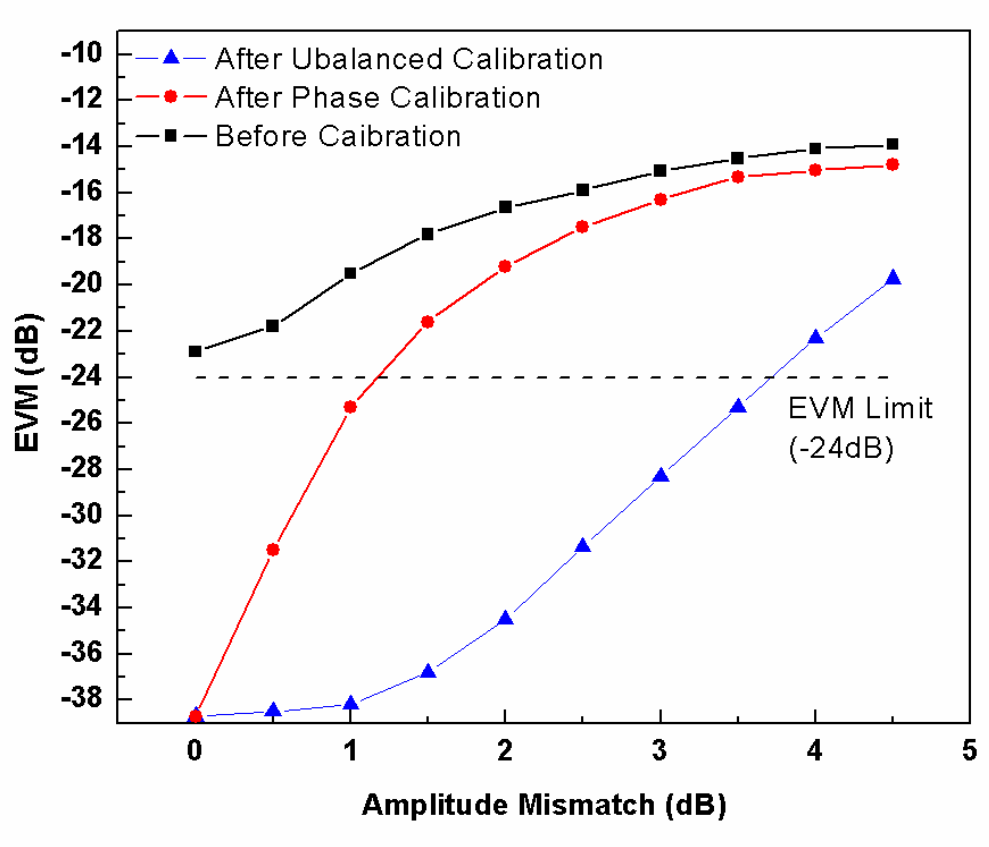

Figure 25. Measured EVM vs. amplitude mismatch for the 64-QAM WiMAX system.

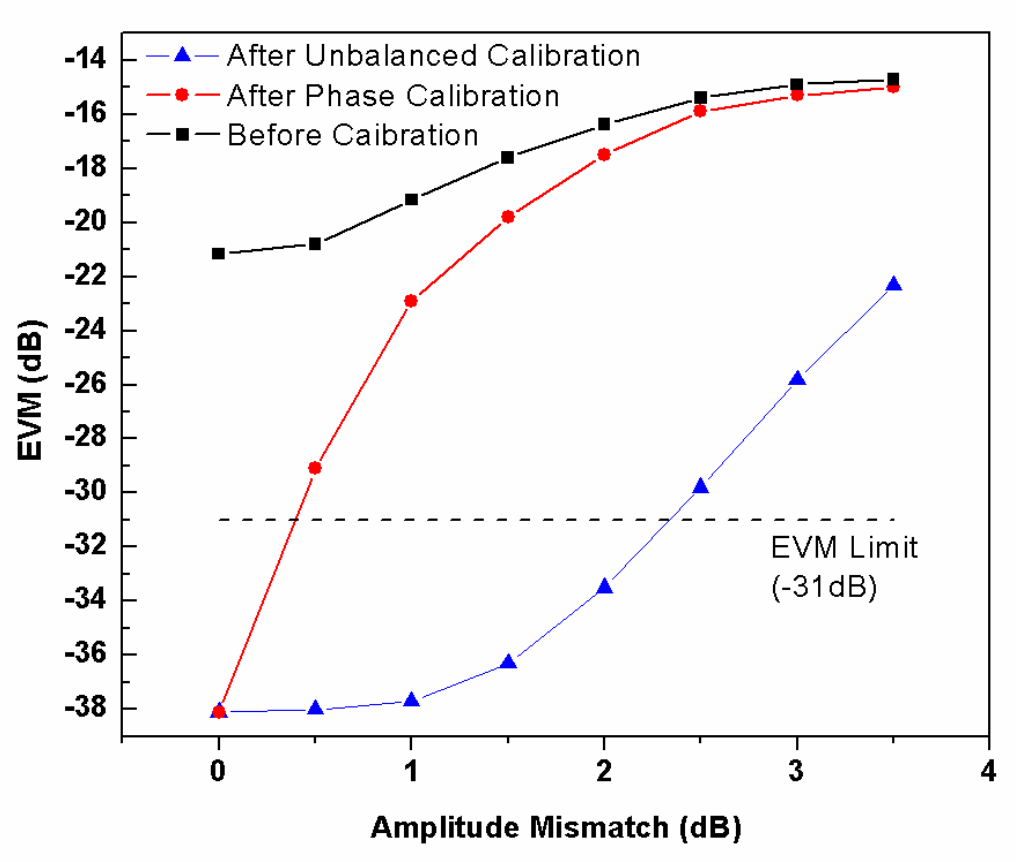

Figure 26. Measured EVM vs. amplitude mismatch for the 16-QAM WiMAX system.

As shown in Figure 25, without the proposed unbalanced phase calibration, the EVM specification of the 64-QAM WiMAX system cannot be satisfied with a 0.5dB amplitude mismatch, even if no phase mismatch occurs. For a 16-QAM WiMAX system, the EVM specification cannot be satisfied with a 1.2 dB amplitude mismatch without the proposed calibration as shown in Figure 26. However, after applying the proposed unbalanced phase calibration technique, the EVM specification of the 64-QAM WiMAX system (-31 dB) is satisfied with a 2.35 dB amplitude mismatch, and the EVM specification of the 16-QAM WiMAX system (-24 dB) with a 3.8 dB amplitude mismatch.

3.7 CONCLUSIONS

In this chapter, we proposed a novel mismatch calibration technique and designed and evaluated a LINC system based on the technique. The proposed technique easily detected both amplitude and phase mismatches using only five test vector signals and calibrated both amplitude and phase mismatches between the switching PAs without additional amplitude mismatch compensation blocks such as a DC/DC converter or an LDO. Because the proposed LINC system does not change the output powers of the PAs, it does not require iterations due to AM/AM and AM/PM distortions in the PA. Experimental measurements have been performed using 16-QAM and 64-QAM OFDM modulated signals with a 7 MHz bandwidth. With the proposed LINC system, overall linearity significantly improved without any iteration or any additional amplitude control block of the PA. Regarding to the measurement results, the proposed calibration technique satisfied EVM requirements with a 3.8dB amplitude mismatch for the 16-QAM WiMAX and 2.35dB for the 64-QAM WiMAX.

CHAPTER 4

HIGHLY EFFICIENT MULTI-LEVEL LINC ARCHITECTURES

4.1 INTRODUCTION

Recently, orthogonal frequency division multiplexing (OFDM) is frequently employed because of its good spectrum efficiency and robustness against inter-symbol interference (ISI) and multi-path fading. The high peak-to-average power ratio (PAPR) of the OFDM system, however, requires a highly linear amplifier. A linear power amplifier (PA) with high back-off can achieve linear amplification, but it yields very low power efficiency.

For example, when using ideal components, the average efficiency of a Class A linear amplifier can be written as shown below [32].

$$\bar{\eta}_{CLASS\ A} = mean\left(0.5 \times \frac{P_{out}}{P_{max}}\right) = 0.5 \times \frac{1}{PAPR(SYSTEM)} \tag{4.1}$$

Although the LINC architecture, which separates a non-constant envelope input signal into two constant envelope signals, is highly efficient, by using two highly efficient nonlinear PAs, the overall efficiency of the transmitter is not drastically improved, because, when the two different signals are added together, the power of the out-phased factors of signals is wasted. Even if, the efficiency of nonlinear PA in the LILNC system is 100%, the average system efficiency of the conventional LINC amplifier can be

expressed as (4.2), because the out-phase terms are waited in power combiner . With the assumption of the efficiency of an ideal class E amplifier to be 100%, the average system efficiency of the conventional LINC amplifier can be expressed as (4.2) [33].

$$\bar{\eta}_{LINC} = mean\left(\frac{P_{out}}{P_{dc}}\right) = \frac{1}{PAPR(SYSTEM)} \tag{4.2}$$

where P_{dc} is the power summed of $|GS_1|$ and $|GS_2|$ and P_{out} is in the power of S_{out}. Based on (4.2), the efficiency of the conventional LINC system is only twice that of the class A amplifier.

In this section, the two efficiency improvement technique of Multi-level LINC (MLINC) transmitter and Uneven Multi-level LINC (UMLINC) transmitter are presented. These new structures have good efficiency by adopting a switched power supply and also demonstrate good linearity with the use of digital phase offset cancellation.

4.2 MULTI-LEVEL LINC (MLINC) USING A DYNAMIC POWER SUPPLY

4.2.1 Basic Principle of MLINC

Figure 27 illustrates the overall structure of the Multi-level LINC (MLINC).

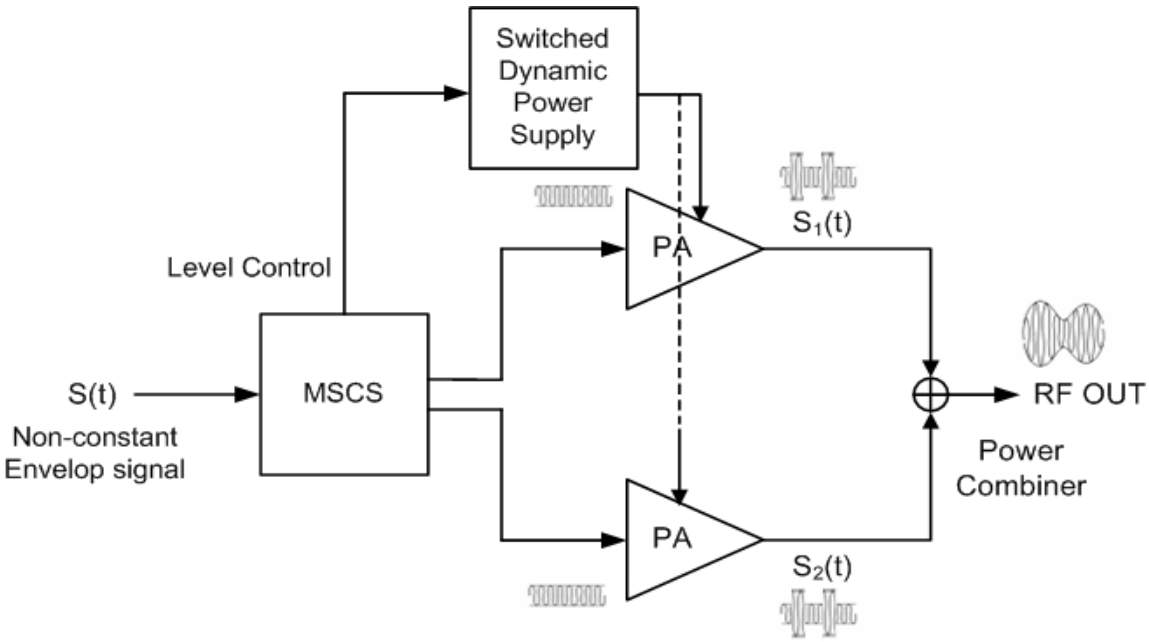

Figure 27 Overall Structure of MLINC

MLINC system consists of a Multi-level Signal Component Separator (MSCS), a switched dynamic power supply, high efficiency switching PAs, and an isolated power combiner. The MSCS generates two RF phase signals that are fed to the PAs. The MSCS also generates a level control used by the fast and high-efficient switched dynamic power supply to change the supply voltage of the PAs. To prevent linearity problems associated with a non-isolated combiner, MLINC used an isolated combiner, whose efficiency is

maximized when both inputs are in phase. Thus, the number of maximum efficiency points of an MLINC equals the number of levels of the power supply, n.

A non-constant envelope signal such as OFDM can be represented as a polar form such as

$$S(t) = r(t)\angle \Phi(t) \tag{4.3}$$

This signal can be separated into two signals, S_1 and S_2, whose magnitudes are constant with the maximum value of the envelope of S(t), r_{max}, as shown in Figure 28(a). This separation can be expressed using the conventional LINC equations as below [34].

$$S_1(t) = S(t) + e(t) \tag{4.4}$$

$$S_2(t) = S(t) - e(t) \tag{4.5}$$

where

$$e(t) = jS(t)\sqrt{\frac{{r_{max}}^2}{|S(t)|^2} - 1} \tag{4.6}$$

These two signals are separately amplified with two nonlinear PAs and their outputs are combined, thus cancelling the e(t) terms and yielding the desired OFDM signal as shown in (5).

$$S_{out}(t) = G \times S_1(t) + G \times S_2(t) = 2G \times S(t) \tag{4.7}$$

where G is the gain of nonlinear PA

In this method, e(t) terms are always wasted when combining as shown in (4.6).

However, by using smaller constant envelope signals such as r_{small} for the small vectors as shown in Figure 28(b) e(t) can be changed to e'(t) as shown in (4.7).

$$e'(t) = jS(t)\sqrt{\frac{r_{small}{}^2}{|S(t)|^2} - 1} \tag{4.7}$$

In this case, e'(t) which is smaller than e(t) is wasted at the same output. By reducing the redundant power, the power efficiency is improved.

Assuming the efficiency of switching amplifier and dynamic power supply is ideal, the efficiency of proposed level shifting LINC represented as

$$\bar{\eta}_{proposedLINC} = \left\{\frac{P_H}{PAPR(HIGH)} + \frac{P_L}{PAPR(LOW)}\right\} \tag{4.8}$$

where P_H is the probability of the high mode (when the symbol amplitude is bigger than r_{small}), and P_L is the probability of the low mode (when the symbol amplitude is smaller than r_{small}). The high mode PAPR(HIGH) becomes smaller than the overall system PAPR(SYSTEM) since the average power of symbols in the high mode is greater than that of the system. Moreover, the low mode PAPR(LOW) also becomes smaller than the overall system PAPR(SYSTEM) because the peak power of low mode symbols are smaller than the system's peak power. Therefore, the overall efficiency of the level shifting LINC is greatly improved than that of conventional LINC.

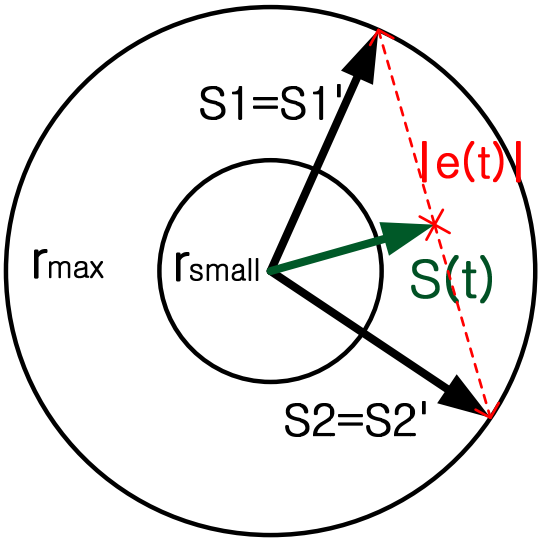

(a)

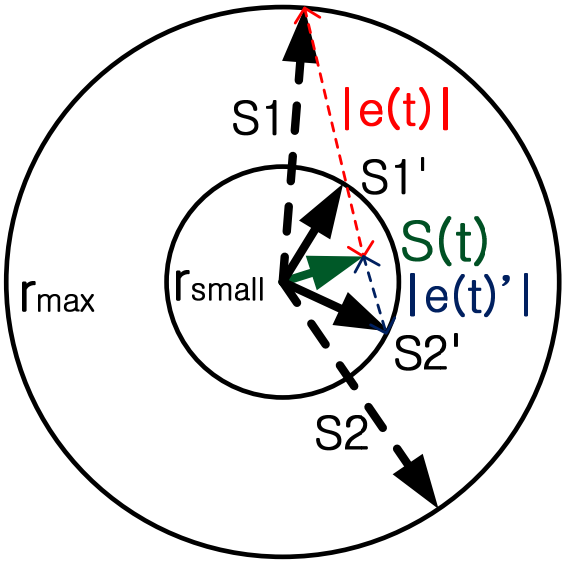

(b)

Figure 28 Level Shifting LINC Concept: (a)$|S(t)|>r_{small}$,(b)$|S(t)|\leq r_{small}$

4.2.2 Simulations and Comparison

To verify the efficiency improvement, Class A, conventional LINC, and proposed LINC amplifiers were designed utilizing ADS™ with standard 0.18um CMOS technology. To obtain more accurate results, packaging effects such as bond wires and pad capacitances were incorporated.

After getting the efficiency with ADS simulation, the total system efficiency was simulated with the data of 64-QAM 7MHz bandwidth WiMax OFDM system with MATLAB™.

Figure 29 is the schematic of the level shifting RF amplifier with the switched dynamic power supply.

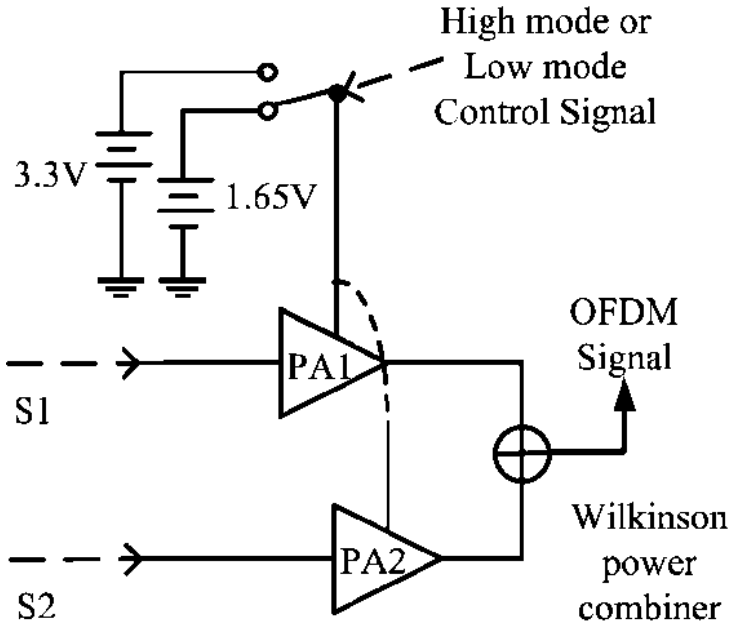

Figure 29. Switched dynamic power supply & Class E PAs

The switched dynamic power supply changes the supply voltage of the class E PAs from a high supply voltage to a low supply voltage according to the amplitude of the OFDM. The two inputs, S_1 and S_2, for the Class E PAs are provided by the digital phase modulator [35], which has the phase information corresponding to high and low modes. A Wilkinson power combiner sums the outputs of the PA to produce the desired OFDM signal.

The schematic diagram of dynamic power supply is shown in Figure 30. For the dynamic power supply design, a PMOS switch is used for high supply voltage to avoid threshold voltage drop and a NMOS switch is used for low supply voltage due to its higher mobility. Both of them are designed with thick-oxide MOSFET to avoid an oxide breakdown of the transistor.

The sizes of the switches are determined by considering the trade-off between the dynamic power supply's efficiency and chip area as shown in Figure 31.

In Figure 31, large width of switch makes the efficiency of dynamic power supply better because turn-on resistance of switch is inversely proportional to the switch width. An inverter chain is used at the input of the switch to provide delay for synchronization with the input signal phase.

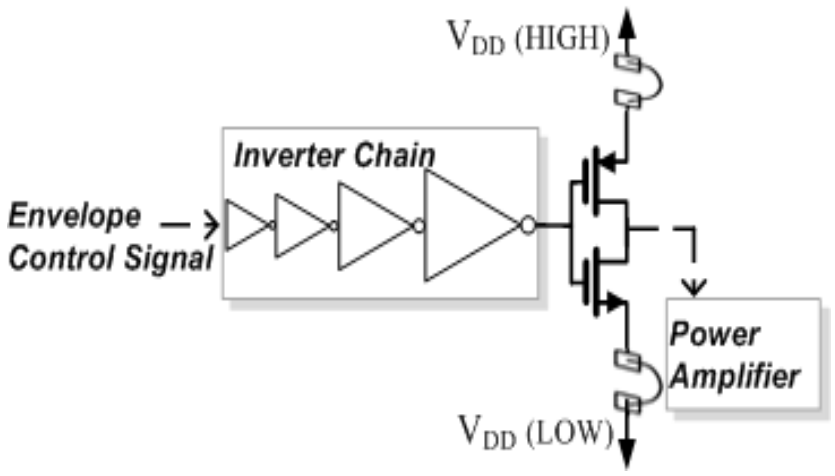

Figure 30. Schematic diagram of dynamic power supply

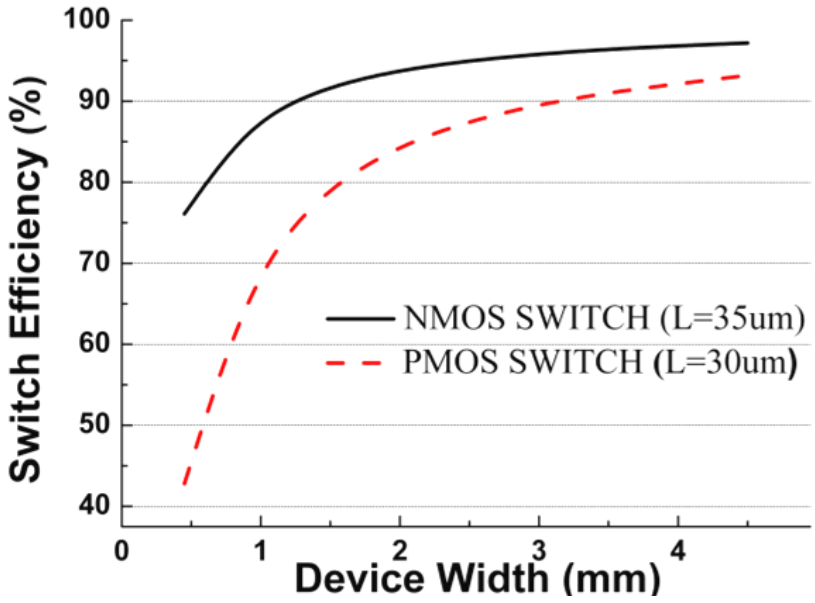

Figure 31. Efficiency of Dynamic power supply

The size and number of inverters are also considered for fast switch performance. The class E power amplifier is implemented with a cascode topology to overcome the breakdown issues of CMOS technology. The PAE was flat to 66% for both 3.3 V and

1.65 V voltage supply. For the output matching networks and Wilkinson power combiners, off-chip component models were employed in the simulation.

The simulation results of the three amplifier efficiencies are listed in Table 1, which are obtained using a 64-QAM WiMax OFDM system as the signal source. This particular system's PAPR of 7.45dB is used to calculate the theoretical efficiency values. The optimal level of high supply voltage and low supply voltage was decided by the probability density function of input signal and the optimum level of the low supply voltage was half of that of the high power supply voltage. And the percentage of low supply mode was nine times that of high supply mode. The simulation result is slightly smaller than the theoretical result due to non-ideal components of the amplifiers and switched dynamic power supply.

Table 1. Efficiencies of the Amplifiers

AMPLIFIERS	THEORETICAL	SIMULATION
Class A	9%	5.76%
LINC	18%	11.88%
Proposed LINC	38.6%	24.5%

4.2.3 Phase Offset Cancellation

4.2.3-A. AM-AM and AM-PM Distortion

AM-AM and AM-PM distortions are the envelope and phase differences between original signal and RF modulated signal. These differences introduce distortion due to the nonlinear relationship between input and output. In the proposed system, AM-AM and AM-PM distortions are calculated using a single tone phase input with changing the power supply voltage from high to low. Figure 32 shows the phase different with using deferent bias voltage.

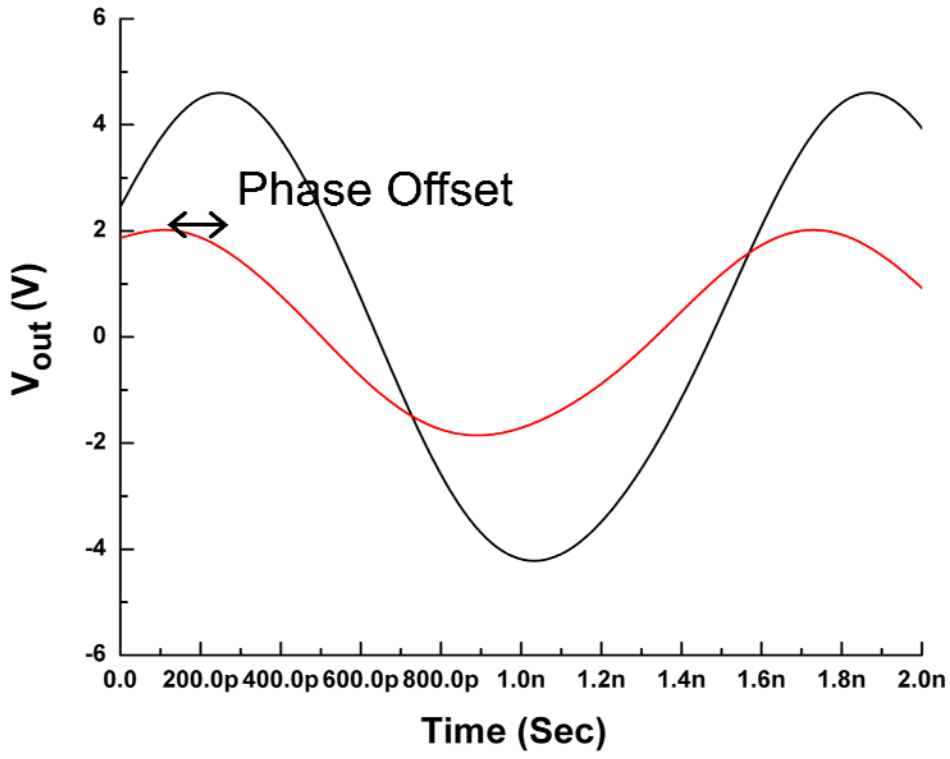

Figure 32 AM/PM phase offset

The AM-AM distortion in the designed PA is minimal because the turn-on resistance of the switch is small and supply voltages for both modes are high enough to operate the power transistor in saturation mode. However, the AM-PM distortion due to Miller capacitance of C_{gd} on CMOS PA cannot be ignored. This originates from the feed forward current through the large gate drain capacitor. When the drain bias is changed, the Miller feed forward capacitor is also changed, which introduces a phase difference according to the supply voltage.

4.2.3-B. Digital Phase Offset Cancellation

To compensate for the AM-PM distortion, digital phase offset cancellation is employed. The constant phase offset caused by the different power supply voltages is measured for a single tone input at multiple bias levels, and it is corrected by introducing a constant phase inverse offset to the digital signal component separator (SCS). The detailed functional block diagram is shown in Figure 33.

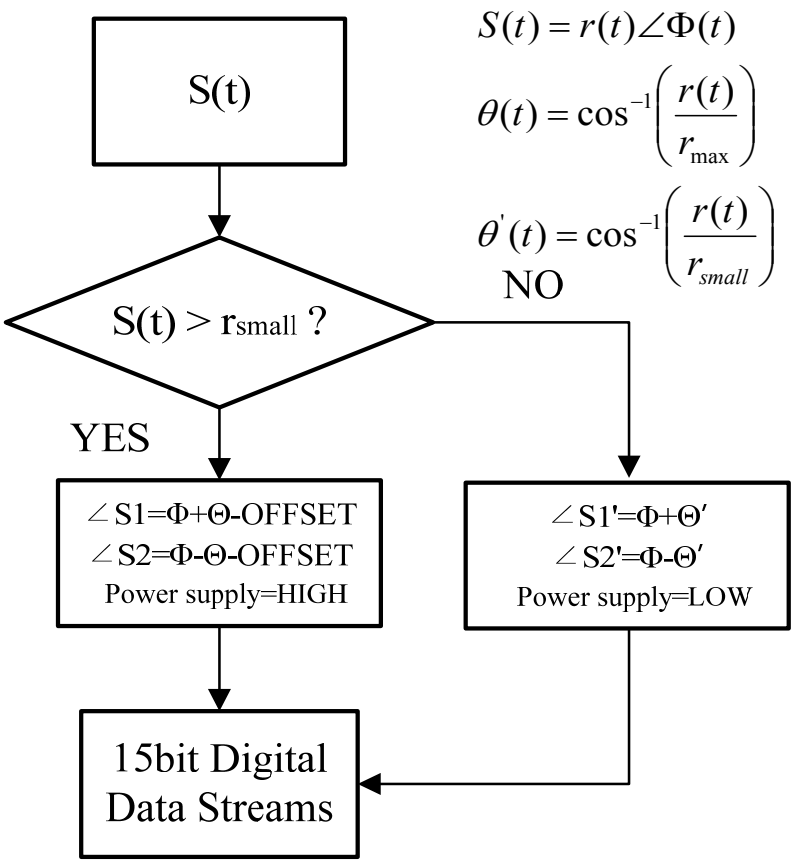

Figure 33. The flow chart of SCS with phase offset cancellation

First, the SCS compares the magnitude of the input signal with threshold level, r_{small}. The threshold level is optimized for the efficiency. The MATLAB simulation results for the threshold level using WiMAX 64QAM signal is shown in Figure 34. When the magnitude of the input signal is bigger than r_{small}, SCS changes the input signal to phase information of S1 and S2 corresponding to r_{max} and deducts the phase offset and sets the power supply control bit to the high. Otherwise, SCS adjusts the phase of S1 and S2 signals corresponding to r_{small}, and sets the supply control bit low.

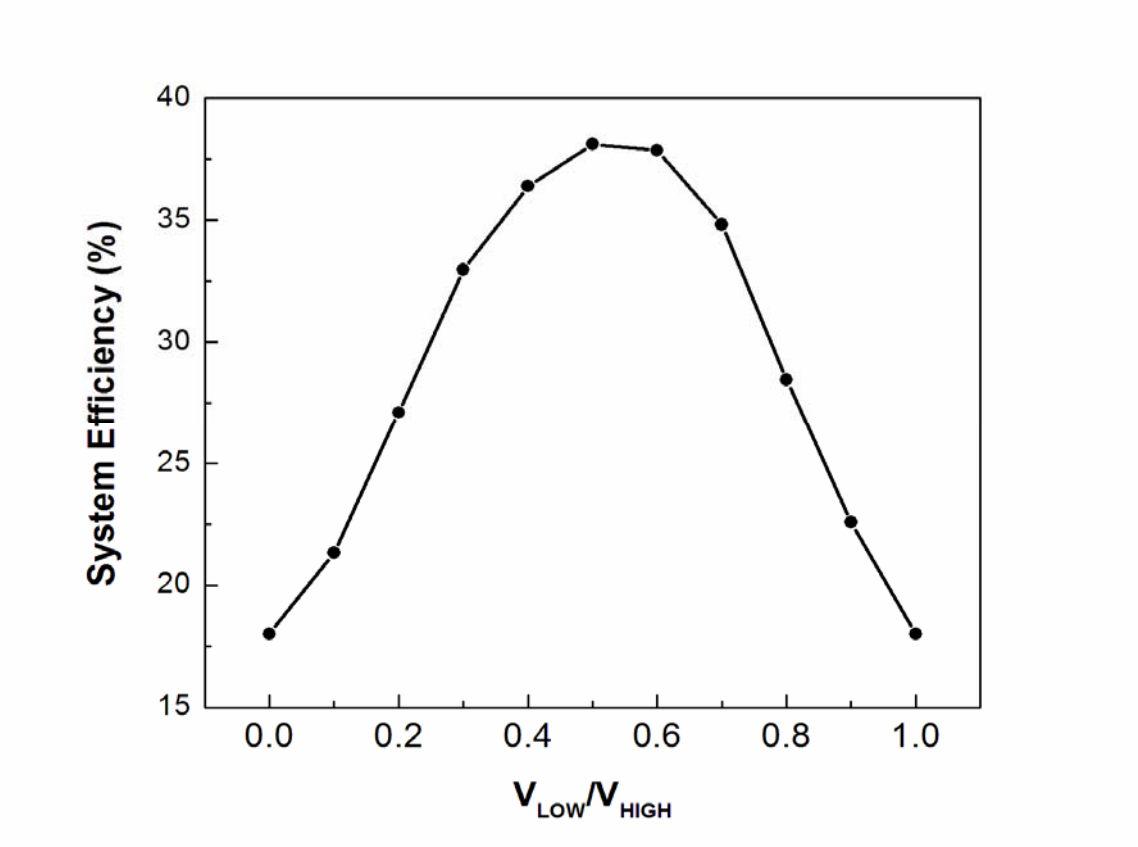

Figure 34. Simulation for the threshold level.

C. Simulations and Comparison

Figure 35 is the simulation setup for linearity measurement. To perform both baseband and RF circuit simulations together, digital and circuit co-simulation in ADSTM is utilized. For the digital base band design, the digital phase modulator is implemented considering all quantization error. Some digital modulation schemes, such as quadrature phase shift keying (QPSK) and quadrature amplitude modulation (QAM), have discrete phase values in modulated RF signals.

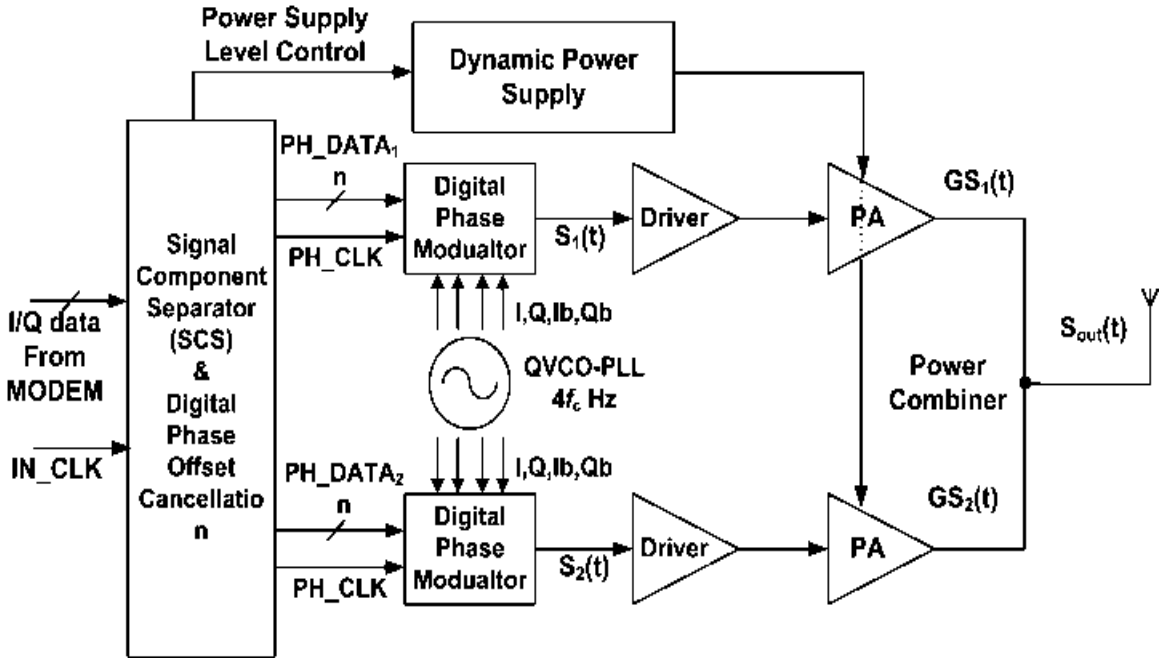

Figure 35. System simulation setup

However, modulators are often required to generate continuous phase values for oversampled baseband symbols or more complex modulation schemes. For example, in OFDM systems, as frequency-domain baseband data are converted to time-domain data by an inverse fast Fourier transform (IFFT), the phases of baseband symbols can be any values between -180° and +180°. To support such modulation schemes, the phase modulator must produce continuous phase values. Moreover, the out-phasing transmitter also requires fine phase tuning for mismatch compensation.

In the digital transmitter, each DPM modulates the clock signal according to a digital phase input, thus it has a finite resolution in phase. Phase quantization may degrade modulation accuracy, as measured by error vector magnitude (EVM) because the

finite resolution generates quantization noise at each phase angle of the out-phasing amplifier. Therefore, it is necessary to determine the minimum number of bits required for a given modulation scheme, which will ensure compliance with the appropriate specification. The relation between signal to noise ratio (SNR_q) and the word length of signal quantization has been well discussed in [36]. The SNR_q after a b_s-bit quantization is given by

$$SNR_q = 6.02 \cdot b_s + 1.76 - 20 \cdot \log_{10} k \text{ [dB]} \tag{4.9}$$

where b_s denotes the number of bits and k denotes the peak factor, the ratio of the peak amplitude to the mean amplitude of the signal.

Every additional bit in signal quantization increases SNR_q by 6.02 dB and its absolute value depends on the PAPR of the original signal. To avoid signal quality degradation due to quantization, the SNR_q should be larger than the SNR of the original signal. Therefore, the number of bits of a DPM, b_{DPM}, should be

$$b_{DPM} \geq \frac{SNR - 1.76 + PAPR}{6.02} \tag{4.10}$$

where both SNR and PAPR are from the original signal in dB before the phase quantization.

To evaluate the quantization effects on OFDM signals, the EVM values of IEEE 802.16e signals were tested with different phase resolution [37]. Figure 36 shows the simulation results. The original signal has the SNR of 40 dB before phase quantization.

From the graph, it is seen that the EVM decreases by 6 dB with an each additional bit until it reaches the original EVM value. Therefore, the DPM of the system must provide at least 5 and 6-bit phase resolution to meet required EVM limit of 16-QAM and 64-QAM, respectively, and 8-bits to avoid significant SNR degradation.

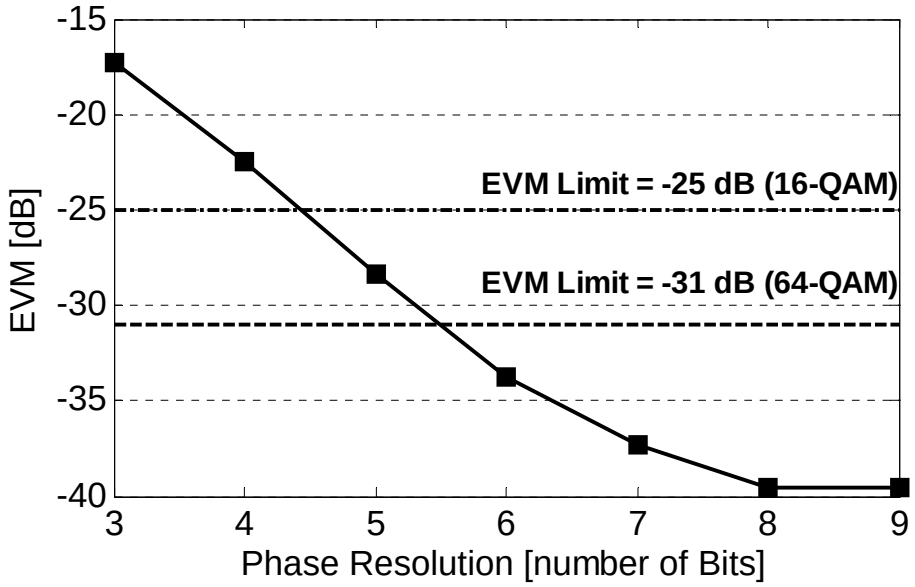

Figure 36. Effects of number of bits in DPM on IEEE 802.16e modulation

The RF circuits are designed in standard 0.18μm CMOS process. Figure 37(a) is the constellation before phase offset cancelation and Figure 37(b) is the constellation after phase offset cancellation. The error vector magnitude (EVM) values are improved from -26 dB to -30 dB with the use of digital phase offset cancellation. A 7 dB enhancement of the adjacent channel power ratio (ACPR) at 10 MHz offset is also observed in the spectrum mask in

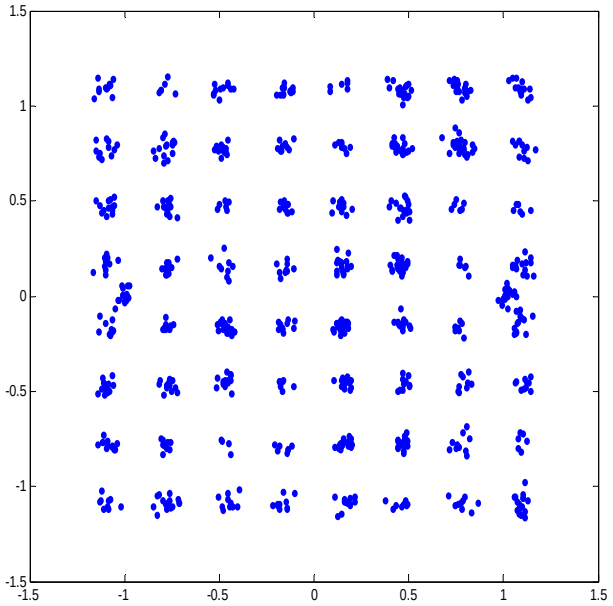

(a)

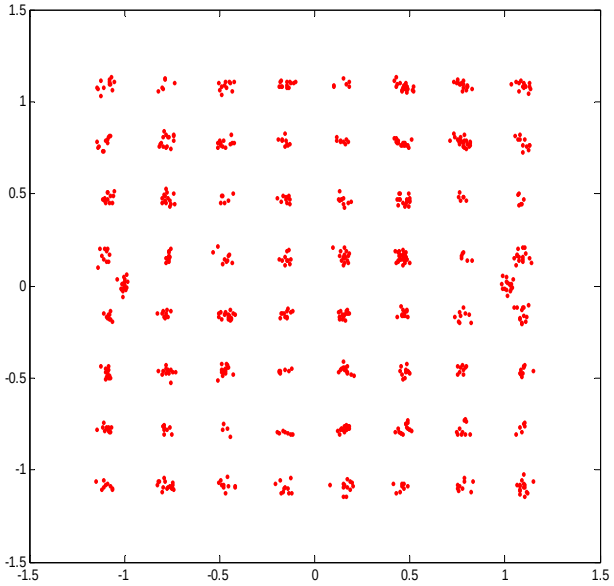

(b)

Figure 37. 64 QAM constellation: (a) Before Phase Offset Cancellation and (b) After Phase Offset Cancellation

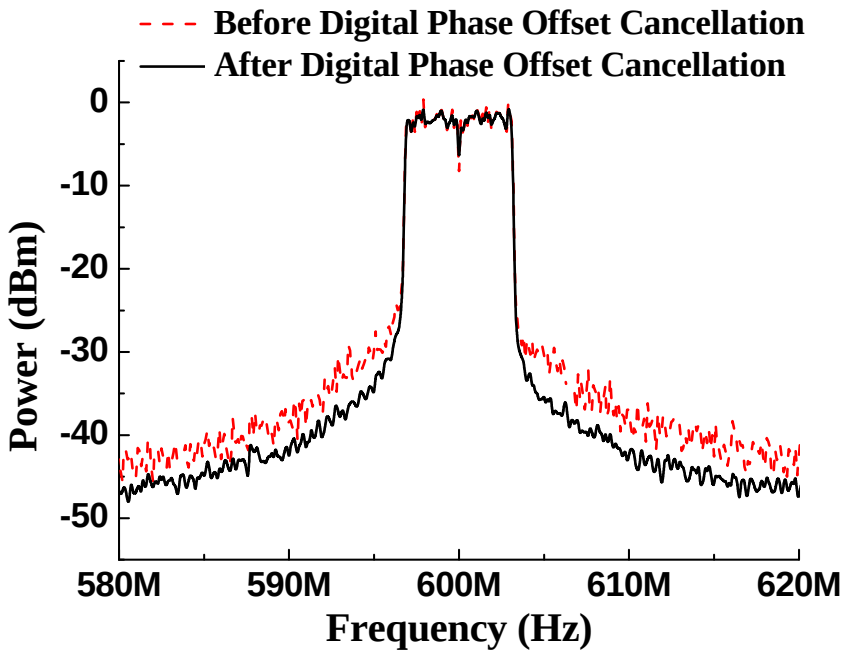

Figure 38. The spectrum mask with and without digital phase offset cancellation

In this section, a level shifting LINC amplifier was presented. The proposed LINC system was designed using standard 0.18μm CMOS technology. The system performance was evaluated with a 64-QAM OFDM modulated signal having 7 MHz bandwidth. By using level shifting technique adopting dynamic switched power supply selection, the total power efficiency was improved from 11.88% to 24.5% compared to a conventional LINC transmitter. Furthermore, a digital phase offset cancellation technique was employed in the proposed LINC amplifier, and improved linearity as measured by a 4 dB improvement in EVM and 7 dB in ACPR at 10 MHz offset.

4.3 UNEVEN MULTI-LEVEL LINC(UMLINC)

An MLINC increases system efficiency by increasing the number of power supplies [29], [38]. However, this increase also increases the complexity of the hardware. In this chapter, a new UMLINC architecture is proposed that further increases system efficiency without increasing complexity with a given number of power supplies. To verify the feasibility of the proposed system, ADS™ and MATLAB™ system simulations are performed.

4.3.1 Basic Principle of UMLINC Structure

Figure 39 illustrates the overall structure of the proposed UMLINC [39]. The structure consists of an UMSCS, a switched dynamic power supply, high efficiency switching PAs, and an isolated power combiner.

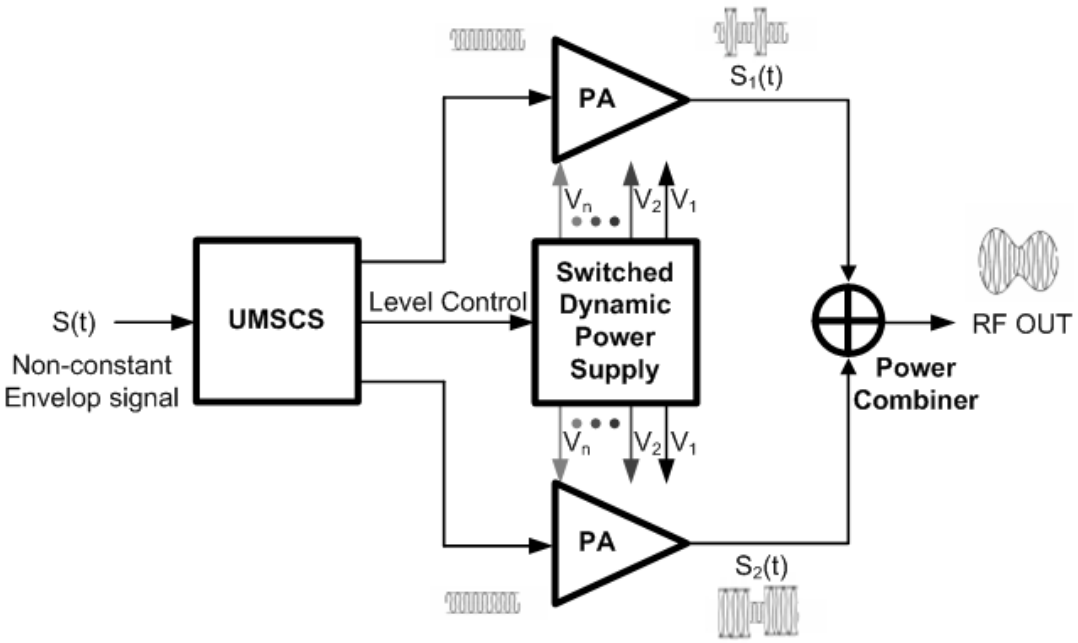

Figure 39. The proposed UMLINC system.

The UMSCS generates two RF phase signals that are fed to the PAs. The UMSCS also generates a level control used by the fast and high-efficient switched dynamic power supply to change the supply voltage of the PAs.

To prevent linearity problems associated with a non-isolated combiner, we used an isolated combiner, whose efficiency is maximized when both inputs are in phase. Thus, the number of maximum efficiency points of an MLINC equals the number of levels of the power supply, n. The proposed UMSCS increases the maximum number of efficiency points from n to n′, defined as

$$n' = {}_{n}H_{2} = {}_{n+1}C_{2} = \frac{(n+1)!}{2!\cdot(n-1)!} \quad . \tag{31}$$

This increase in the number of maximum efficiency points improves the total system efficiency.

4.3.2 Uneven Multi-Level Signal Component Separator (UMSCS)

The UMSCS generates level control and two RF phase signals. Figure 40 presents an example of two power supplies being employed. The outputs of the two power supplies are proportional to r_{small}, which is chosen based on the signal power density function (PDF), and r_{max}, which is half of the maximum signal envelope.

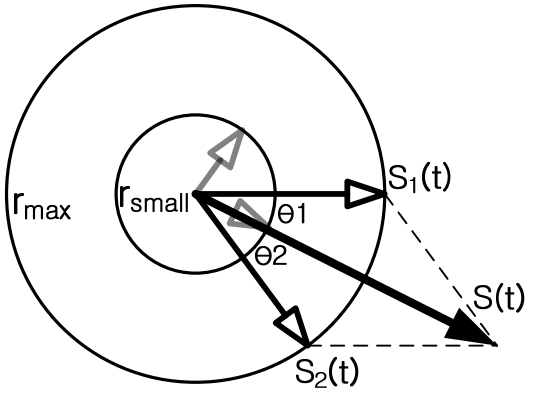

(a)

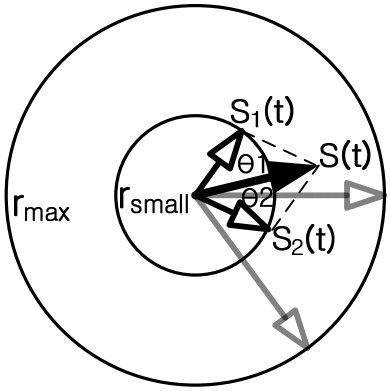

(b)

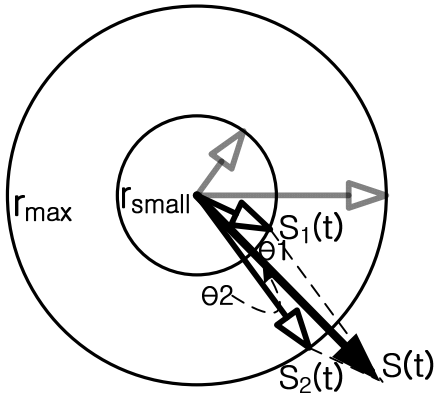

(c)

Figure 40. UMSCS operation: (a) when rsmall + rmax <|S(t)|, (b) when |S(t)| <2·rsmall, (c) when rsmall<|S(t)|<rsmall+rmax.

Figure 40(a) shows the operation of the UMSCS when the input linear signal, S(t), exceeds $r_{small}+r_{max}$. In this case, the UMSCS generates two signals of the same amplitude, r_{max}, yet different phase information. This operation is the same as that of a SCS in a conventional LINC system. When S(t) is smaller than $2 \times r_{small,}$ the UMSCS generates two signals of the same amplitude, r_{small}, as shown in Figure 40(b). When the operations shown in Figure 40(a) and (b) are combined, they are the same as those of a multi-level signal component separator (MSCS) in an MLINC amplifier. When S(t) is larger than $2 \times r_{small}$ and smaller than $r_{small}+r_{max}$, unlike in the previous systems, the UMSCS generates two different envelope signals, r_{small} and r_{max}, as shown in Figure 40(c).

The overall operation of the UMSCS is described as follows. A complex polar representation of S(t) is

$$S(t) = |S(t)| \angle \phi(t) \, . \tag{32}$$

The UMSCS outputs change according to the input signal amplitude and phase. These signals can be expressed as

$$S_1(t) = |S_1(t)| \angle (\phi(t) - \theta_1(t)) \ , \tag{33}$$

$$S_2(t) = |S_2(t)| \angle (\phi(t) + \theta_2(t)) \ , \tag{34}$$

where $|S_1(t)|$ and $|S_2(t)|$ are r_{max} or r_{small} , $S(t) = S_1(t)+S_2(t)$ and θ_1 and θ_2 can be derived from the law of cosines as

$$\theta_1(t) = \cos^{-1}\left(\frac{|S(t)|^2 + |S_2(t)|^2 - |S_1(t)|^2}{2|S(t)| \times |S_2(t)|} \right) \tag{35}$$

$$\theta_2(t) = \cos^{-1}\left(\frac{|S(t)|^2 + |S_1(t)|^2 - |S_2(t)|^2}{2|S(t)| \times |S_1(t)|} \right) . \tag{36}$$

4.3.3 System Measurement Results

Using ADS and MATLAB with a 7MHz bandwidth 64QAM WiMAX signal, both the efficiency improvement and the feasibility of the system were verified. The total system efficiency can be expressed as

$$System\ Efficiency = \int_0^{|S(t)|_{max}} \eta_{PA} \times \eta_{Comb}(|S(t)|) \times P(|S(t)|)\, d|S(t)| \ , \tag{37}$$

where η_{PA} is the PA efficiency, η_{comb} is the power combiner efficiency, and P(|S(t)|) is the PDF according to the signal envelope. The simulations adapted ideal switching PAs and an ideal isolated power combiner.

Figure 41 shows the system efficiency configuration for a LINC, an MLINC, and the proposed UMLINC system for a WiMAX signal.

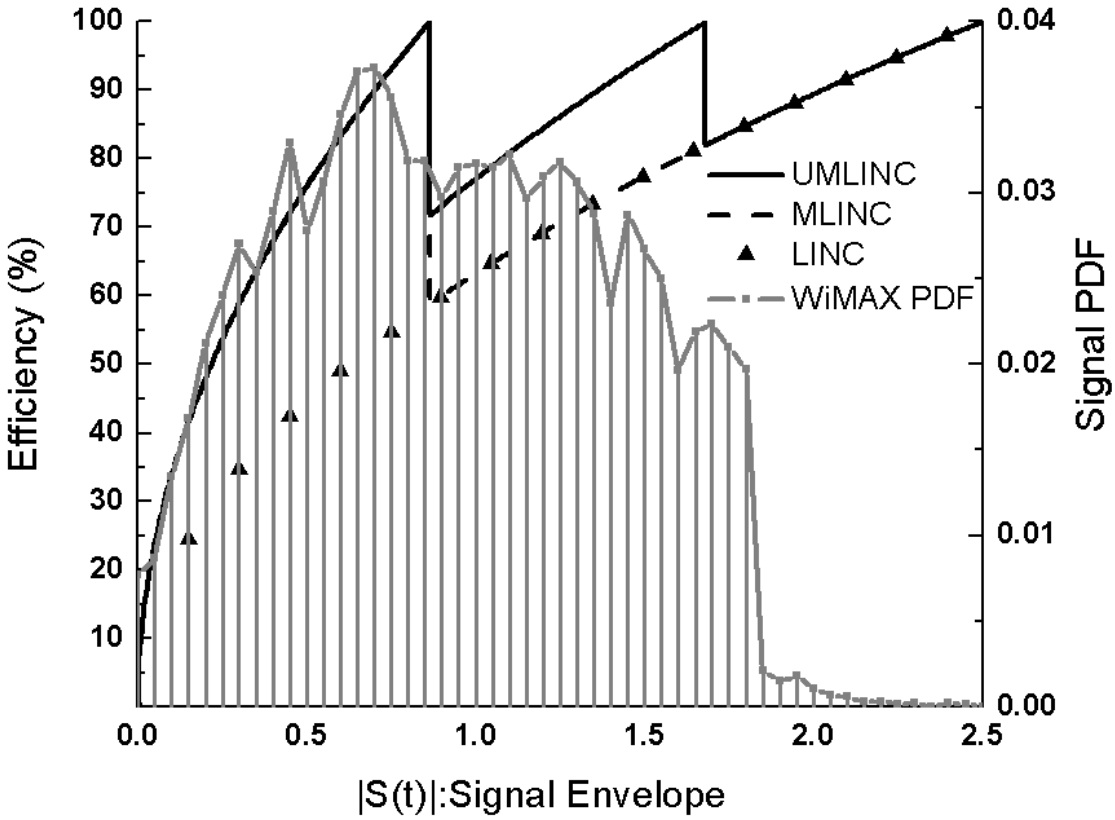

Figure 41. System efficiency configuration.

In Figure 41, for a conventional LINC system, efficiency is maximized when the signal envelope, |S(t)|, is maximal and decreases as |S(t)| decreases. However, as shown in Figure 41, most of the WiMAX signal is in the small envelope range. Therefore, a conventional LINC system yields poor system efficiency. In an MLINC system that employs two power supplies, the efficiency in the low power range increases by using two small envelop signals, r_{small}, when |S(t)| is small. However, the efficiency at the middle power levels is still low because only two maximum efficiency points exist. Using uneven signal envelopes for the middle power range in the UMLINC system improves the efficiency at the middle power levels, as shown in Figure 41. The simulation results for the system efficiency of each system are shown in Table 2.

Table 2. System Efficiency Comparison.

	Conventional LINC	MLINC (# power supply=2)	UMLINC (# power supply=2)
System Efficiency	18%	38.6%	49.72%
Optimum Level	r_{max}	$r_{small}=0.51 \times r_{max}$	$r_{small}=0.346 \times r_{max}$

The overall system efficiency improved from 38.6% to 49.72% with optimum r_{small} values chosen with a system simulation.

To prove the effectiveness of the proposed uneven multilevel technique, a LINC system was built. Figure 42 illustrates a system setup of the uneven LINC system. To minimize the effects of IQ mismatches, a digital intermediate frequency (IF) LINC modulator is employed. The UMSCS block and IQ modulator blocks are implemented with Matlab™. The UMSCS generates two digital phase outputs, which are digitally modulated to IF frequency IQ signals. The digital IF frequency signal is converted to a 30MHz IF frequency analog signal with 100MHz sampling in a DAC board (a Gage Compusen 4300) controlled by Matlab™.

The two outputs of the DAC board are up-converted to 630MHz RF signals using a 600MHz local oscillator (SMU 200ATM) and off-chip mixers (ZX05-42MH). For the PAs, the multi-level switching PA can be employed [40]. In this measurement, PAs are skipped, because the purpose of this measurement is not to verify the PA but to verify uneven multi-level LINC system. The up-converted multi-level LINC RF signals are combined in a power combiner.

The constellation and spectrum measurement results for a WiMAX system are presented in Figure 43. The measurement results exhibit -34dB EVM (sepc: -25dB) and 55dB ACPR with 7MHz offset.

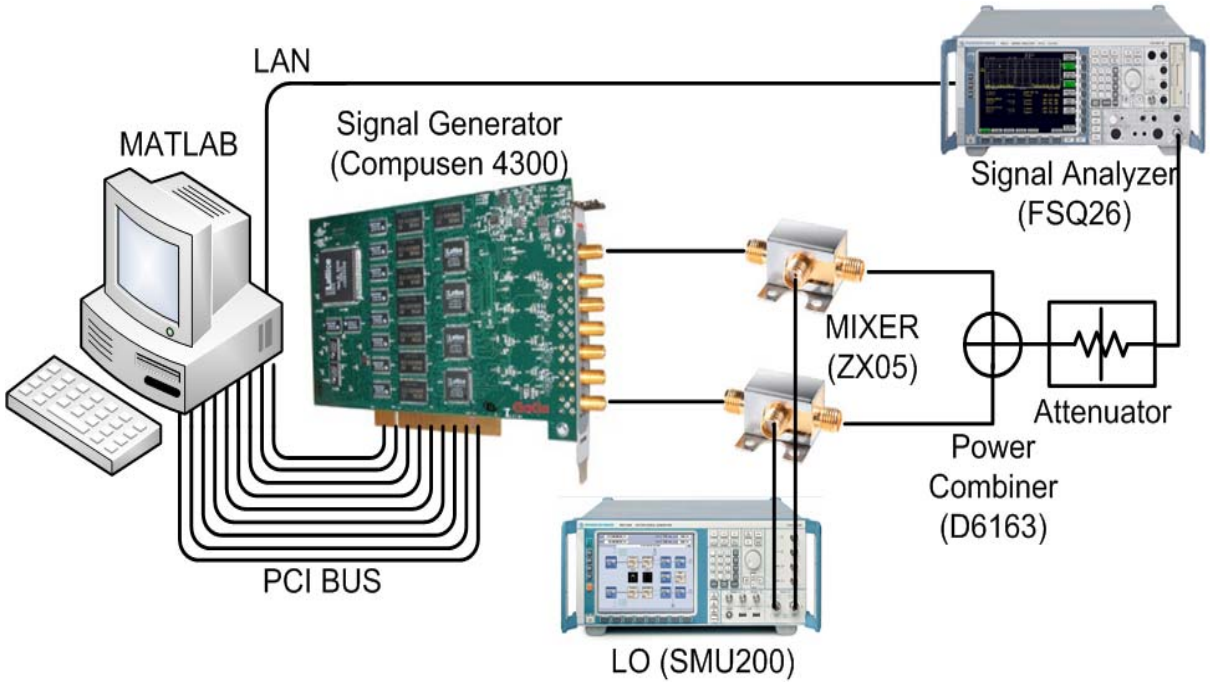

Figure 42. Measurement setup for UMLINC

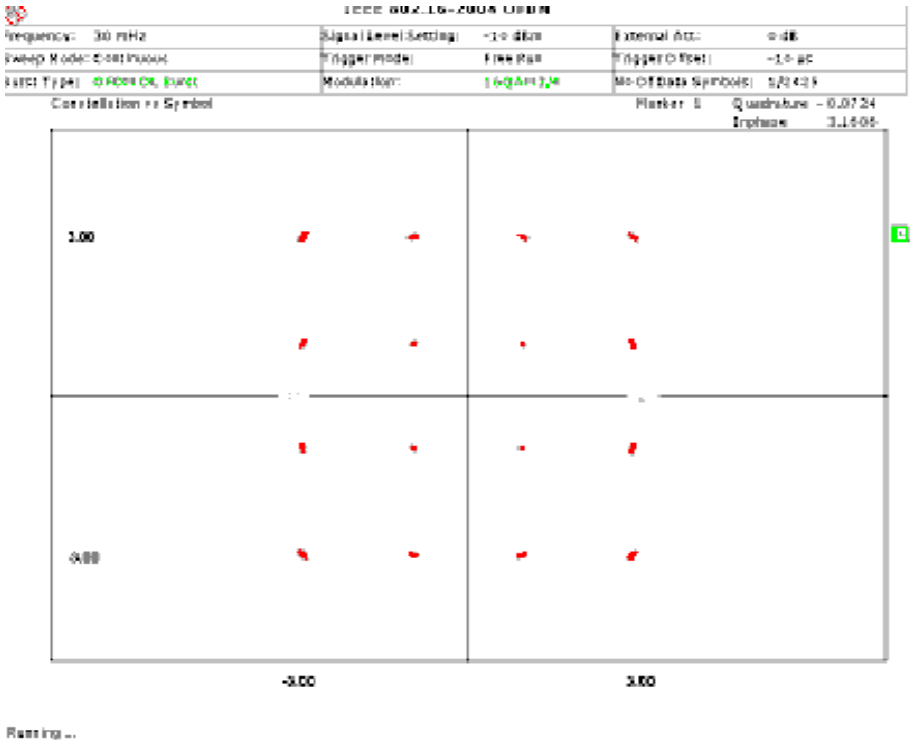

(a)

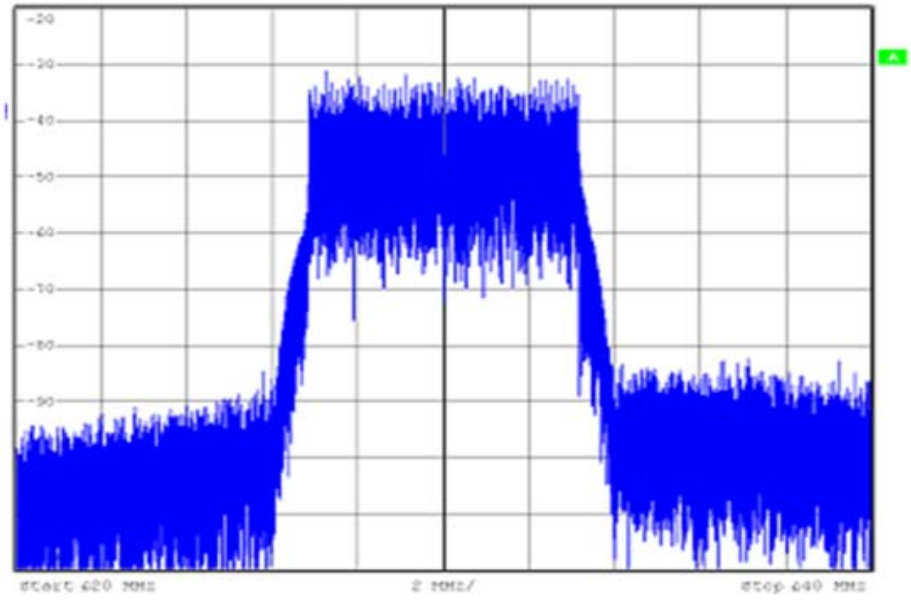

(b)

Figure 43. (a) The constellation and (b) spectrum measurement results.

4.4 CONCLUSIONS

In this chapter, two efficiency improvement techniques for LINC system are presented. The efficiency of these systems is checked with ADS and MATLAB co-simulations using two individual power supplies. MLINC significantly improve the efficiency compared with conventional LINC. Furthermore, UMLINC improve the efficiency more. To verify the linearity performance, error vector magnitude and adjacent channel power ratio are simulated and measured using commercial WiMAX signal source and these systems show good linearity performance.

CHAPTER 5

MULTI-BAND, MULTI-MODE LINC TRANSMITTER

5.1 INTRODUCTION

With the tremendous growth of wireless applications, many spectrum segments have been allocated to the licensed spectrum users. The ever-growing demand for higher user data rates has driven the wireless communication industry to implement more efficient modulation techniques or sophisticated coding schemes in their limited spectrum allocations. These licensees have the privileged rights to use this authorized spectrum for commercial or public use. When the licensed spectrum band is carefully observed, however, some spectrum segments are found to be much less than fully utilized, depending on the time and location.

Recently, cognitive radios (CR) technology has been proposed to increase spectral efficiency for the white, UHF spectrum that provides superior propagation and building penetration [41] [42]. CR systems aim to use the unoccupied spectrum allocations without additional license when the primary (i.e. licensed) users are not present. Therefore, CR system should have flexible transceiver architecture to adapt itself for the varying environment, covering multiple communication standards over a wide frequency range.

Figure 44 shows the basic principle of CR system. In the UHF band, some frequency segment is used by primary licensed users. With using CR system, the vacant band can be occupied by CR user. In order not to violate the licensee's right to

exclusively use the allocated spectrum segments, CR system should avoid using any spectrum band already occupied by primary users. Moreover, even though CR users have been using the vacant spectrum, whenever any primary user wants to use that band, CR users should stop their communication in order not to interfere with primary users as shown in Figure 44.

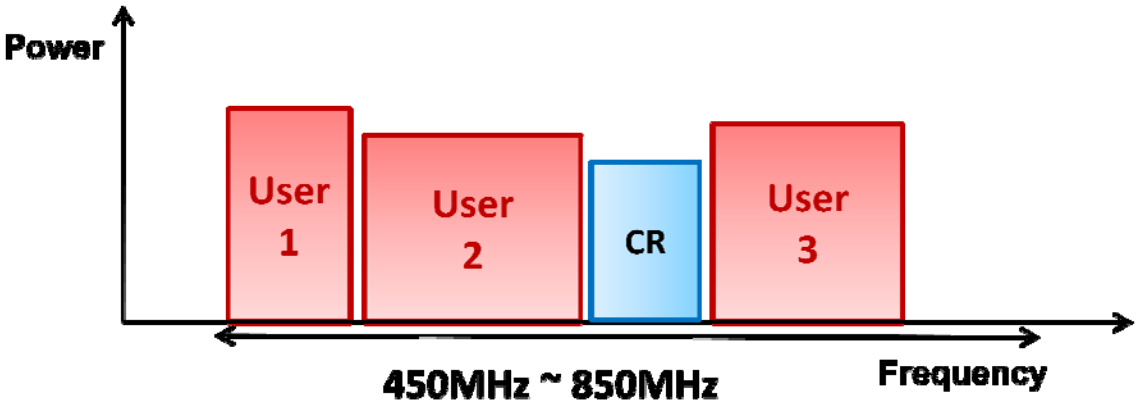

(a)

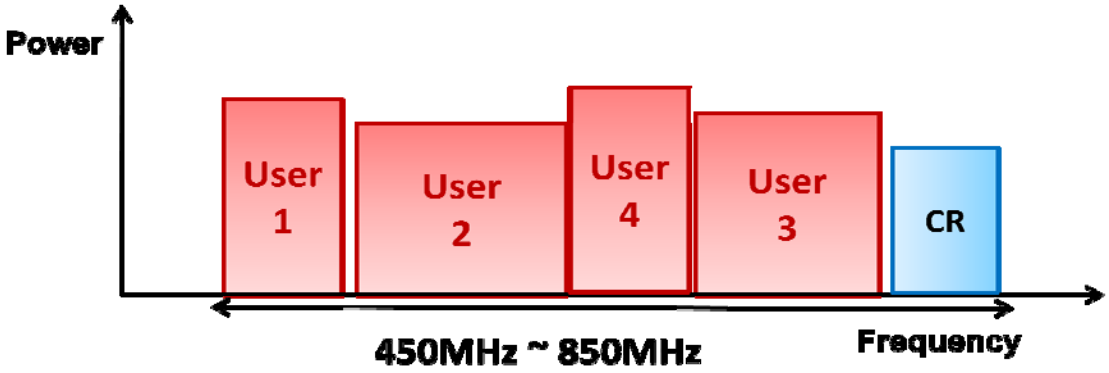

(b)

Figure 44. Principle of Cognitive Radio: (a)first time, (b) when user 4 is activated

If those protections are not provided, CR system would not be allowed to utilize the vacant spectrum resources. Therefore, the successful deployment of CR relies on its ability to accurately sense the spectrum usage status over a wide frequency range serving various wireless communication standards.

Implementing a CR transmitter poses two challenges. In order to handle the highly linear signal source with a long battery life, the PA must be highly linear and efficient. To increase efficiency while maintaining high linearity, multi-level LINCs (MLINC) have been suggested. Implementation of the MLINC system requires a multi-level PA, but the fabrication of such a PA has not been reported yet. Among the possible solutions for multi-level PA architectures, the approach that adopts a switched power supply is faster and more efficient than that uses a low drop output regulator. However, additional power switches increase the die area and reduce efficiency due to on-resistance between a PA and a power supply. The other challenge of a CR transmitter and its PA is its broadband requirement. To maximize the utilization of the available spectrum segments, the bandwidth of the signal has to be highly flexible, so that even a small fraction of spectrum resources can be fully utilized by CR users. In order to cover a broad frequency band, the PA must have multi-band performance.

In this chapter, a multi-level and multi-band Class-D PA for the LINC system for the CR white spectrum application is presented. The proposed PA generates multiple-output power levels without additional switches, using intrinsic PMOS devices of the Class-D topology, and also enables multi-band operation using tunable resonators. The proposed PA was fabricated using a standard 0.18-μm CMOS process.

5.2 DESIGN OF MULTI-LEVEL AND MULTI-BAND CLASS-D PA

Figure 45 shows the LINC system using the proposed PA. For the proposed PA, the voltage-mode Class D topology was used [43]. A Class-D PA uses a pair of devices driven in a push-pull mode and a series output resonator to tune the fundamental frequency. Without an additional power-switch block that decreases efficiency due to a series on-resistor in the switch device, the proposed Class-D PA can generate multi-output power by controlling the PMOS devices in a push-pull configuration of the Class-D PA, resulting in a smaller silicon area and higher efficiency.

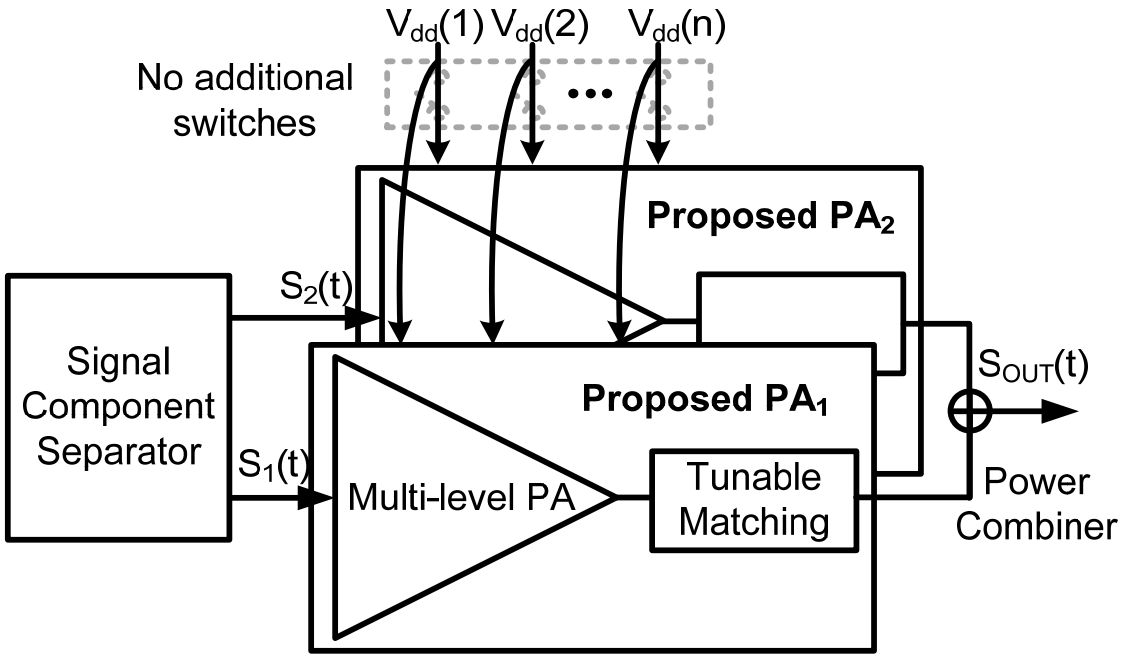

Figure 45. . Proposed LINC system: simplified block diagram.

The LINC system using the proposed PA provides peak efficiency on multiple output power levels due to its multi-level architecture, as shown Figure 46. In addition, the proposed PA enables a multi-band operation by using the tunable output network. A detailed structure of the proposed PA is explained in the following section.

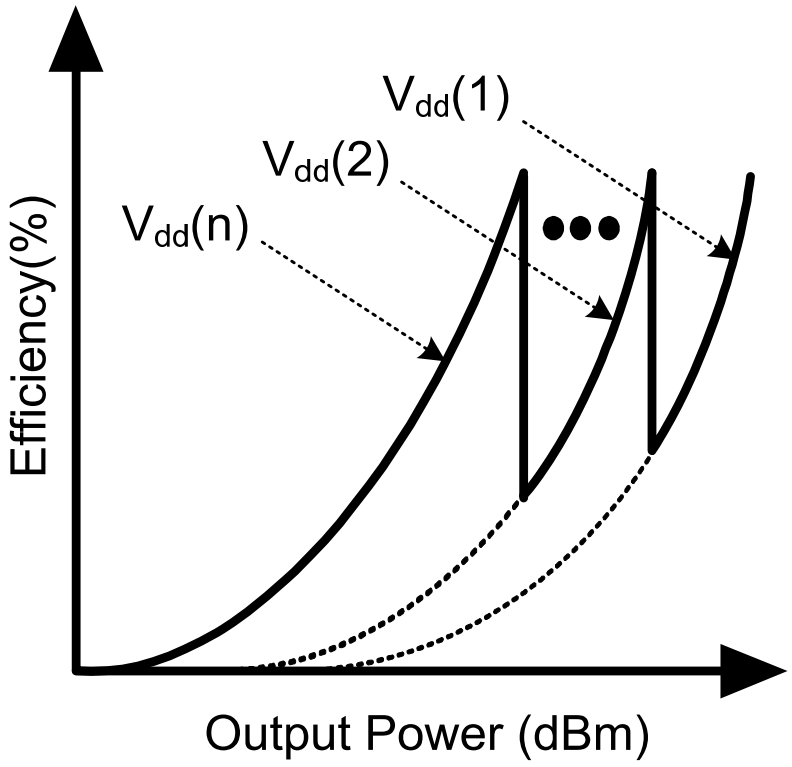

Figure 46. . Proposed LINC system: efficiency vs. output power.

5.2.1 Multi-Level Operation

The total schematic diagram of the proposed Class-D PA is shown in Figure 47.

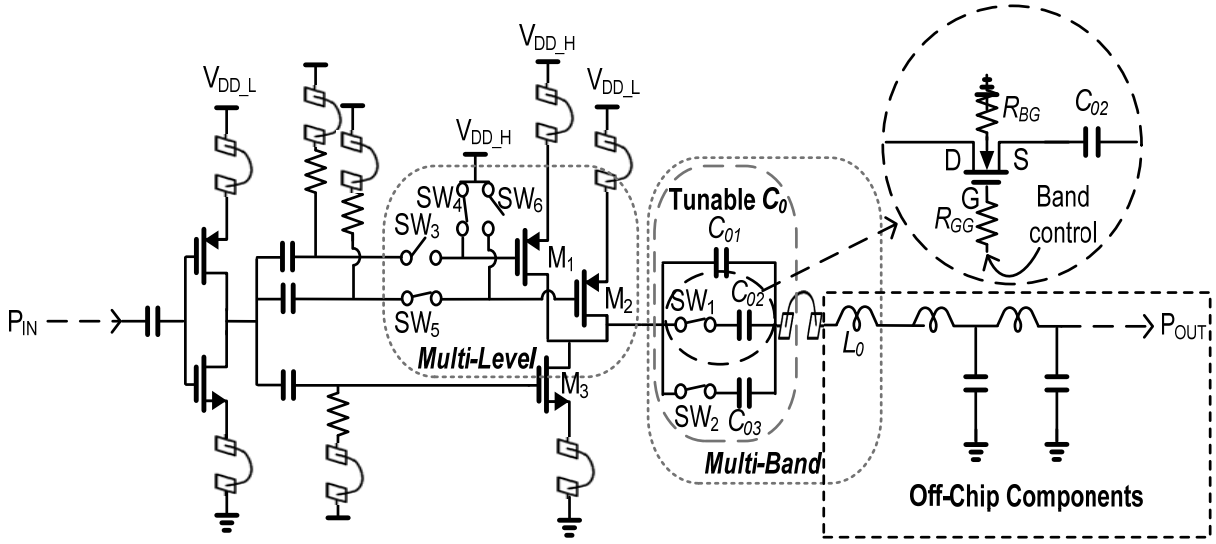

Figure 47. Schematic diagram of the proposed multi-level multi-mode Class-D PA.

In the high power mode, the SW6 is on to tie the gate of M2 to V_{DD_H}, and the M2 works in the cut-off region. In addition, the SW5 is off to block the RF-in signal path from the input gate of M2, the SW3 is on to deliver the RF input signal to M1, and SW 4 is off not to disturb the on-off switching operation of M1. In this case, the proposed PA operates with a push-pull structure of M1 and M3 and generates the maximum output power with the highest power supply, V_{dd_H}, as shown in Figure 48(a).

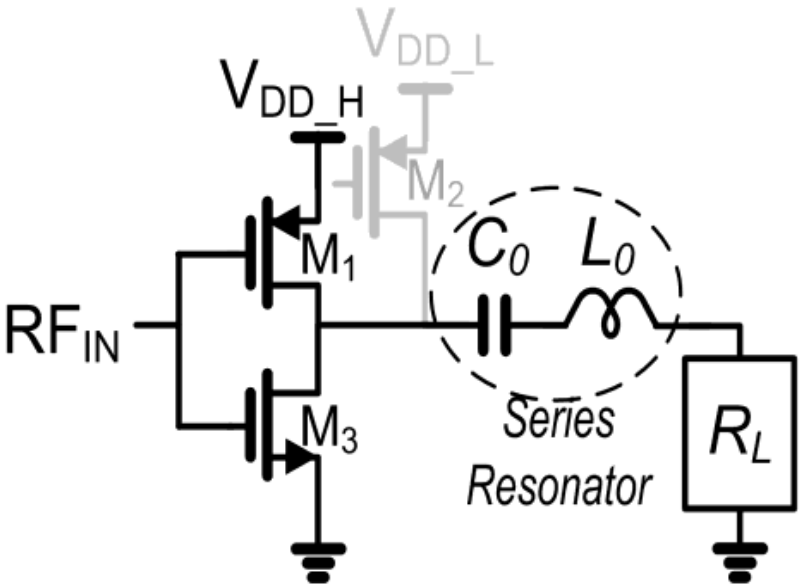

(a)

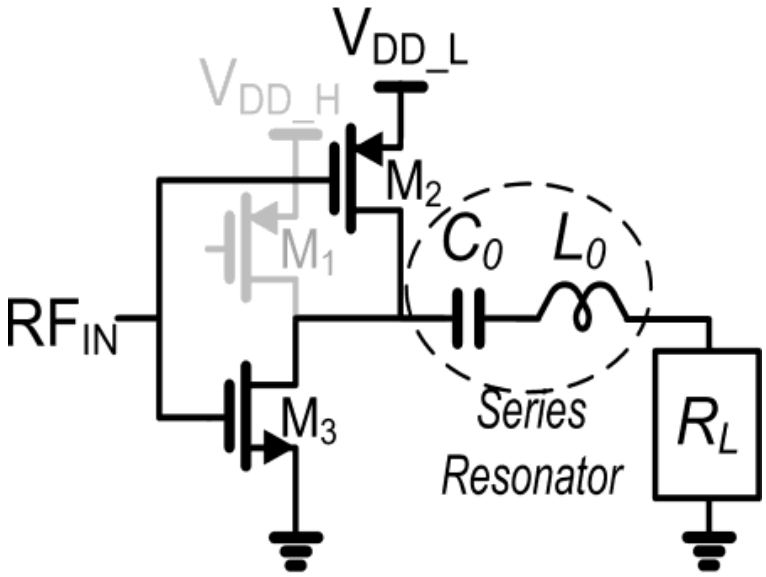

(b)

Figure 48. Multi-level operation or proposed PA: (a) high-power mode, (b) low-power mode.

In the low-power mode, the operations of SW3-SW6 are the opposite of those of the high-power mode. Thus, the M1 is the cut-off region, and the M2 and the M3 operates in the push-pull operation with a low power supply, V_{dd_L}, as shown in Figure 48(b). In this mode, the proposed PA generates low-output power. For both modes, the proposed PA maintains Class-D operation and yields high efficiency.

For reliable circuit design, the thick-oxide MOSFETs are used. The device sizes of M1, M2, and M3 are chosen by considering the optimum push-pull operation in the Class-D topology.

5.2.2 Multi-Bamd Operation

The operating frequency of the voltage-mode Class-D PA is proportional to the square root of the C_0 value in the L_0C_0-series resonator tank. For the multi-band operation, the proposed PA uses a tunable resonator with variable capacitor values, C_0, shown in Figure 24. For the highest frequency operation, the SW1 and the SW2 are open, which gives C_0 the lowest value, C_{01}. When SW1 or both SW1 and SW2 are turned on, the C_0 increases to $C_{01}+C_{02}$, or $C_{01}+C_{02}+C_{03}$, respectively, and the operating frequency band moves to the lower frequency band. For the broad band operation, the output LC matching network is designed with multi-sections [44].

In these tunable switch operations, the voltage swing between the two terminals in the switch device is large because the voltage swing in the resonator is amplified by the

value of loaded Q. The large voltage swing in the off-condition can cause breakdown issues and unintentionally turn on the switches. To prevent these side effects, several methods can be used. First, the thick-oxide MOSFETs can be used to provide high reliability. Secondly, the resistive body-gate floating technique can be applied in a deep N-well to prevent gate-source and gate-drain breakdowns with a low insertion loss [45]. Figure 49 shows the V_{GS} and V_{GD} voltage swing of the switches when they are in the off-operation.

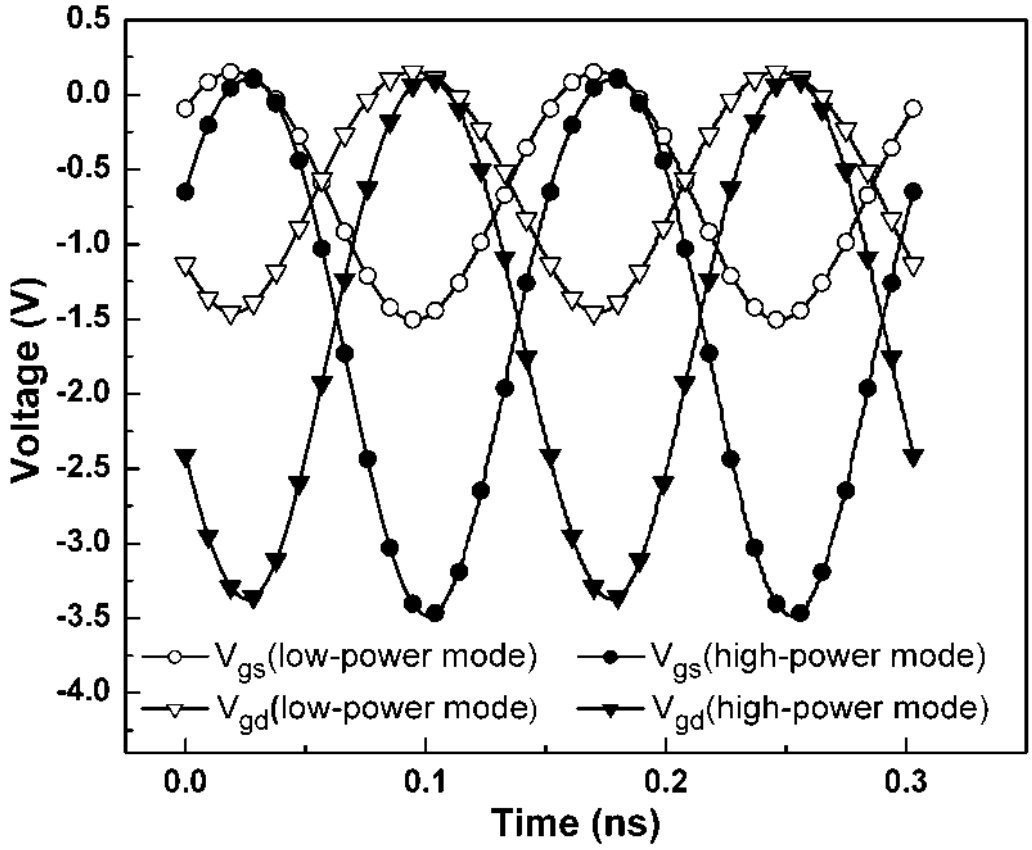

Figure 49. Voltage difference between the gate and the drain/source of the multi-band switch in off-operation.

The simulation results show that both V_{GD} and V_{GS} always fall below the threshold voltage of 0.67 V. The voltage swings between each terminal are under the thick-oxide breakdown voltage of 6.8 V.

5.2 MEASUREMENT RESULTS

A photograph of the implemented PA using a standard 0.18-μm CMOS process is shown in Figure 50.

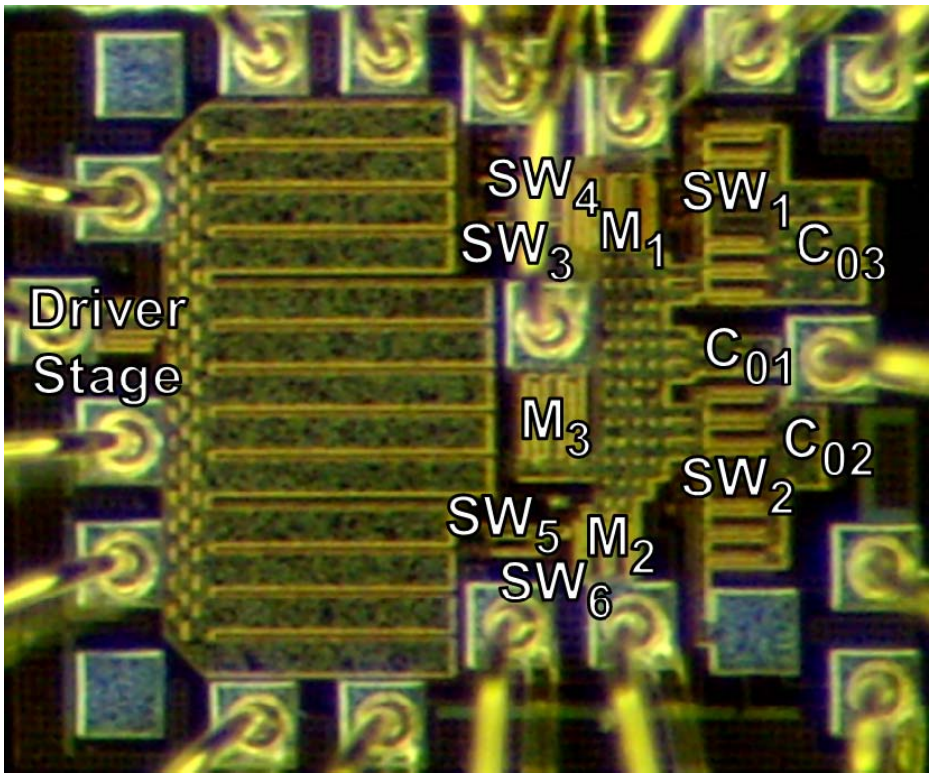

Figure 50. Die photograph of the proposed PA

The die area is 670 μm × 850 μm. The die is attached onto a PCB board with an off-chip output matching network. The system setup for the measurement is shown in Figure 51.

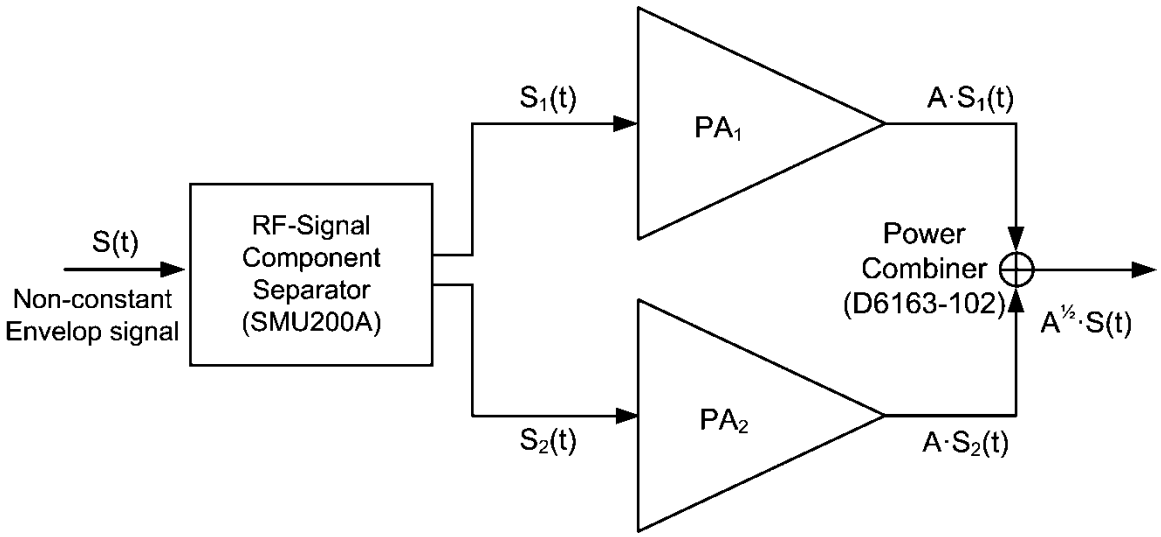

Figure 51. System Measurement Setup

The two RF input signals are generated from a RF arbitrary signal generator (SMU200A), and the outputs of the PAs are combined with a broad band combiner (Walenton D6163-102). The output power, the gain, the overall power added efficiency (PAE), and the drain efficiency (DE) of the power stage are measured with in-phase input signals to the two paths of the LINC system. To apply a power mode change, the SW3~SW6 operates according to each mode. Figure 52 shows the measured gain, output power, and efficiency versus input power at the center frequency of the operation frequency band, or 540MHz.

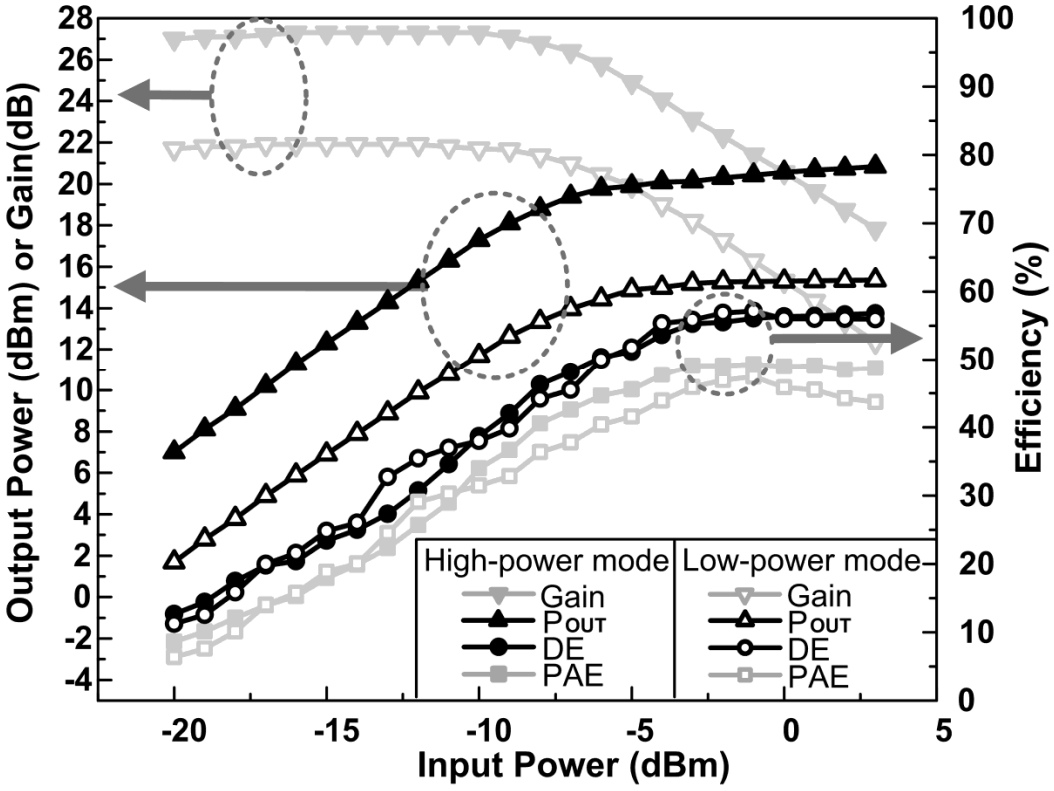

Figure 52. Measured gain, output power, DE, and PAE vs. input power in the low- and high-power mode at 540 MHz

With an input power of -1dBm, the proposed PA shows a DE of 57%, a PAE of 46%, a gain of 16.3dB, and a DC power consumption of 67.5mW in the low-power mode operation; and a DE of 56%, a PAE is 50%, a gain of 22.4dB, and a DC power consumption of 218mW in the high-power mode operation. The output power and efficiency versus frequency of the proposed PA at -1dBm input power are shown in Figure 53.

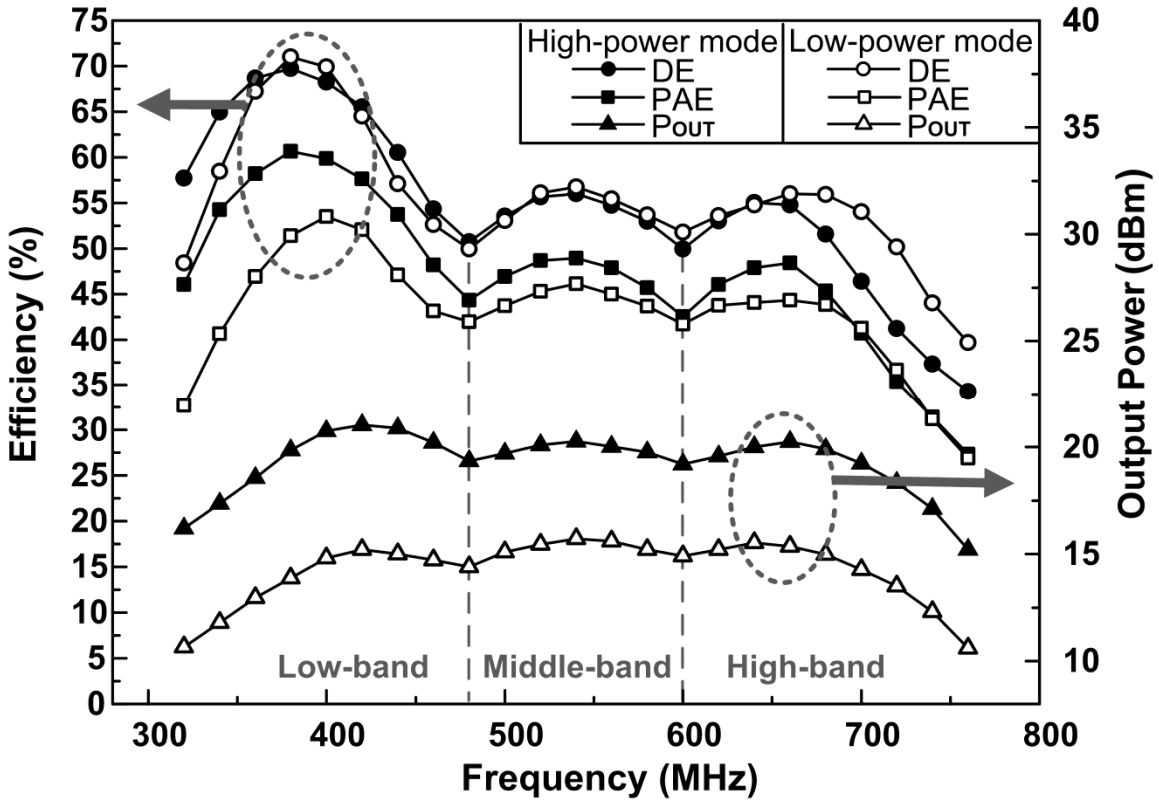

Figure 53. Measured output power, DE, and PAE of proposed PA vs. frequency with multi-power and multi-band operation

The maximum DE is 72% with 20dBm output power in the high-power mode and 70% with 15.1dB output power in the low-power mode. With the on-off operation of SW1 and SW2, the 3dB bandwidth of the proposed PA is 380MHz from 350 to 730MHz. The efficiency of the proposed PA in the high frequency band is lower than that in the low frequency band due to the parallel parasitic capacitance at the drain node of the power device. However, the efficiency degradation can be improved by using a parallel tuning inductor [46].

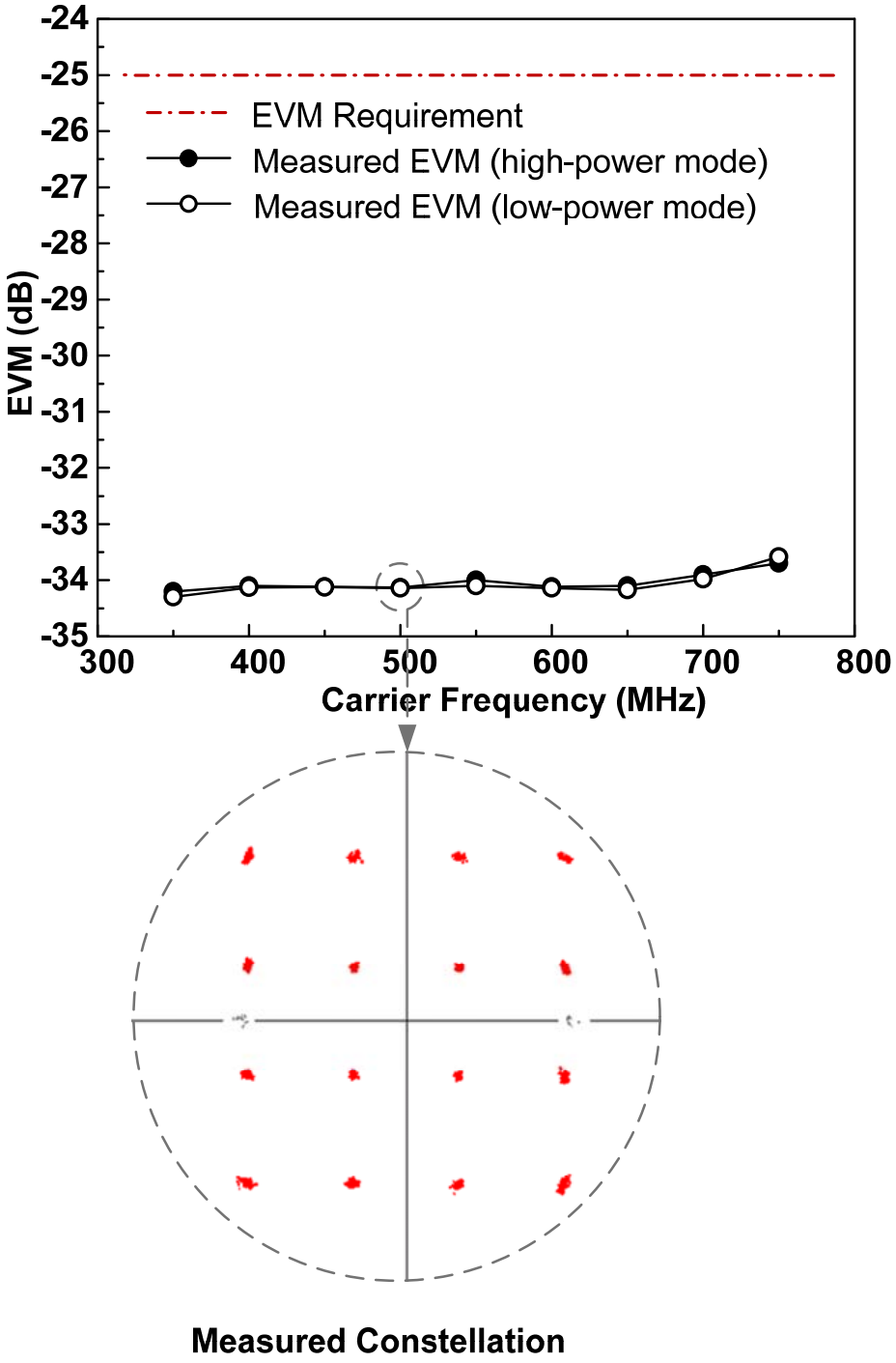

Figure 54. Measured EVM and constellation of LINC system with proposed PA using the WiMAX 7MHz bandwidth 16QAM OFDM signal

The error vector magnitude (EVM) and constellation are measured with a vector signal analyzer, an FSQTM. A WiMAX 802.16e 16QAM OFDM signal with 7Mbps bandwidth is used in the measurement, shown in Figure 54. The measured EVMs are around -34dB for both the low- and high-power modes. Thus, the linearity requirement, less then -25dB, is satisfied in both the high- and low-power modes.

5.4 CONCLUSION

This chapter proposes a multi-mode and multi-band Class-D PA in a 0.18-μm CMOS process for the LINC system in the cognitive radio application. By using the intrinsic PMOS of Cass D topology, the proposed PA provides both the high- and low-power modes with high efficiency in a simple structure. Using tunable resonating capacitors, the proposed PA provides wide-bandwidth, from 350 to 730MHz. The proposed Class-D PA with the LINC system is a high-efficient and high-linear solution for the cognitive radio white spectrum application.

CHAPTER 6

TECHNICAL CONTRIBUTIONS OF THE DISSERTATION

Over the past decade, the RF transmitter has been incredibly improved in terms of linearity, efficiency, and bandwidth. The increasing demand of customers for higher data rate and multi-band functionality has driven this trend for the decade. For instance, RF transmitter for cognitive radio should be able to support multiple RF frequency band.

Out-phasing transmitter, which uses two highly efficient switching PAs, can be a good solution for highly linear and efficient transmitter. However, more efficient and linear transmitter which has multi-band operation is required.

In this dissertation, some new architectures of out-phasing transmitter were presented. The summary is shown in Figure 55.

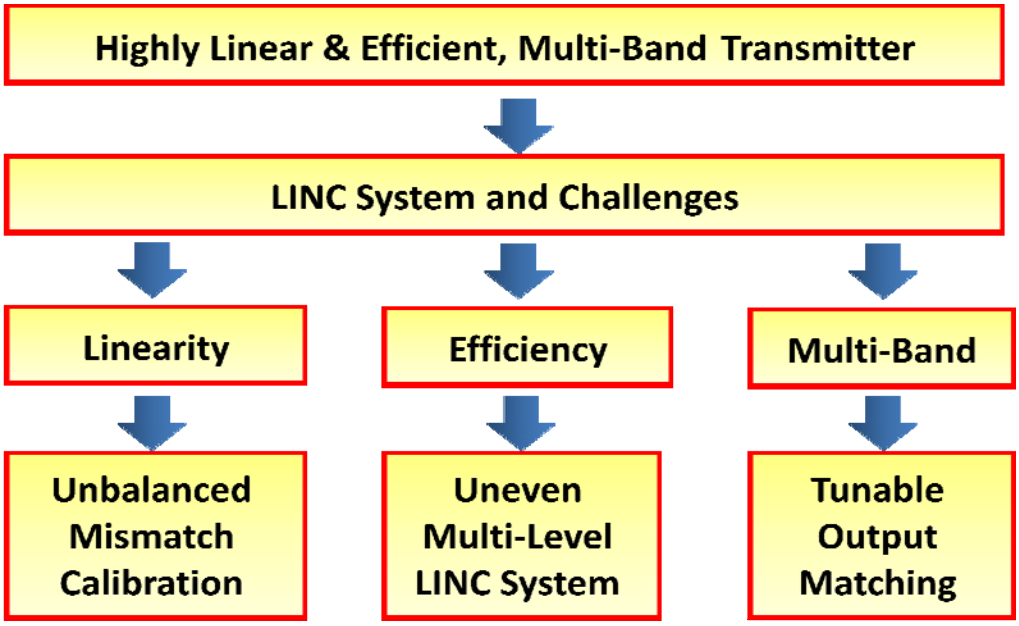

Figure 55. Summary of Thesis

The technical contributions of this dissertation can be summarized as follows.

- The LINC system is easily degraded by amplitude and phase mismatches between the two paths. In this dissertation, a novel mismatch calibration technique for the LINC system that calibrates both phase and amplitude mismatches with only phase control was presented. The technique detects mismatches between two paths without any iteration using pre-defined five test vector signals. In addition, this technique corrects the path mismatches using unbalanced phase control. Therefore, the proposed scheme does not require additional amplitude mismatch control blocks such as DC/DC converters or LDOs. The linearity performance of the proposed LINC system is measured with 7MHz bandwidth WiMAX signals. According to the measurement results, the proposed technique significantly enhances linearity.

- An efficiency improvement technique of the LINC transmitter has been developed. The developed technique utilizes Multi-level and Uneven Multi-level LINC structure to decrease the wasted power in the power combiner. Compared to an average power efficiency of conventional LINC transmitter, the average power efficiency of proposed LINC transmitter which employs a new uneven multi-level signal component separator (UMSCS) that significantly improves transmitter efficiency. This work was verified by ADS simulations and system measurements.

- In this dissertation, a multi-level and multi-band Class-D CMOS power amplifier (PA) in a standard 0.18-μm CMOS process is presented. Using multiple PMOS devices with control switches, the proposed PA improves efficiency with the multi-level operation. In order to enable the multi-band operation, the proposed PA employs a tunable series resonator. The measured maximum drain efficiencies were 72% and 70% for the low power mode and high power mode, respectively. The 3dB bandwidth of the proposed system was from 450 MHz to 730 MHz, which covers the cognitive radio white spectrum standard. The measured EVM using a commercial 16QAM OFDM signal was -34dB with a LINC system.

REFERENCES

[1] J. D. Chimeh, "Mobile services: Trends and evolution," in *Advanced Communication Technology, 2009. ICACT 2009. 11th International Conference on*, 2009, pp. 946-948.

[2] G. Hanington*, et al.*, "High-efficiency power amplifier using dynamic power-supply voltage for CDMA applications," *Microwave Theory and Techniques, IEEE Transactions on,* vol. 47, pp. 1471-1476, 1999.

[3] D. Cox, "Linear Amplification with Nonlinear Components," *Communications, IEEE Transactions on,* vol. 22, pp. 1942-1945, 1974.

[4] F. J. Casadevall and A. Valdovinos, "Performance analysis of QAM modulations applied to the LINC transmitter," *Vehicular Technology, IEEE Transactions on,* vol. 42, pp. 399-406, 1993.

[5] F. Casadevall and J. J. Olmos, "On the behavior of the LINC transmitter," in *Vehicular Technology Conference, 1990 IEEE 40th*, 1990, pp. 29-34.

[6] A. Birafane and A. B. Kouki, "On the linearity and efficiency of out-phasing microwave amplifiers," *Microwave Theory and Techniques, IEEE Transactions on,* vol. 52, pp. 1702-1708, 2004.

[7] F. H. Raab*, et al.*, "Power amplifiers and transmitters for RF and microwave," *Microwave Theory and Techniques, IEEE Transactions on,* vol. 50, pp. 814-826, 2002.

[8] S. C. Cripps, *RF Power Amplifiers for Wireless Communications, 2nd ed*. Norwood, MA: Artech House Inc., 2006.

[9] P. Hyun-Min, *et al.*, "A predistortion linearizer using envelope-feedback technique with simplified carrier cancellation scheme for class-A and class-AB power amplifiers," *Microwave Theory and Techniques, IEEE Transactions on,* vol. 48, pp. 898-904, 2000.

[10] D. Seok Joo, *et al.*, "Pulsed Active Load–Pull Measurements for the Design of High-Efficiency Class-B RF Power Amplifiers With GaN HEMTs," *Microwave Theory and Techniques, IEEE Transactions on,* vol. 57, pp. 881-889, 2009.

[11] A. Reatti and M. K. Kazimierczuk, "Comparison of the efficiencies of class D and class E rectifiers," in *Circuits and Systems, 1993., Proceedings of the 36th Midwest Symposium on*, 1993, pp. 871-874 vol.2.

[12] S. Lungu, *et al.*, "Simulation and design of a Class E power amplifier," in *Electronics Technology, 2009. ISSE 2009. 32nd International Spring Seminar on*, 2009, pp. 1-4.

[13] J. N. Kitchen, *et al.*, "Polar SiGe Class E and F Amplifiers Using Switch-Mode Supply Modulation," *Microwave Theory and Techniques, IEEE Transactions on,* vol. 55, pp. 845-856, 2007.

[14] K. Bumman, *et al.*, "High Efficiency RF Transmitter Architectures Modulating Power Supply," in *Telecommunications in Modern Satellite, Cable and Broadcasting Services, 2007. TELSIKS 2007. 8th International Conference on*, 2007, pp. 149-155.

[15] J. Zhuang, *et al.*, "A Technique to Reduce Phase/Frequency Modulation Bandwidth in a Polar RF Transmitter," *Circuits and Systems I: Regular Papers, IEEE Transactions on,* vol. 57, pp. 2196-2207, 2010.

[16] S. Tomisato, *et al.*, "Phase error free LINC modulator," *Electronics Letters,* vol. 25, pp. 576-577, 1989.

[17] L. Sundstrom, "Automatic adjustment of gain and phase imbalances in LINC transmitters," *Electronics Letters,* vol. 31, pp. 155-156, 1995.

[18] S. Ampem-Darko and H. S. Al-Raweshidy, "Gain/phase imbalance cancellation technique in LINC transmitters," *Electronics Letters,* vol. 34, pp. 2093-2094, 1998.

[19] S. A. Olson and R. E. Stengel, "LINC imbalance correction using baseband preconditioning," in *Radio and Wireless Conference, 1999. RAWCON 99. 1999 IEEE*, 1999, pp. 179-182.

[20] Z. Xuejun and L. E. Larson, "Gain and phase error-free LINC transmitter," *Vehicular Technology, IEEE Transactions on,* vol. 49, pp. 1986-1994, 2000.

[21] X. Zhang, *et al.*, "Calibration scheme for LINC transmitter," *Electronics Letters,* vol. 37, pp. 317-318, 2001.

[22] Z. Xuejun, *et al.*, "A gain/phase imbalance minimization technique for LINC transmitter," *Microwave Symposium Digest, 2001 IEEE MTT-S International,* vol. 2, pp. 801-804 vol.2, 2001.

[23] J. N. Kitchen, *et al.*, "Combined Linear and delta-Modulated Switch-Mode PA Supply Modulator for Polar Transmitters," *Solid-State Circuits, IEEE Journal of,* vol. 44, pp. 404-413, 2009.

[24] M. Seong-Sik, *et al.*, "Mismatch Detection and Compensation Method for the LINC System Using a Closed-Form Expression," *Microwave Theory and Techniques, IEEE Transactions on,* vol. 56, pp. 3050-3057, 2008.

[25] H. Joonhoi, *et al.*, "A novel unbalanced phase calibration technique for the LINC transmitter," in *Radio and Wireless Symposium (RWS), 2010 IEEE*, 2010, pp. 188-191.

[26] L. Chung-Wei and L. Yen-Jen, "A Power Efficient and Fast Transient Response Low Drop-Out Regulator in Standard CMOS Process," in *VLSI Design, Automation and Test, 2006 International Symposium on*, 2006, pp. 1-4.

[27] N. Joongjin and K. Bumman, "The Doherty Power Amplifier With On-Chip Dynamic Bias Control Circuit for Handset Application," *Microwave Theory and Techniques, IEEE Transactions on,* vol. 55, pp. 633-642, 2007.

[28] P. Reynaert and M. S. J. Steyaert, "A 1.75-GHz polar modulated CMOS RF power amplifier for GSM-EDGE," *Solid-State Circuits, IEEE Journal of,* vol. 40, pp. 2598-2608, 2005.

[29] H. Joonhoi, *et al.*, "Highly efficient and linear level shifting digital LINC transmitter with a phase offset cancellation," in *Radio and Wireless Symposium, 2009. RWS '09. IEEE*, 2009, pp. 211-214.

[30] S. Yamanouchi, *et al.*, "An efficient algorithm for simulating error vector magnitude in nonlinear OFDM amplifiers," in *Custom Integrated Circuits Conference, 2004. Proceedings of the IEEE 2004*, 2004, pp. 129-132.

[31] V. W. Leung, *et al.*, "An improved digital-IF transmitter architecture for highly-integrated W-CDMA mobile terminals," in *Vehicular Technology Conference, 2003. VTC 2003-Spring. The 57th IEEE Semiannual*, 2003, pp. 1335-1339 vol.2.

[32] S. Azam, *et al.*, "The limiting frontiers of maximum DC voltage at the drain of SiC microwave power transistors in case of class-A power amplifier," in *Semiconductor Device Research Symposium, 2007 International*, 2007, pp. 1-2.

[33] M. El-Asmar, *et al.*, "Impact of the PA Mismatching in Chireix-Out-phasing System without Stubs," in *Signals, Systems and Electronics, 2007. ISSSE '07. International Symposium on*, 2007, pp. 201-204.

[34] X. Zhang, Larson L.E., Asbeck, P., *Design of Linear RF Out-phasing Power Amplifiers*: Artech House Publishers, 2003.

[35] K. Kwan-Woo, *et al.*, "A 600MHz CMOS OFDM LINC transmitter with a 7 bit digital phase modulator," in *Radio Frequency Integrated Circuits Symposium, 2008. RFIC 2008. IEEE*, 2008, pp. 677-680.

[36] L. Sundstrom, "The effect of quantization in a digital signal component separator for LINC transmitters," *Vehicular Technology, IEEE Transactions on,* vol. 45, pp. 346-352, 1996.

[37] L. Doo hwan and H. Morikawa, "Performance Analysis of Ranging Process in IEEE 802.16e OFDMA Systems," in *Wireless and Mobile Computing, Networking and Communications, 2007. WiMOB 2007. Third IEEE International Conference on*, 2007, pp. 16-16.

[38] C. Yuan-Chuan, *et al.*, "Multilevel LINC System Design for Wireless Transmitters," in *VLSI Design, Automation and Test, 2007. VLSI-DAT 2007. International Symposium on*, 2007, pp. 1-4.

[39] J. Hur, *et al.*, "Highly efficient uneven multi-level linc transmitter," *Electronics Letters,* vol. 45, pp. 837-838, 2009.

[40] J. Hur, *et al.*, "A Multi-Level and Multi-Band Class-D CMOS Power Amplifier for the LINC System in the Cognitive Radio Application," *Microwave and Wireless Components Letters, IEEE,* vol. 20, pp. 352-354, 2010.

[41] Y. Hur, *et al.*, "A Cognitive Radio (CR) Testbed System Employing a Wideband Multi-Resolution Spectrum Sensing (MRSS) Technique," in *Vehicular Technology Conference, 2006. VTC-2006 Fall. 2006 IEEE 64th*, 2006, pp. 1-5.

[42] A. B. MacKenzie, *et al.*, "Cognitive Radio and Networking Research at Virginia Tech," *Proceedings of the IEEE,* vol. 97, pp. 660-688, 2009.

[43] Y. Jingshi and S. I. Long, "Power Amplifier Selection for LINC Applications," *Circuits and Systems II: Express Briefs, IEEE Transactions on,* vol. 53, pp. 763-767, 2006.

[44] T. H. Lee, *The Design of CMOS Radio-Frequency Integrated Circuits, 2nd ed.* Cambridge, U.K.: Cambridge Univ. Press, 2004.

[45] Y. Mei-Chao, *et al.*, "Design and analysis for a miniature CMOS SPDT switch using body-floating technique to improve power performance," *Microwave Theory and Techniques, IEEE Transactions on,* vol. 54, pp. 31-39, 2006.

[46] H. Tsai-Pi, *et al.*, "CMOS Out-phasing Class-D Amplifier With Chireix Combiner," *Microwave and Wireless Components Letters, IEEE,* vol. 17, pp. 619-621, 2007.

PUBLICATIONS

[1] **J. Hur**, et al., “A Novel Automatic Amplitude and Phase Mis-matches Calibration Technique for the LINC Transmitter with an Unbalanced Phase Control,” under review in *IEEE Transactions On Microwave Theory And Techniques*.

[2] **J. Hur**, et al., “A Multi-Level and Multi-Band Class-D CMOS Power Amplifier for the LINC System in a Cognitive Radio Application,” *IEEE Microwave and Wireless Components Letters (MWCL),* Volume 20, Issue 6, June. 2010, pp. 352 - 354.

[3] **J. Hur**, et al., "A Novel Unbalanced Phase Calibration Technique for the LINC Transmitter,” *IEEE Radio and Wireless Symposium (RWS)*, Jan. 2010, pp. 188 – 191.

[4] **J. Hur,** et al., "Highly efficient uneven multi-level LINC transmitter," *Electronics Letters,* Volume 45, Issue 16, July 30 2009, pp. 837 - 838.

[5] **J. Hur**, et al., “Highly Efficient and Linear Level Shifting Digital LINC Transmitter with a Phase Offset Cancellation,” *IEEE Radio and Wireless Symposium (RWS)*, 18-22 Jan. 2009 pp. 211 - 214.

[6] K. Lim, **J. Hur**, et al., “Emerging Techniques for All Digital Multi-level Multi-band RF Out-phasing Transmitter,” Accepted in *Telecommunication Review,* 2010.

[7] K. Kim, **J. Hur**, J. Choi, K. Chae, O. Lee, S. Byun, C.-H. Lee, K. Lim, and J. Laskar, “A Fully-Integrated All-Digital Out-phasing Transmitter for OFDM System,” under review in *Circuits and Systems I, IEEE Transaction of,* submitted.

[8] J. Laskar, K. Lim, **J. Hur**, K..Kim, O. Lee and C. H. Lee, ”Emerging Multi-Level Architectures and Unbalanced Mismatch Calibration Technique for High-Efficient

and High-Linear LINC systems," *IEEE International Symposium on Circuits and Systems*, 2010, pp. 821 - 824.

[9] J. Park, T. Song, **J. Hur**, et al., "A Fully Integrated UHF-band CMOS Receiver with Multi-Resolution Spectrum Sensing (MRSS) Functionality for IEEE 802.22 Cognitive Radio Applications," *Solid-State Circuits, IEEE Journal of*, vol. 44, no. 1, Jan. 2009, pp. 258-268.

[10] J. Park, T. Song, **J. Hur**, et al., "A Fully Integrated UHF Receiver with Multi-Resolution Spectrum Sensing (MRSS) Functionality for IEEE 802.22 Cognitive Radio Applications," in *Solid-State Circuits Conference, 2008. ISSCC 2008. Digest of Technical Papers. IEEE International*, 2008, pp. 526-633.

[11] K. Kim, J. Choi, **J. Hur**, O. Lee, C.-H. Lee, K. Lim, and J. Laskar, "All-Digital Out-phasing Modulator with Digital Mismatch Compensation," under review in *Circuits and Systems II (TCAS-II), IEEE Transaction of.*

[12] K. Kim, J. Choi, **J. Hur**, C.-H. Lee, K. Lim, and J. Laskar, "All-Digital Out-Phasing Transmitter," in *International Solid-State Circuits Conference Student Forum, 2009. ISSCC 2009 Student Forum. IEEE*, Feb. 2009.

[13] S. Suh, K. Kim, **J. Hur**, et al., "MAC Controlled LINC Calibration using Pilot-aided LSE Channel Estimator for OFDM Systems," *IEEE Vehicular Technology Cenference (VTC),* Apr. 2009, pp. 1 - 5.

[14] T. Song, J. Park, S. Lee, **J. Hur**, et al., "An SRAM-based On-Chip Arbitrary Waveform Generator for Analog Signal Processing," accepted in *IEEE Transaction On Instruments and Measurement.*

[15] J. Park, K. Kim, T. Song, S. Lee, **J. Hur**, et al., "A Cross-layer Cognitive Radio Testbed for the Evaluation of Spectrum Sensing Receiver and Interference Analysis," in *Cognitive Radio Oriented Wireless Networks and Communications, 2008. CrownCom 2008. 3rd International Conference on*, 2008, pp. 1 - 6.

[16] K. Lim, C. Lee, H. Kim, J. Laskar, **J. Hur**, et al., "Systems and Methods for a Level-shifting High-Efficiency LINC Amplifier Using Dynamic Power Supply", submitted for Patent (US) Patent application number: 20100073084

VITA

Joonhoi Hur was born in Seoul, Korea, in 1979. He received his B.S. in electrical engineering from Korea University, Seoul, Korea, in 2002. From 2002 to 2005, he worked at WinTelecom in Seoul, Korea, where he was involved in wireless network device design. He received his M.S. in electrical and computer engineering from Georgia Institute of Technology, in 2008. In summer 2010, he worked as an intern in Texas Instruments, Dallas, TX where he was involved in H/W and System design. He is currently working toward his Ph.D. in electrical and computer engineering in Georgia Institute of Technology. His research interests include RF, baseband system design, and analog and RF-integrated circuit design.